SEASONAL PRECIPITATION VARIABILITY AND ITS IMPACT ON VEGETATION DYNAMICS UNDER CLIMATE CHANGE AND ARIDITY SPECTRA OF THE SOUTHWEST UNITED STATES ECOSYSTEMS

A Dissertation

by

DAGBEGNON CLEMENT SOHOULANDE DJEBOU

Submitted to the Office of Graduate and Professional Studies of
Texas A&M University
in partial fulfillment of the requirements for the degree of

DOCTOR OF PHILOSOPHY

Chair of Committee,	Vijay P. Singh
Committee Members,	Patricia Smith
	Oliver Frauenfeld
	Rusty Feagin
Head of Department,	Stephen Searcy

May 2015

Major Subject: Biological and Agricultural Engineering

ABSTRACT

This study combines hydro-climatological and biological components for addressing variability in precipitation and vegetation patterns under climate change. We explore the marginal and interactive effects of vegetation and atmospheric variables in order to better understand the plausible changes in terrestrial hydrological processes. We target the southwest United States, known for its diversified ecosystem and depleting water resources. Specifically, we employ an entropy-based disorder index to address precipitation variability and evaluate the marginal effect of watershed topography. Results show that the variability gradually increases westward. We concluded a significant watershed topography effect, which suggests that hilly reliefs have a stabilizing effect on seasonal precipitation variability in time and space. We conclude the necessity to include watershed topography information in climate model parameterizations. However, the implication of a spatial precipitation gradient raises questions regarding vegetation dynamics. In order to understand these dynamics, we analyze the inclusion of precipitation variability in conjunction with the Normalized Difference Vegetation Index (NDVI) during the growing season. We identify three climatic regions based on the United Nations Aridity Index (AI): a relatively humid region with $AI \geq 0.65$, an intermediate region with $0.50 \leq AI < 0.65$, and a relatively dry region with $AI < 0.50$. We target four types of vegetation covers: deciduous forest, shrubland, pasture, and grassland. We conclude significant positive trends in the NDVI series for both relatively humid and intermediate climatic regions. In the arid region, we find distinct responses to precipitation for perennial

vegetation versus annual vegetation types. The magnitude of these responses tends to increase with environmental aridity. Later we apply the entropy theory to investigate the joint inclusion of precipitation, soil moisture, and temperature in vegetation dynamics analysis. Results reveal trends toward maximum entropy; however, the variable precipitation remained particularly determinant from a marginal point of view. We use a probabilistic approach to analyze the climate change impact on future precipitation patterns. We conclude significant drifts in seasonal precipitation regimes and a meaningful spatial weight. Finally, we emphasize the plausible implications of our findings for future water management. Nevertheless, we suggest further studies on the topic particularly at a global scale.

DEDICATION

To GOD be the glory, for the unbounded love and mercy

ACKNOWLEDGMENTS

I would like to express my gratitude to my academic advisor, Professor Vijay P. Signh for his meaningful guidance and contribution to this work. His encouragement and support were determinant during my years at Texas A&M University. I am so grateful for the opportunity I got to study under Professor Singh. His tremendous background in hydrology and environmental engineering associated with his great trans-disciplinary knowledge, gave me the flexibility to extend freely my research scope. Besides the scientific knowledge, I learned from him the virtue of patience and self-confidence, which I believe are essential for great achievements. I will always be proud of him and give my best to have a fruitful career, which he can be proud of as well.

I would like to thank Dr Patricia Smith, Dr Oliver Frauenfeld and Dr Rusty Feagin for their insightful guidance and support throughout the course of this research. I truly appreciate their constructive contribution. I also appreciate my colleagues at Texas A&M and friends here in USA, particularly Dr. Virginia Daughety, Dr. Ken Hilner and his wife Debbie Hilner, Dr. Shahriar Kibriya, Dr. Tom Jondiko, Raghu Modala, Ana Monzon, and Francine Rodriguez for their friendship and encouragement.

I would like to acknowledge the Spatial Sciences Laboratory at the Department of Ecosystem Sciences Management, the Climate Science Laboratory at the Department of Geography and the Texas A&M Supercomputing Facility for using their resources during my research. Likewise, I want to acknowledge the Borlaug Institute and the Conflict and Development Center for their financial contribution to my academic fees; the Asian-

Pacific-Economic-Community APEC's Climate Center, for providing me a training on "Climate Prediction". Special thanks to Dr. Edwin Price and his wife Hallethaire Price, the donor of the African Scholar scholarship for which I was awarded twice by the College of Agriculture and Life Science.

Finally, I am very grateful for all my parents in Benin Republic for all their prayers and moral support, may GOD bless them.

NOMENCLATURE

AI	Aridity Index
AMSR	Advanced Microwave Scanning Radiometer
AVHRR	Advanced Very High Resolution Radiometer
CV	Coefficient of Variation
DEM	Digital Elevation Model
DI	Disorder Index
DJF	December-January-February
DN	Digital Number
ENSO	El Niño and Southern Oscillation
EPA	Environmental Protection Agency
EVI	Enhanced Vegetation Index
FNEP	Full Network Estimated Precipitation
GCHN	Global Historical Climatological Network
GCM	General Circulation Model
GFDL	Geophysical Fluid Dynamics Laboratory
HUC	Hydrologic Unit Codes
IDW	Inverse Distance Weighted
IPCC	Intergovernmental Panel on Climate Change
IQR	Interquartile Range
JJA	June-July-August

LAI	Leaf Area Index
MAM	March-April-May
MJO	Madden-Julian Oscillation
NAM	North American Monsoon
NARCCAP	North American Regional Climate Change Assessment Program
NASA	National Aeronautics and Space Administration
NCDC	National Climatic Data Center
NDVI	Normalized Difference Vegetation Index
NHD	National Hydrography Datasets
NLCD	National Land Cover Database
NOAA	National Oceanic and Atmospheric Administration
PCA	Principal Component Analysis
PDF	Probability Density Functions
PET	Potential Evapotranspiration
RCM	Regional Climate Model
RMSE	Root Mean Squared Errors
SAVI	Soil Adjusted Vegetation Index
SMAP	Soil Moisture Active Passive
SON	September-October-November
UNEP	United Nations Environmental Program
USGS	United States Geological Survey
WRS-2	Worldwide Reference System 2

TABLE OF CONTENTS

Page

ABSTRACT ii

DEDICATION iv

ACKNOWLEDGMENTS v

NOMENCLATURE vii

TABLE OF CONTENTS ix

LIST OF FIGURES xii

LIST OF TABLES xvi

CHAPTER I INTRODUCTION 1

1.1. Background and justification 1
1.2. Objectives 4
1.3. Study region 5
1.4. Methodology 6
1.5. Relevance and limitations 8
1.6. Structure of the dissertation 10

CHAPTER II ANALYSIS OF WATERSHED TOPOGRAPHY EFFECTS ON SUMMER PRECIPITATION VARIABILITY 11

2.1. Synopsis 11
2.2. Introduction 12
2.3. Study area and importance of the JJA period 14
2.4. Data and methods 19
2.4.1. Elevation data 19
2.4.2. Precipitation data 19
2.4.3. Measurement of precipitation disorder 21
2.4.4. Investigating watershed topography effect on summer precipitation disorder 22
2.5. Results and discussion 23
2.5.1. Summer precipitation variability in time and space 23

2.5.2. Seasonal precipitation variability analysis at watershed level 26
2.5.3. Analyzing the influence of watershed topography on summer precipitation disorder.....29
2.5.3.1. Approach based on a linear regression.....29
2.5.3.2. Approach based on combined principal component and cluster analyses.....33
2.6. Conclusions 37

CHAPTER III VEGETATION RESPONSE TO PRECIPITATION ACROSS THE ARIDITY GRADIENT OF THE SOUTHWESTERN UNITED STATES 40

3.1. Synopsis 40
3.2. Introduction 41
3.3. Climate classification across the study domain.....43
3.4. Characteristics of vegetation types.....47
3.5. Methodology 48
3.5.1. Remote sensing and vegetation index data.....48
3.5.2. Precipitation data.....51
3.5.3. Vegetation dynamics metrics 51
3.6. Results 54
3.6.1. Analysis of trends in NDVI series.....54
3.6.2. Analysis of trends in precipitation series 56
3.6.3. Cross-correlation analysis between vegetation growth and precipitation.....58
3.6.4. Comparative analysis of vegetation response to precipitation characteristics 60
3.7. Discussion 62
3.8. Conclusions 64

CHAPTER IV RETRIEVING VEGETATION GROWTH PATTERNS FROM SOIL MOISTURE, PRECIPITATION AND TEMPERATURE USING ENTROPY 66

4.1. Synopsis 66
4.2. Introduction 67
4.3. Data and theory 70
4.3.1. Data and study domain.....70
4.3.2. Vegetation growth metrics 73
4.3.3. Description of joint entropy 73
4.4. Results and discussion.....77
4.4.1. Entropy scaling of system vegetation, soil moisture, precipitation, temperature.....77

4.4.2. Month-wise analysis of vegetation response to soil moisture, temperature and precipitation during the vegetation growth period 79
4.4.3. Entropy-based clustering of vegetation growing seasons 83
4.4.4. Estimate of vegetation growth from soil moisture, temperature, precipitation.....87
4.5. Synthesis and conclusions.....93

CHAPTER V IMPACT OF CLIMATE CHANGE ON PRECIPITATION

PATTERNS: A COMPARATIVE APPROACH 96

5.1. Synopsis 96
5.2. Introduction 97
5.3. Methodology 99
5.3.1. Data and study region.....99
5.3.2. Bias correction procedure.....103
5.3.3. Pooled analysis of changes in precipitation pattern 106
5.3.4. Non-parametric analysis of changes across precipitation ranges.109
5.3.4.1. Kernel estimate.....109
5.3.4.2. Trends analysis.....115
5.3.5. Probabilistic estimate of changes in precipitation patterns 118
5.4. Discussion of results.....128
5.5. Conclusions 131

CHAPTER VI CONCLUSION AND RECOMMENDATIONS FOR FUTURE

STUDIES 134

6.1. Conclusion.....134
6.2. Recommendations 137

REFERENCES.....138

LIST OF FIGURES

Page

Figure 1 Watersheds involved in the study spatial domain 6

Figure 2 Study region showing the watershed boundaries and the location of the rain gauge stations involved in the study 17

Figure 3 Comparison of time series of yearly JJA precipitation from 1895–2011 for Arkansas (AR), New Mexico (NM), and Texas (TX) 17

Figure 4 Average annual precipitation (mm) across the study area for the period 1895-2011 18

Figure 5 Average percentage of JJA precipitation across the study area for the period 1895–2011. 18

Figure 6 Entropy-based spatial distribution of DI of JJA number of precipitation events across the study area 25

Figure 7 Entropy-based spatial distribution of DI of JJA precipitation depth across the study area 25

Figure 8 Entropy based seasonal precipitation variability across the Lower Colorado watershed 27

Figure 9 Entropy based seasonal precipitation variability across Texas gulf watershed 28

Figure 10 Entropy based seasonal precipitation variability across the study domain's part of the Arkansas Red-White and Lower Mississippi watersheds 28

Figure 11 Entropy based seasonal precipitation variability across the U.S part of the Rio Grande watershed 29

Figure 12 Locations selected across the Lower Colorado watershed (right) and the related distribution of percentage terrain slope (left) 31

Figure 13 Scatter plot of the disorder index by the corresponding terrain slope (%) based on the 204 locations across the Lower Colorado watershed 32

Figure 14 Boxplots of z-score time series of number of JJA precipitation events (>13 mm) for 50 stations randomly selected, 25 from the flat region (left) and 25 from the hilly region (right) 35

Figure 15 Boxplots of z-score time series of JJA precipitation depth for 50 stations randomly selected, 25 from the flat region and 25 from the hilly region..... 35

Figure 16 Scree plot used for selecting the PCs. The bars describe each of the first 30 PCs and their corresponding eigenvalues. The curve describes the percentage of cumulative variance accounted for by the PCs..... 36

Figure 17 Spatial domains resulting from the cluster analysis performed on the selected PCs, identified based on JJA precipitation depth (right) and number (left) based on precipitation stations in the Lower Colorado watershed..... 36

Figure 18 Regions identified based on JJA precipitation depth and number of rainy days. Region A is the intersection of the two Regions 1 in Figure 17. Region B is the intersection of the two Regions 2 in Figure 17. Region C is the intersection of the two Regions..... 37

Figure 19 UNEP Aridity Index variability and selected satellite scene (footprint) locations across the study region..... 45

Figure 20 Trends in vegetation greenness as an indicator of primary productivity . (a) Deciduous forests, (b) shrublands, (c) pastures, and (d) grasslands. Group 1: moist region with AI≥0.65. Group 2: intermediate region with 0.50≤AI<0.65. Group 3: dry region with 55

Figure 21 Seasonality effect on Kendall's τ for four types of vegetation. Red lines represent 95% upper and lower significance limits for Kendall's τ. Group 1: moist region with AI≥0.65. Group 2: intermediate region with 0.50≤AI<0.65. Group 3: dry region with AI<0.50..... 56

Figure 22 Cross-correlations between NDVI for different types of vegetation and precipitation amounts. Correlations exceeding ±0.05 are statistically significant (95%-level). Group 1: moist region with AI≥0.65. Group 2: intermediate region with 0.50≤AI<0.65. Group 3: dry region with AI<0.50..... 59

Figure 23 Cross-correlation between NDVI as a measure of vegetation growth, and different precipitation variables: total precipitation, number of precipitation events > 13 mm, number of precipitation events > 3 mm. The dry region (group 3 with AI<0.50) was target as an example for this plot..... 61

Figure 24 The Texas Gulf watershed showing the location for the land-based stations considered for the study. The location of each satellite scene considered is represented by the corresponding footprint.....72

Figure 25 Schematic illustration of the joint entropy approach. H(P, SM, VI) stands for the three dimensional joint entropy including soil moisture and precipitation (P, SM) and vegetation growth index (VI). H(P, VI) and H(SM, VI) represent two dimensional joint entropies 76

Figure 26 Three dimensional entropy scaling of vegetation index VI, precipitation P, temperature T and soil moisture SM. Based on joint entropy computation.....78

Figure 27 Analysis of NDVI, NDVIRatio, NDVISlope responses to soil moisture, precipitation and temperature for each month of the vegetation growing season (May, June, July, August and September). 81

Figure 28 Probability Distribution of NDVI, soil moisture, temperature and cumulative precipitation. 82

Figure 29 Diagram presenting the nested statistical model used for vegetation index VI estimate. SM = Soil Moisture a 5 cm, P=Cumulative Precipitation, T=Mean Temperature, x=month of the growing season; a, b, c, d, e are the parameters identified base on a least square errors approach 91

Figure 30 Three dimensional scatter-plots of Vegetation Index (NDVI) as a function of coupled atmospheric variables [soil moisture (SM), precipitation (P) and temperature (T)].....92

Figure 31 Map of the Texas Gulf watershed showing the selected RCM3-GFDL grid cells (referred to by letters), the land-based precipitation stations considered for the bias correction and the annual precipitation gradient.....102

Figure 32 Boxplots of the percentage of changes in monthly precipitation series. Comparing the RCM3-GFDL precipitation series for historical (1971-2000) and future periods (2041-2070).....108

Figure 33 Comparing the probability density estimates for past (blue curve) and future (red curve) monthly precipitation during the seasons of DJF (December-January-February), MAM (March-April-May), JJA (June-July-August) and SON (September-October-November). We estimated the probability density using a Gaussian kernel. Example based on grids A, H, Q and X (figure 31).....112

Figure 34 Comparing the probability density estimates for past (blue curve) and future (red curve) monthly number of precipitation events (>3mm) during the seasons of DJF (December-January-February), MAM (March-April-May),

JJA (June-July-August) and SON (September-October-November). We estimated the probability density using a Gaussian kernel. Example based on grids A, H, Q and X. 113

Figure 35 Comparing the seasonal precipitation series between historical (1971-2000) and future (2041-2070) climate. 117

Figure 36 Probit estimate of monthly precipitation total (mm). A seasonal comparison of historical and future trends. 122

Figure 37 Probit estimate of monthly number of precipitation events (>3mm). A seasonal comparison of historical and future trends. 123

Figure 38 Estimate of seasonal changes in the probability of occurrence for the quartiles of monthly precipitation total. Q1, Q2 and Q3 represent the 1st, 2nd and 3rd quartiles, respectively 124

Figure 39 Estimates of seasonal changes in the probability of occurrence for the quartiles of monthly number of precipitation events (>3mm). Q1, Q2 and Q3 represent the 1st, 2nd and 3rd quartiles, respectively. 125

LIST OF TABLES

Page

Table 1 Frequency of JJA precipitation contribution to yearly totals for the period 1895–2011 19

Table 2 Summary statistics of the relationship between the entropy based Disorder Index and the percentage terrain slope 32

Table 3 Characteristics of selected satellite scenes across the study region; the Worldwide Reference System 2 (WRS-2) identifies the selected satellite scenes shown in Figure 19. Group 1: moist region with AI≥0.65. Group 2: intermediate region with 0.50≤ AI<0 46

Table 4 Summary of the Mann-Kendall test performed on the 23-year precipitation variables for each of the groups. Group 1: moist region with AI≥0.65, group 2: intermediate region with 0.50≤AI<0.65, and group 3: dry region with AI<0.50. The significant Kendall's τ values (95% level) are in bold. 57

Table 5 Temporal lags of vegetation response based on cross-correlation analysis; maximum correlation ρ(l,t) indicates the highest positive response of vegetation at lag l. Note that only the maximum values of positive cross-correlations are provided. Group 1: moist region with AI≥0.65, group 2: intermediate region with 0.50≤AI<0.65, and group 3: dry region with AI<0.50. The significant correlations (95% level) are in bold. 60

Table 6 Coefficients of determination based on the Pearson correlations computed pair-wise between cross-correlation series. The cross correlation series are computed between NDVI and precipitation variables (number of precipitation events >3 mm, events >13 mm) and total precipitation cross-correlation series. Group 1: moist region with AI≥0.65. Group 2: intermediate region with 0.50≤AI<0.65. Group 3: dry region with AI<0.50. 62

Table 7 Spatial characteristics of satellite scenes selected across the Texas Gulf watershed; the Worldwide Reference System 2 (WRS-2) identifies the selected satellite scenes shown in Figure 24. The geographic coordinates indicate the central point of each scene 72

Table 8 Illustration of a three-way contingency table employed to infer joint probability distribution. In this example we consider series X, Y and Z.

Each variable is categorized into 2 classes (n=2). Observations are cross-classified and the discrete PDF is estimated 76

Table 9 Summary of temperature series during the growing season; CV=coefficient of variation 82

Table 10 Clustering the growing season month using an entropy based stopping rule process. The number of group at each stage of the process is n. *Optimum value of the discriminating criteria indicating the optimum number of clusters. 86

Table 11 Bivariate fitting of deciduous forest and grassland's NDVI series. Analyses are conducted cluster-wise for each type of vegetation with each of the atmospheric variables (soil moisture SM, cumulative precipitation P, mean temperature T). Quadr.= quadratic, Corr.=correlation., Equ. = equation..... 90

Table 12 Summarizing the results of the nested model. VI = Vegetation Index; P = Precipitation; T=Temperature; SM = Soil Moisture; Corr. = correlation coefficient; RMSE = Root Mean Square Errors..... 90

Table 13 References corresponding to the selected grids in Texas Gulf watershed..... 103

Table 14 Estimated parameters for the bias correction algorithm [equation (5.2)]; example with grid cells A, H, Q and X are presented. 105

Table 15 Comparison of RCM3-GFDL's historical and future precipitation series in the Texas Gulf watershed. The monthly precipitation total and number of events (>3mm) are considered for seasons DJF, MAM, JJA and SON. μ= monthly mean, σ=standard deviation, and CV=coefficient of variation..... 107

Table 16 Binary bivariate contingency table obtained by pairing past P and future P' precipitation series. 114

Table 17 Values of $\chi^2 = N\phi^2$; estimating the degree of association between past *P* and future *P'* monthly precipitation total using RCM3-GFDL ensemble model simulations. The critical χ^2 for 1 degree of freedom and a p-value = 0.05 is 3.84 and the significant values are marked with "*". Q1, Q2 and Q3 represent the 1st, 2nd and 3rd quartiles. Example based on grids A, H, Q and X (figure 31). 114

Table 18 Values of $\chi^2 = N\phi^2$ estimating the degree of association between past P and future P' monthly number of precipitation events (>3mm) using RCM3-GFDL ensemble model simulations. The critical χ^2 for 1 degree of freedom and a p-value = 0.05 is 3.84 and the significant values are marked

with "*". Q1, Q2 and Q3 represent the 1st, 2nd and 3rd quartiles, respectively. Example based on grids A, H, Q and X (figure 31).....115

Table 19 Report of Mann-Kendall's non-parametric trend test. The table presents the Kendall's tau values computed with the seasonal precipitation series. 118

Table 20 Probit estimates of monthly precipitation total for grid cells. The table reports the probit parameters β0 and β1, as well as the model significance p. ** indicates a p-value <0.01; *indicates p-value <0.05. 126

Table 21 Probit estimates of monthly number of precipitation events (>3mm). The table reports the probit parameters β0 and β1, as well as the model significance p. ** indicates a p-value <0.01; *indicates p-value <0.05.....127

CHAPTER I

INTRODUCTION

1.1. Background and justification

The effects of climate change are increasingly manifested in many parts of the world with substantial impact on vegetation (Huntington, 2006; IPCC, 2012). However, there is still significant uncertainty related to future projections of climate. This sustains the debate on the plausible impact of climate change on precipitation patterns (Easterling et al., 2000; Salve et al., 2011). Yet, it is widely accepted that climate change will result into a disturbance in regular hydrological patterns. For instance, several studies have projected the future with high frequencies of extreme events, such as floods, droughts, extreme temperatures and desertification (Groisman et al., 2004; Overpeck et al., 2011; Wehner et al., 2011). During this last decade, questions regarding climate change impact in water resources were extensively addressed (Butcher et al., 2014; Lespinas et al., 2014). The complexity of the interactive relation between atmospheric variables and vegetation calls for a particular attention by water managers. In most regional watersheds, the vegetation is natural and spatially diversified. Often, there is a noticeable trend between precipitation type and vegetation density. It is common to find high density canopies in regions with high amounts of precipitation, while the vegetation density decreases as the precipitation amount decreases in space. Under the spectrum of climate change projected with high uncertainty, the sustainability of the natural balance of soil-water-atmosphere deserves a particular attention for its potential implications in water resources.

Although advances in climate models motivated several impact studies, consistent disparities are reported within models simulations (Butcher et al., 2014; O'Gorman, 2012). Increased extreme precipitation is consistently represented across climate models (O'Gorman, 2012). In the same geographic region, some models project increased inland precipitation amount, while other models project the opposite. This is an evidence of the uncertainty imbedded in the projections. Reviewing studies related to the impacts of climate change on hydrological processes, Whitehead et al., (2009) concluded with a consensual view of potential increase in temperature and significant change in precipitation. Maestre et al. (2012) asserted that the potential benefit of an increased precipitation amount would be likely cancelled by an increase in evapotranspiration related to the increase in temperature. Based on multimodels ensemble simulations, Seager et al. (2007) projected a consistent drier climate in the southwest United States for the 21st century.

The expected behavior of vegetation under climate change can hardly be dissociated from the subsequent precipitation variability. Precipitation and natural vegetation growth are customarily characterized by seasonal patterns. Several studies addressing climate change emphasize seasonality. The hydrological importance of different seasons vary more or less depending on the geographic location. Oreskes et al. (2010) identified summer precipitation as a critical component for water supply, agricultural productivity, and risk of floods and droughts. Physically based models are developed to project future biomass behavior. However, the difficulty to integrate the complex interactive relationships is likely to affect the reliability of these models. Changes

in precipitation amount and frequency are likely to affect vegetation dynamics differently. At the regional watershed scale, understanding the future behavior of the natural vegetation is critical, as changes in land cover have shown a significant impact on hydrologic processes (Yang et al., 2010). At a large watershed scale, the flux in water budget depends significantly on the vegetation. For that reason, it is critical to have a good understanding of how the vegetation would respond to future climate change and particularly to precipitation variability. Our study aims to emphasize seasonality and the need of understanding particularly in the southwest United States region.

Primarily, our research aims to investigate the seasonal precipitation variability and prospect the behavior of natural vegetation as a response to climate change. Actually, studies on precipitation and vegetation dynamics often employ data derived from satellite images. For instance, Schmidt and Karnieli (2000) concluded a meaningful correlation between the normalized difference vegetation index NDVI and precipitation series, but with a time lag. At a large scale, remote sensing approaches are reliable and practical for vegetation dynamics analysis (Le Maire et al., 2011; Roerink et al., 2003). Specifically we consider the NDVI series in the study.

The study describes the actual disorder in rainfall sequences and examines the effect on vegetation dynamics. The southwest U.S. is relatively dry compared to the rest of the country. Water resource depletion is a real issue in this area, which certainly needs more attention under climate change. At that point, our study aims to contribute for an improved understanding of the plausible vegetation behavior under perturbations related to climate change.

1.2. Objectives

This dissertation research investigates interactions between vegetation, precipitation and watershed morphology over the southwest region of the United States. The study considers the past real time vegetation response to precipitation variability and examines the plausible future implications in terrestrial hydrological processes. The primary objective is to improve the understanding of the plausible behavior of natural vegetation under the context of changes in precipitation patterns. Beside this primary motivation, we intend to consider remote sensing products and also examine the inclusion of soil moisture, and temperature. Explicitly, we address five specific research objectives which are:

i) Expound the spatial and temporal variability of precipitation using entropy based rainfall disorder index and analyze the influence of watershed topography across regional watersheds in the southwestern US.

ii) Use the last two decades of NDVI series to investigate trends of vegetation dynamics in relation to aridity gradient across the southwest US and evaluate statistical relationships with precipitation patterns.

iii) Investigate the inclusion of precipitation, soil moisture, and temperature in vegetation dynamics analysis using entropy theory; and propose an algorithm for retrieving the joint patterns.

iv) Explore the climate change impact on future precipitation scenarios, based on regional climate model simulations of future climate scenarios and propose a probabilistic approach for impact assessment.

v) Discuss the implications of results by emphasizing plausible changes in future hydrological processes.

1.3. Study region

We conduct the research on the monsoon region of the southwest United States. As indicated by Gutzler (2000), the monsoon region of the southern United States covers mainly the states of Arizona, New Mexico and Texas. However, the regional watersheds in those states span neighboring states as well. To have a better view of the interactive relations between watersheds and seasonal precipitation variability, it was essential to extend our study zone to six states of the southwest United States, including the states of Arizona, New Mexico, Texas, Oklahoma, Arkansas and Louisiana. In the selected region, the long-term availability of water represents a real issue. The study region is presented in the Figure 1. The regional watersheds involved in the study are: Lower Colorado basin (United States Geological Survey Hydrologic Unit Codes USGS-HUC 15), Rio Grande (HUC 13), Texas Gulf (HUC 12), Arkansas Red-White (HUC 11) and Lower Mississippi (HUC 08). The region offers a diversified range of vegetation, climate and watershed characteristics. The diversifications mentioned are used for analysis.

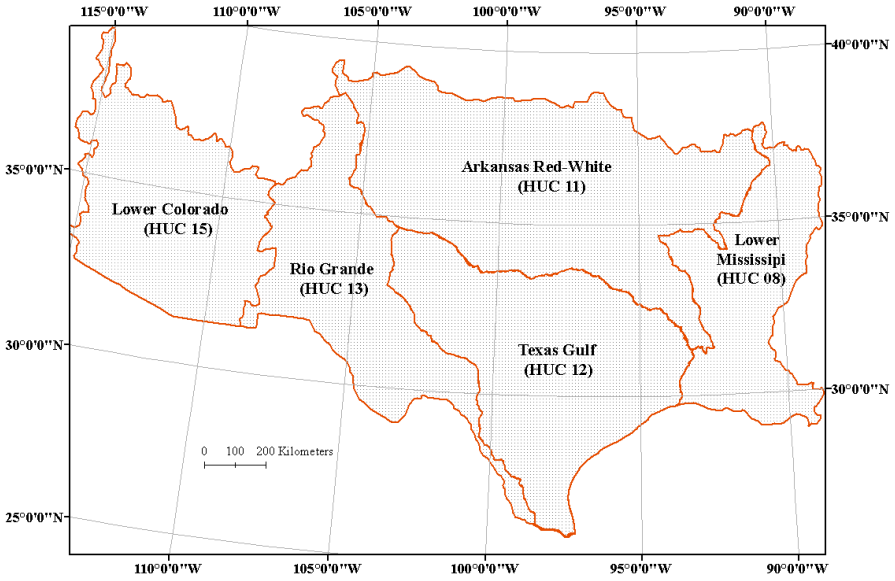

Figure 1 Watersheds involved in the study spatial domain

1.4. Methodology

We employ different methods for the accomplishment of each objective of the study. We present the details of approaches in each chapter. In sum, we present our methods in four sections in accordance with chapters as follow:

i) In the chapter II reporting the analysis of precipitation variability and the watershed topography effects, we employ the theory of information entropy developed by Shannon (1948). Shannon entropy is probabilistic and applies for random events and its applicability in water resources has been consistently

demonstrated (Kawachi et al., 2001; Singh, 1997b). Specifically, we select 360 land-based stations from the National Oceanic and Atmospheric Administration NOAA website (www.noaa.gov) and collect precipitation series over the period 1960 to 2010. We utilize the entropy disorder index (Mishra and Singh, 2009) and evaluate the magnitude of precipitation variability in time and space across the southwest US region.

ii) In chapter III, we investigate vegetation dynamics in relation to precipitation variability. We emphasize the plant growing season May-September and the aridity gradient in the southwest US. The NDVI series derived from the Advanced Very High Resolution Radiometer (AVHRR) composite images are reliable and relevant for long-term vegetation dynamic studies (Fontana et al., 2012). We collect the NDVI series for a 23 years period with 15 days temporal resolution for four vegetation types: deciduous forest, shrubland, pasture and grassland. We use the NDVI series along with precipitation series, and estimate the trends in vegetation dynamics.

iii) Chapter IV examines the inclusion of precipitation, soil moisture and temperature along with the NDVI series for vegetation dynamics analysis. We explore both marginal and joint effects using the entropy theory. Specifically, we employ the joint entropy and the entropy scaling approach. Foremost, we propose an entropy-based clustering method for seasonality analysis. Finally, we propose a mathematical algorithm to retrieve meaningful relationships between atmospheric variables and vegetation growth patterns.

iv) Chapter V expounds the magnitude of climate change impacts on plausible future precipitation scenarios. We evaluate a few customary statistical approaches in climate change assessment. We apply a probabilistic method for climate impact analysis. We address plausible changes in future precipitation seasonality using the North American Regional Climate Change Assessment Program's Regional Climate Model NARCCAP RCM3-GFDL simulations. We conduct the analysis at the watershed scale and develop maps of plausible changes in which we distinguish the perturbation for different quartile ranges.

1.5. Relevance and limitations

Water resources depletion is a real challenge in the southwest US. During the last century, the region has experienced an important population growth associated with an increase of irrigated lands. Subsequently, the pressure on water resources became a real concern and deficit in water budget was frequently reported. Unfortunately, the need for water is projected to increase in the future. Therefore, it is essential that future water demand are planned in advance in the region. Although wastewater reuse represents a realistic alternative for the future, a wise management of precipitation water may contribute significantly to mitigate future water issues. At the watershed level, vegetation represents a major biophysical component that plays a critical function in the hydrological processes. Under climate change, the difficulty for realistic water resources planning is exacerbated as consistent perturbations are projected in future precipitation patterns. For that reason, it is meaningful to anticipate the behavior of natural vegetation and evaluate

the plausible implications for water resources. The present dissertation research explores the mentioned aims. The results would contribute to the understanding of future changes in precipitation patterns and vegetation dynamics. The outcomes of the research would be globally beneficial for the society in the long term.

Nevertheless, it is important to report a few limitations related to the method employed in the study. The main limitation we noted is about the remote sensing products, which we employed. Regarding the use of remote sensing for vegetation dynamics assessment, Fisher (1994) stated clearly that crops with the same phenology behave as the same canopy in a spectral view. Alternatively, the use of Land Use Land Cover interface helped to differentiate vegetation types. However, it is important to know that Land Use Land Cover map is static and is not updated yearly. Another limitation is associated with the resolution of the satellite images used. Indeed we employed NOAA's AVHRR images which have a spatial resolution of 1.1 km. This means that the margin of error in vegetation assessment can be meaningful particularly in locations that do not have features spread continuously and homogeneously at a large scale. In other words, 1.1 km resolution pixels will generate the same DN for all the features that fall in the corresponding area without any distinction within the different features involved. However, the benefit of using 1.1 km resolution remote sensing images in vegetation assessment is justified by its long term availability and its capacity to be used for large scale studies, as it is the case in our research.

1.6. Structure of the dissertation

This dissertation reports the study through five chapters in accordance with the objectives stated above. The first chapter assesses the precipitation variability patterns and the related watershed topography effect. The second chapter examines the actual vegetation dynamics in precipitation and aridity gradient. The third chapter explores for a regional watershed and explores the joint effect of precipitation, temperature and soil moisture on vegetation dynamics. The fourth chapter evaluates the extent of climate change impact on precipitation. Finally, the fifth chapter recaps and discusses all the results under the scope of plausible changes on water resources.

CHAPTER II

ANALYSIS OF WATERSHED TOPOGRAPHY EFFECTS ON SUMMER PRECIPITATION VARIABILITY*

2.1. Synopsis

With climate change, precipitation variability is projected to increase. The present section investigates the potential interactions between watershed characteristics and precipitation variability. The watershed is considered as a functional unit that may affect seasonal precipitation. The study uses historical precipitation data from 370 meteorological stations over the last five decades, and digital elevation data from regional watersheds in the southwestern United States. This domain is part of the North American Monsoon (NAM) region, and the summer period (June-July-August, JJA) was considered. Based on an initial analysis for 1895–2011, the JJA precipitation accounts, on average, for 22–43% of the total annual precipitation, with higher percentages in the arid part of the region. The unique contribution of this research is that entropy theory is used to address precipitation variability in time and space. An entropy-based disorder index was computed for each station's precipitation record. The JJA total precipitation and number of precipitation events were considered in the analysis. The precipitation variability potentially induced by watershed topography is investigated using a spatial

*Reprint with permission from "Analysis of watershed topography effects on summer precipitation variability in the Southwestern United States" by D.C. Sohoulande Djebou, V.P. Singh, O.W. Frauenfeld, 2014. *Journal of Hydrology*, 511, 838-849, Copyright [2015] by Elsevier.

regionalization based on a combined principal component and cluster analysis. It is found that the disorder in precipitation total and number of events tends to be higher in arid regions. The spatial pattern shows that the entropy-based variability in precipitation amount and number of events gradually increases from east to west in the southwestern United States. Regarding the watershed topography influence on summer precipitation patterns, hilly reliefs have a stabilizing effect on seasonal precipitation variability in time and space. Results show the necessity to include watershed topography in global and regional climate model parameterizations.

2.2. Introduction

In recent decades, a number of studies have shown that the sustainability of the natural soil-water-atmosphere balance is threatened by climate change (Thomas et al., 2004; Junk et al., 2013). Several authors concur that an increase in sea surface temperature should induce an increase in atmospheric humidity (Huntington, 2006). However, there still remains a debate on whether, in general, climate change effects will result in decreased or increased precipitation amounts (Easterling et al., 2000; Salve et al., 2011). Nevertheless, it has been widely shown that climate change will result in higher frequencies of extreme events, such as floods, droughts, extreme temperatures, high precipitation variability, and desertification (e.g., Groisman et al., 2004; Overpeck et al., 2011; Wehner et al., 2011; IPCC 2012).

Under climate change, Oreskes et al. (2010) clearly designated summer precipitation as one of the critical components of climate affecting water supply,

agricultural productivity, and risk of floods and droughts. In contrast, projections from general circulation models (GCMs) are not consistent enough for decision making at the local level (Oreskes et al., 2010). Worldwide, studies addressing seasonal and annual precipitation variability have focused more attention on the large-scale causes, such as El Niño and Southern Oscillation (ENSO), the Madden-Julian Oscillation (MJO), and monsoons (Mohino et al., 2011; Giannini et al., 2003; Krishnamurthy and Shukla, 2000). At the regional scale, the potential forcing effect of the watershed topography has been less considered.

Changnon and Vogel (1981) indirectly indexed the role of watershed topography by indicating that, unlike cloud movement, storm movement is from upstream to downstream. It was suggested that the morphologic characteristics of the watershed were a driving factor. Along similar lines, using warm-season precipitation events to examine the spatial variability of precipitation around Oklahoma City, Hand and Shepherd (2009) showed a significant effect of urbanization on spatial precipitation variability. However, again, at regional watershed scales the forcing effects of watershed biophysical characteristics have been less reported. This should also be a critical improvement to climate model parameterizations, to improve simulations of future precipitation extremes under climate change (O'Gorman, 2012).

In addition to analyzing summer precipitation using an entropy/disorder approach, this study investigates how the watershed topography affects disorder of summer precipitation patterns in both time and space. Of all the interactions between precipitation and terrain complexity, the impact of orography is one of the most well-documented

phenomena (Roe, 2005). In the vicinity of large mountain barriers, orographic effects are so dominant that they sustain ecosystems and regional climates. Notable transitions can be observed between vegetation on the drier leeward flank, and the vegetation on the wetter windward side of mountain ranges (Roe, 2005). However, at the watershed scale and in regions which do not feature large mountain barriers, the terrain complexity's effects on precipitation patterns have not been documented. The aim of this study is to investigate the disorder in summer precipitation to uncover the potential interactions between summer precipitation variability and the physical watershed characteristics for regional watersheds in the southern United States.

2.3. Study area and importance of the JJA period

The spatial domain encompasses six states in the southwestern United States: Arizona, New Mexico, Texas, Oklahoma, Arkansas, and Louisiana. This region covers an area of 1,780,636 km^2 and represents more than 18% of the contiguous United States. As presented in Figure 2, the regional watersheds within this domain are the Lower Colorado basin (United States Geological Survey Hydrologic Unit Codes USGS-HUC 15), Rio Grande (HUC 13), Texas Gulf (HUC 12), Arkansas Red-White (HUC 11), and Lower Mississippi (HUC 08).

The focus of our study is on JJA, because a large portion of the precipitation in the course of the year occurs during this period. This was determined by computing the yearly percentage of JJA precipitation over the period 1895 to 2011. We used climate division monthly precipitation from the Full Network Estimated Precipitation (FNEP) dataset

(McRoberts and Nielsen-Gammon, 2011), released by the Atmospheric Sciences Department at Texas A&M University. Based on an equal-area weighted average among the climate divisions, statewide monthly and yearly precipitation values were computed for 1895–2011. Aggregating the yearly JJA precipitation amount, we derived the yearly percentage for each state over the entire period.

We found that JJA seasonal precipitation accounts for a significant portion of the yearly total precipitation in the region. By way of example, Figure 3 represents a time series of the yearly percentage of JJA precipitation amount over the period 1895 to 2011 for Arkansas, Texas, and New Mexico. During 1895–2011, the overall average yearly percentages of JJA precipitation amounts varied from 22 to 43% in the region. Figure 4 presents the spatial distribution of long-term average annual precipitation totals and Figure 5 presents the average percentage of yearly JJA precipitation amounts. Analyzing these two maps, it is evident that the contribution of the JJA precipitation to the yearly precipitation increases, moving westward from humid to arid regions. In addition, Table 1 shows the frequencies of JJA percentages of yearly precipitation in each state. Over the 117-year time period (1895 to 2011), the JJA precipitation contribution is very high in the far western and arid states (New Mexico, Arizona), while it decreases in the eastern and humid states (Louisiana, Arkansas). Meanwhile, Texas and Oklahoma show more transitional characteristics.

The importance of JJA precipitation in this region is due to the North American Monsoon (NAM). The NAM is a yearly phenomenon that controls the warm season climate over North America and causes summer precipitation in the southwestern regions

(Higgins and Shi, 2001). The moisture originating from the Gulf of Mexico and Gulf of California is driven by the NAM over the desert areas including the states of Arizona and New Mexico (Higgins et. al, 1997). Reviewing the southwestern United States climate, Sheppard et al. (2002) indicated that the July-August-September precipitation in Arizona and New Mexico account for 50% of the annual precipitation. The onset date of NAM is variable and the July–August period is considered to be the mature phase of the NAM. Our choice of the JJA period thus includes this mature phase of the NAM as well as the warmer summer period. Heat and humidity are two main components that control biophysical processes, such as plant growth and evapotranspiration. In regard to the socioeconomic importance of farming in the southwestern United States, the JJA period is of great importance for summer precipitation studies.

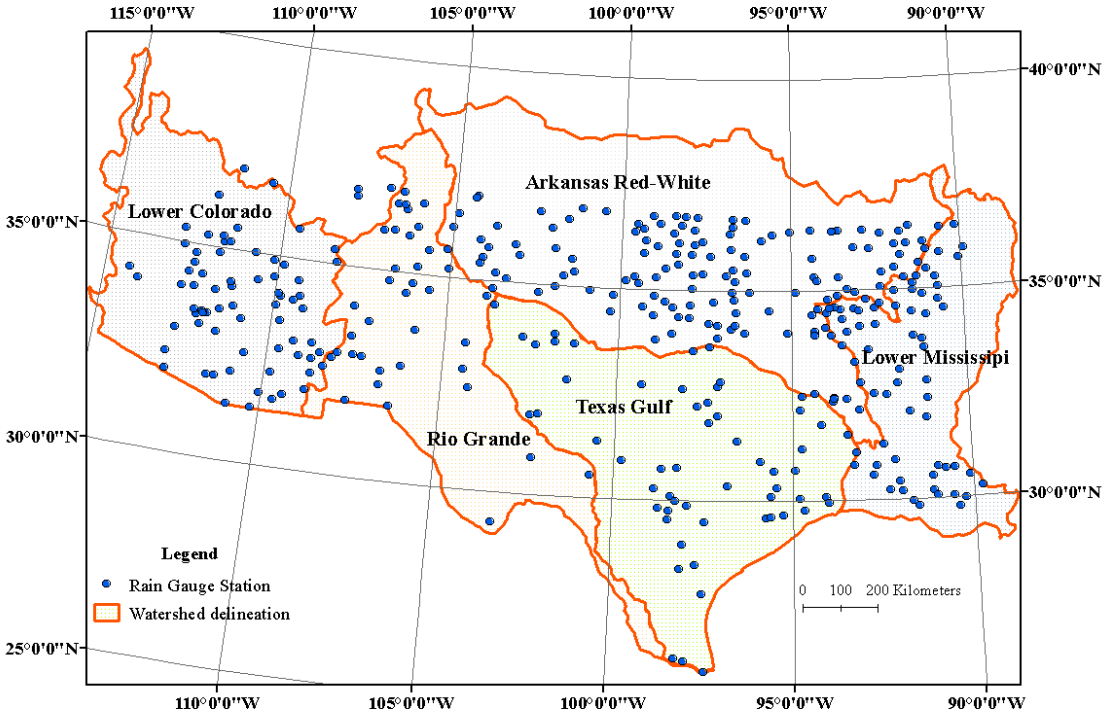

Figure 2 Study region showing the watershed boundaries and the location of the rain gauge stations involved in the study

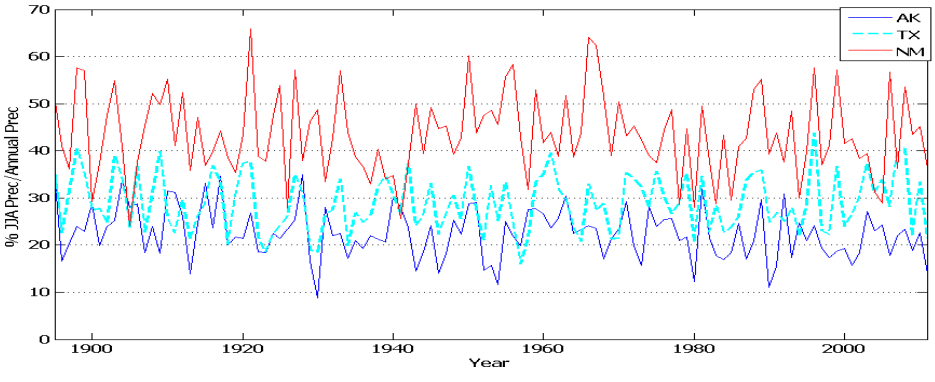

Figure 3 Comparison of time series of yearly JJA precipitation from 1895–2011 for Arkansas (AR), New Mexico (NM), and Texas (TX)

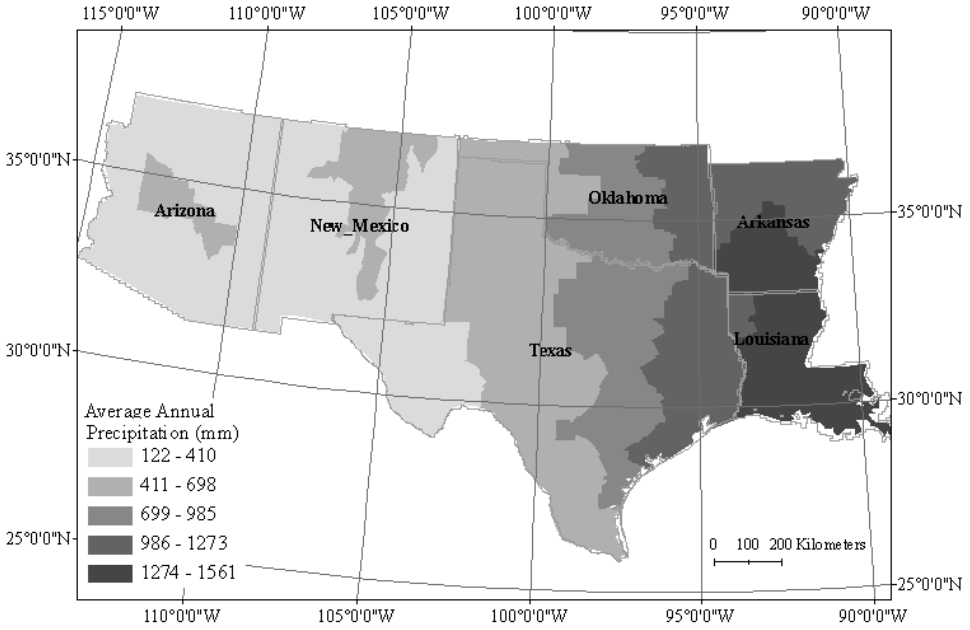

Figure 4 Average annual precipitation (mm) across the study area for the period 1895–2011

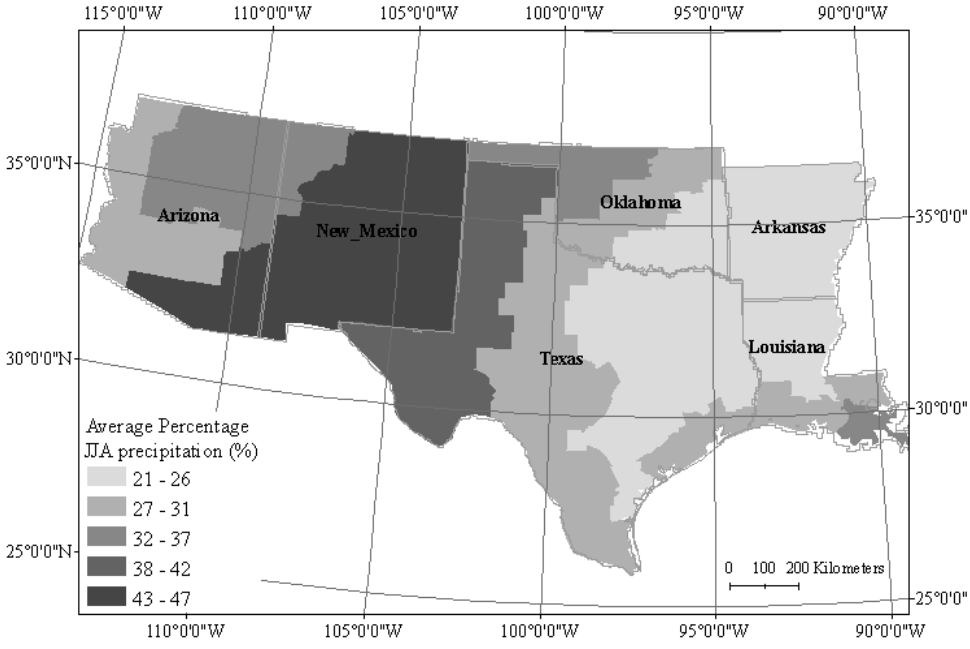

Figure 5 Average percentage of JJA precipitation across the study area for the period 1895–2011.

Table 1 Frequency of JJA precipitation contribution to yearly totals for the period 1895–2011

%JJA	New Mexico	Arizona	Texas	Oklahoma	Louisiana	Arkansas
>50%	24%	6%	0%	2%	0%	0%
>40%	63%	21%	5%	11%	0%	0%
>30%	92%	60%	44%	25%	28%	11%

2.4. Data and methods

2.4.1. Elevation data

For each watershed, we used a digital elevation model (DEM) with 30 m resolution. We obtained the National Hydrography Datasets (NHDPlus) DEM from the Horizon System Corporation website (www.horizon-systems.com). NHDPlus was developed with the assistance of the United States Environmental Protection Agency (EPA) in collaboration with the United States Geological Survey (USGS). Based on the DEM, watershed slopes were computed to differentiate hilly terrains from plains. In particular, the variability in slope across the watersheds was determined using a 5% slope as a threshold. This threshold was chosen based on previous studies involving the Lower Colorado watershed (e.g., Wang et al., 2009; Ahmad et al., 2010), which reported that the spatial contrast in topography is best resolved by applying a 5% threshold.

2.4.2. Precipitation data

The spatial domain is characterized by a sharp east-west precipitation gradient. Studying summer precipitation in the monsoon region of the southwestern United States,

which coincides with our study domain, Gutzler (2000) considered precipitation data for the months of July and August. Here, we consider monthly precipitation amount and number of wet days with precipitation greater than 13 mm (i.e. 0.5 inches) for JJA. The correlation between the rain event days and monthly precipitation totals was higher when the threshold for the rain event days definition was set lower. Across the precipitation stations considered, on average the number of rain event days with precipitation depth >3 mm (0.1 inches) explained more than 72% of the variance in JJA total precipitation time series , while this variance was less than 58% for depth >13 mm. However, defining rain event days as days with precipitation >13 mm reduces the potential collinearity inference on the robustness of the study.

Precipitation data for the last five decades, 1960–2010, were used from 370 precipitation stations over the selected watersheds (Figure 2). We collected the data from the National Oceanic and Atmospheric Administration (NOAA) National Climatic Data Center (NCDC) (http://www.ncdc.noaa.gov). NOAA's NCDC provides historical precipitation data from land based stations. Of those 370 stations, 62 are in Arizona, 71 in Arkansas, 36 in Louisiana, 59 in New Mexico, 69 in Oklahoma, and 73 in Texas. A number of criteria were defined for selecting precipitation stations. First, we only considered stations with historical data for the period 1960 to 2010. Note that from the thousands of operating rain gauge stations, only a low percentage of them met this criterion. As a second criterion, we only retained rain stations having less than 5% of missing data. We used the inverse distance weighted (IDW) method (Di Luzio et al., 2008), based on the three nearest stations to in-fill missing values.

2.4.3. Measurement of precipitation disorder

Various indices and statistics have been used to analyze the variability of biophysical phenomena in time and space. Among them, approaches based on variance are common. Variance is an expression of the dispersion from the mean. However, variance is unit based and is amplified, depending on the scale of measurement. The unit issue can be corrected using the coefficient of variation (CV), which is the ratio of the standard deviation (σ) to the mean (μ), $CV = \sigma / \mu$. The coefficient of variation can be viewed as the rate of departure from the mean. In the case of seasonal precipitation the magnitude depends on the spatial location. Two precipitation stations may have records following the same probability distribution but they may have different statistics because the range of precipitation totals is high at one station and low at another. Thus, it may be problematic to compare an arid region to a humid region using standard deviation for assessing variability in precipitation records. However, there are unique approaches to overcome these shortcomings in quantifying precipitation variability that are not biased by the spatial heterogeneity of precipitation. One of these approaches is based on Shannon entropy, which has been successfully used in a number of studies (e.g., Kawachi et al., 2001; Singh, 1997).

The entropy theory, developed by Shannon (1948), is probabilistic and therefore applies to random events. Two locations with precipitation data of similar probability distributions will have the same entropy value. At each rain gage *k*, the historical precipitation data were binned in order to derive a probability distribution. The Shannon entropy H_k was then computed using the formula:

$$H_k = -\sum_{i=1}^{n} p_i Log_2 p_i \quad (1)$$

where H_k has units in bit, N is the number of discrete intervals for events (precipitation amount, number of rainy days), and p_i is the probability associated with bin i. While assessing the entropy based precipitation variability over the state of Texas, Mishra et al. (2009) used a Disorder Index (*DI*), which is the difference between the maximum entropy value H_{max} and the computed entropy value at a specific rain gage k (H_k):

$$DI_k = H_{\max} - H_k = Log_2 N - \sum_{i=1}^{n} p_i Log_2 p_i \quad (2)$$

The maximum entropy here is the entropy value of a scenario of uniform precipitation distribution (Mishra et al., 2009). The *DI* is a measurement of the difference between the maximum entropy and the actual entropy. A lower entropy value is equivalent to a bigger difference, or *DI*, which indicates higher variability.

We also employ this DI approach and, from the entropy based disorder indices generated for the stations, produce maps of the precipitation variability distribution across our domain. Combined maps of precipitation disorder and terrain slope were constructed for each watershed and comparative analyses are then employed.

2.4.4. Investigating watershed topography effect on summer precipitation disorder

We compare how precipitation disorder varies across hilly versus flat terrains to infer the potential role of watershed topography. We focus on the lower Colorado basin, as it presents a clear differentiation between these two reliefs (hilly/plain). The central part of the Lower Colorado River basin, which also encompasses central Arizona, is particularly hilly and was therefore also considered by Wang et al. (2009) as part of the

intermountain region of the Western United States. Using a threshold of 5% slope, we produce a map where hilly regions are differentiated from the plains regions and the intermountain region of the watershed (Wang et al. 2009).

To assess the role of watershed topography on the disorder in summer precipitation patterns, we first selected transects of 2 km regions across the watershed. The averaged slope and entropy-based disorder indices were derived for each region and analyzed via regression analysis. We then used spatial regionalization based on principal component analysis (PCA). PCA is widely used in climate regionalization analyses (e.g., White et al., 1991; Comrie and Glenn, 1998; Frauenfeld and Davis, 2002; Gutzler, 2004). Our purpose is to identify similar topographic regions in the Lower Colorado basin based on the disorder in summer precipitation records. Indeed, in the western U.S region, the topography influences warm season precipitation, particularly in terms of precipitation totals (Leung et al., 2003).

2.5. Results and discussion

2.5.1. Summer precipitation variability in time and space

During the period 1960 to 2010, monthly summer precipitation totals and monthly number of days with precipitation events greater than 13 mm were considered at each station. Entropy values were then derived for the JJA monthly records. Figure 6 presents the spatial distribution of disorder in summer precipitation events across the study region.

Theoretically, the maximum value of entropy corresponds to a scenario of uniform probability distribution (Mishra et al., 2009) of summer precipitation records. Therefore,

the higher the precipitation variability at a station, the less its entropy value will be. Here we use the entropy-based DI.

Figure 6 shows a notable pattern of increasing variability as we move from east to west. Relating Figure 6 to Figure 5, we observe that disorder in summer precipitation, in terms of the number of events, tends to be higher in arid regions when compared to humid regions. However, we still note some isolated patches indicating discontinuity in the spatial variability. These patterns can potentially be explained by the biophysical characteristics of the watershed, which interact with the precipitation variability. Figure 7 illustrates the variability in the JJA precipitation totals across the region for 1960–2010. Summer precipitation totals exhibit more disorder moving from north to south. This may suggest that variability in precipitation totals is more susceptible to regional climate forcing, rather than local factors such as watershed characteristics, as we emphasized the above precipitation variability.

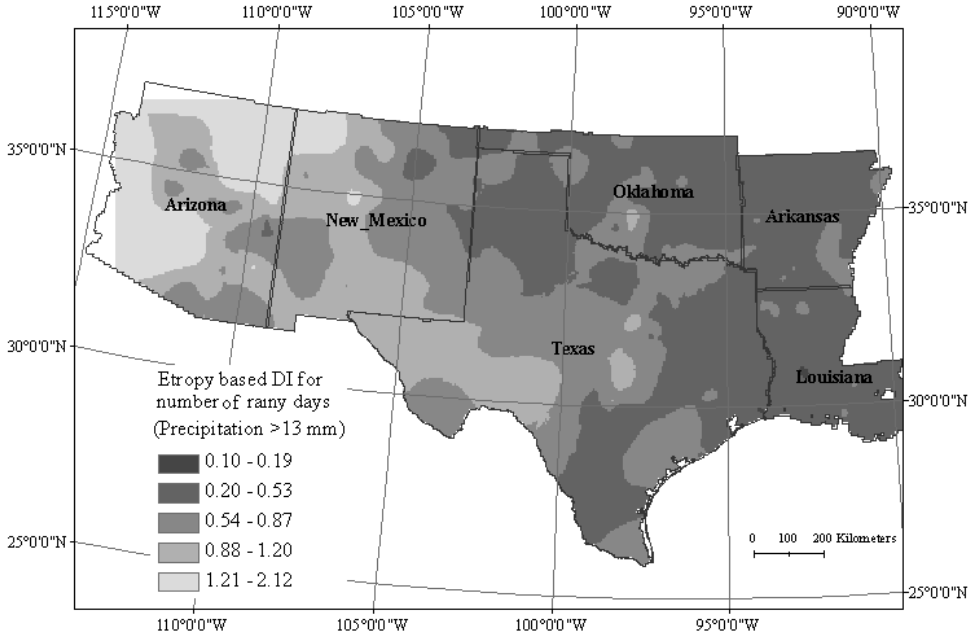

Figure 6 Entropy-based spatial distribution of DI of JJA number of precipitation events across the study area

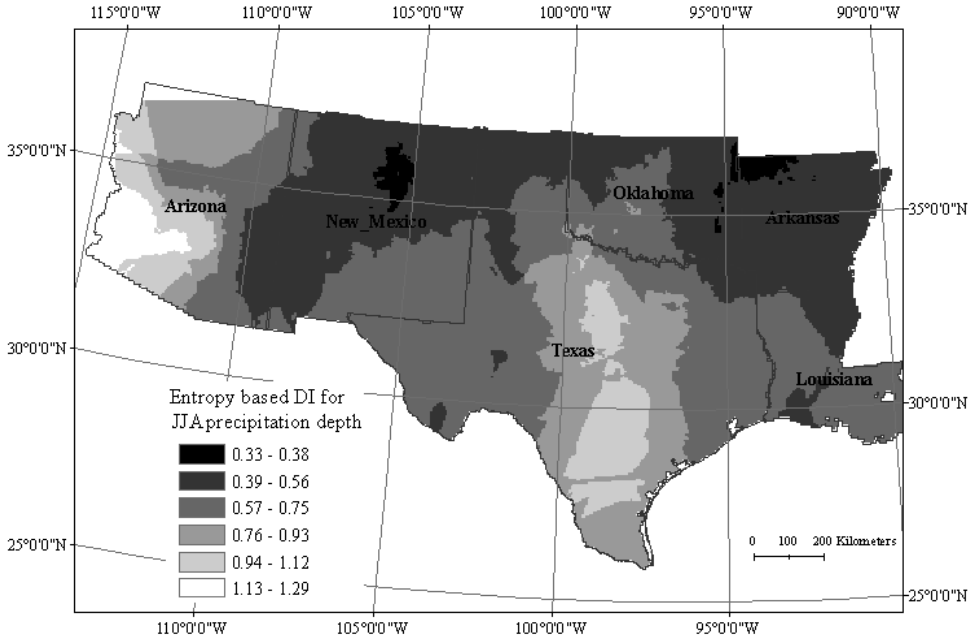

Figure 7 Entropy-based spatial distribution of DI of JJA precipitation depth across the study area

2.5.2. Seasonal precipitation variability analysis at watershed level

Of all the watersheds in this study, the Lower Colorado exhibits a very pronounced relief. Many locations with high slopes (>5%) are evident, particularly in the central part of the watershed, extending from east to west (Figure 8). When comparing the variability in seasonal precipitation events (precipitation depth >13 mm), a sharp gradient in variability is evident within the region of high slopes. Similarly, the seasonal variability in terms of precipitation totals shows contours with sharp gradients around the regions with high slopes.

In general, the variability in the seasonal precipitation characteristics (totals and number of events) decreases (increasing entropy value) as we move from low-slope regions to high-slope regions. This suggests that the seasonal precipitation characteristics tend to be steadier in regions with high relief compared to flat regions. Note that in the Texas Gulf (Figure 9), the combined Arkansas Red-White and Lower Mississippi (Figure 10), and the Rio Grande (Figure 11) watersheds, high slopes (>5%) were not very frequent, i.e. these watersheds are relatively flat. However, similar patterns observed in the Lower Colorado's seasonal precipitation characteristics are evident based on the entropy contours in the Texas Gulf (Figure 9) and the Rio Grande watersheds (Figure 11). We note some breaks in the continuity of the entropy contours, which are located in the regions of the watersheds having high slopes.

The results suggest a potential influence of watershed topography on the JJA precipitation variability. The orographic influence on precipitation is well known. Particularly in the Southwest United States, which includes our study region, Sheppard et

al. (2002) related the orographic effect with annual precipitation amounts. However, the watershed topography effect on the disorder in precipitation needs to be further clarified.

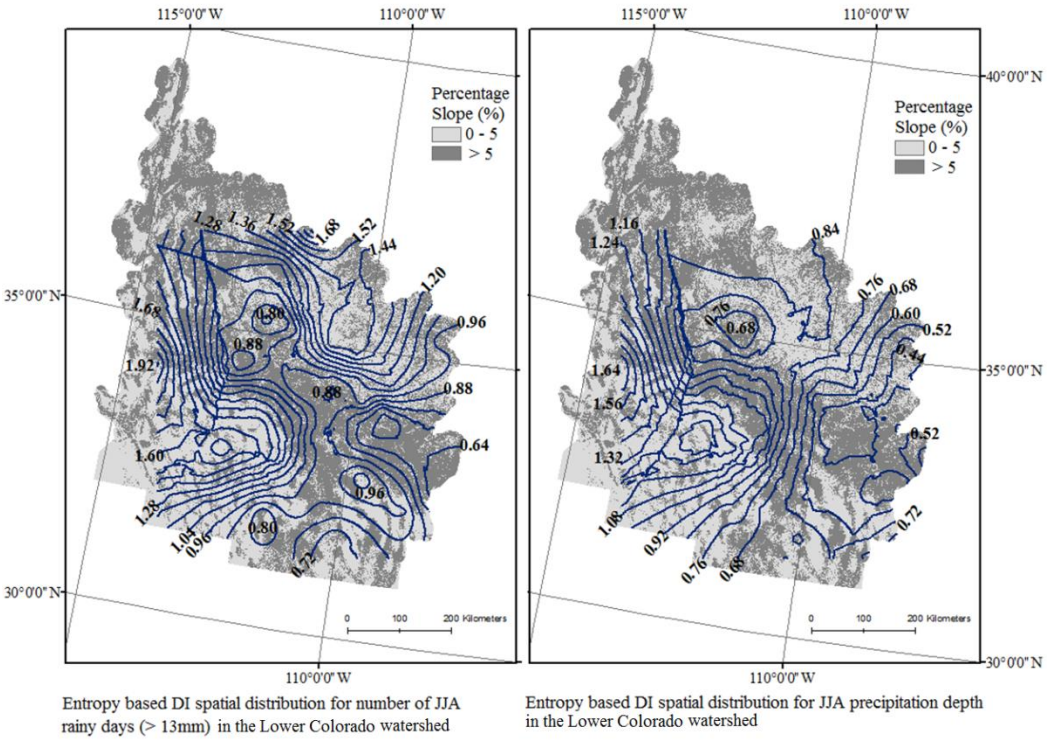

Figure 8 Entropy based seasonal precipitation variability across the Lower Colorado watershed

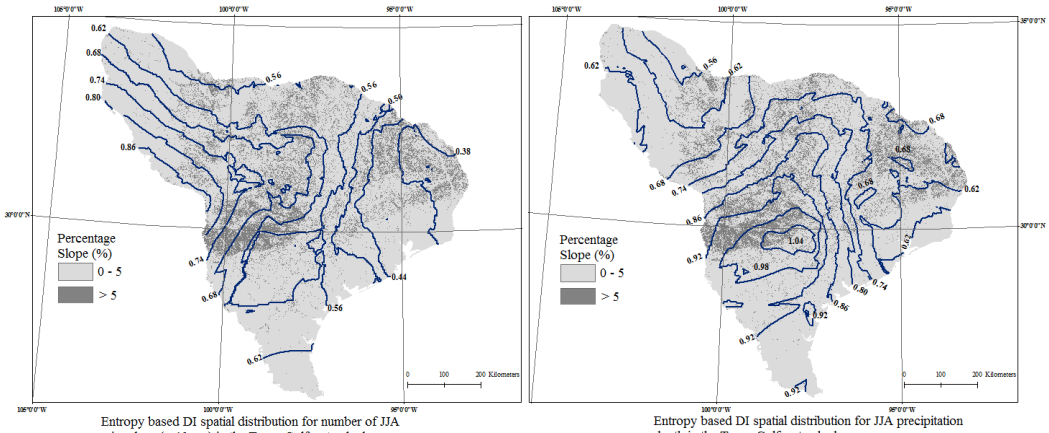

Figure 9 Entropy based seasonal precipitation variability across Texas gulf watershed

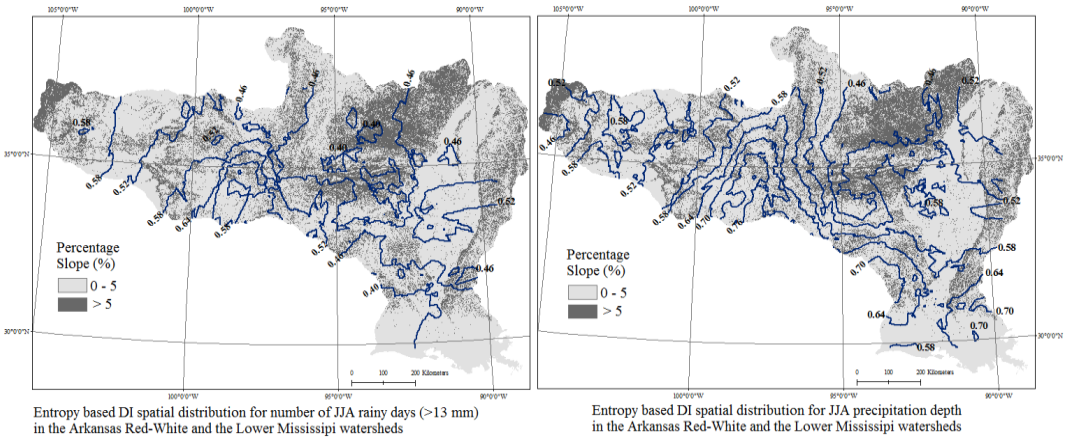

Figure 10 Entropy based seasonal precipitation variability across the study domain's part of the Arkansas Red-White and Lower Mississippi watersheds

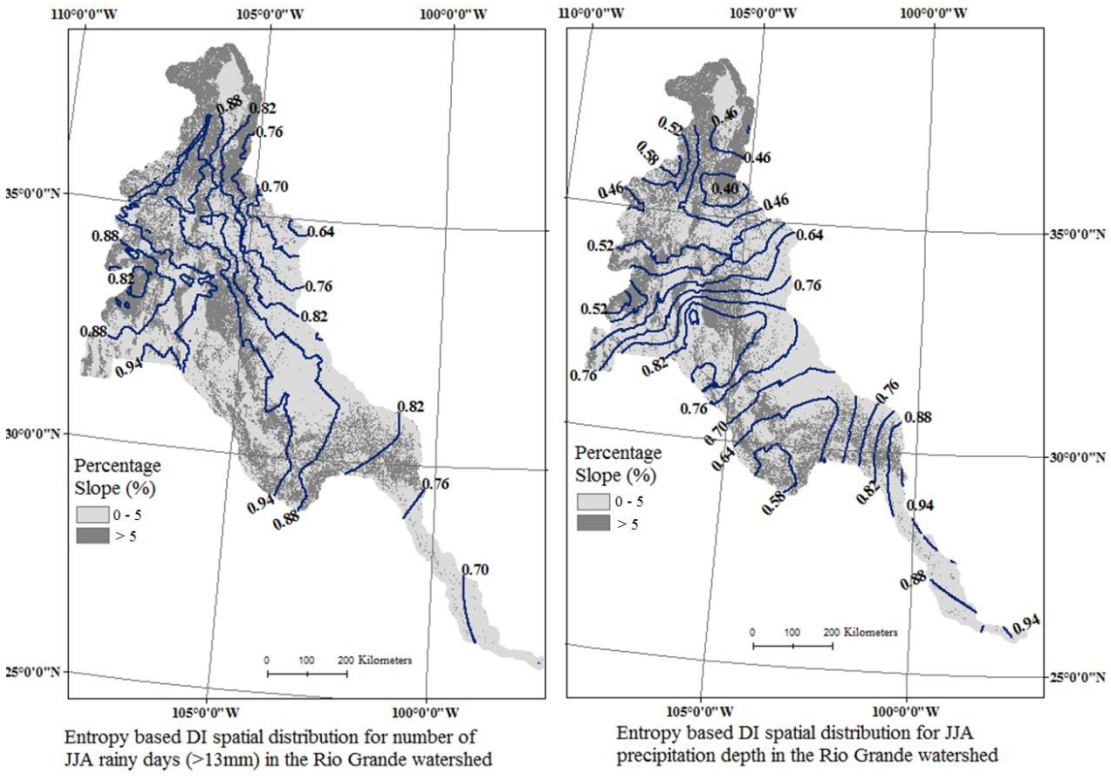

Figure 11 Entropy based seasonal precipitation variability across the U.S part of the Rio Grande watershed

2.5.3. Analyzing the influence of watershed topography on summer precipitation disorder

2.5.3.1. Approach based on a linear regression

Across the Lower Colorado watershed, a total of 160 locations were selected along transects presented in Figure 12. Each location represents a 2 km diameter region associated with a terrain slope and an entropy-based DI value. Consecutive locations were selected 5 km apart in order to avoid overlap along transects. For individual locations, the corresponding DI and slope values were derived by averaging the values of all the pixels

within its 2 km region. The slope distribution across the Lower Colorado (Figure 12) confirms the terrain contrast in the watershed topography.

The scatter plots of JJA precipitation DI by the percentage terrain slope (Figure 13) show decreasing trends for both the JJA precipitation depth and the number of events. The computed Pearson correlation coefficients between the terrain slope and the JJA precipitation's DI ($r=-0.52$ for number of rainy days, $r=-0.44$ for precipitation depth) are significant at the 99% level. These values are also similar to Spearman's rank correlation coefficient (Table 2). The negative correlation coefficients indicate that the DI decreases when the terrain slope increases. This confirms the trends observed in section 4.2, which indicate that the disorder in precipitation patterns tends to decrease in hilly regions compared to flat areas. Furthermore, the coefficients of determination indicate that even in the absence of major orographic forcing such as from mountain barriers, the terrain variability still accounts for 27% of the variance of JJA number of events' DI ($r^2=0.27$), while it accounts for 19% of the variance in JJA precipitation total's DI ($r^2=0.19$).

The computed mean absolute error (MAE) and root mean square error (RMSE) seem to indicate a better estimation of the JJA precipitation total's DI. In contrast, a higher correlation is obtained between terrain slope and JJA's rainy days' DI. In sum, the statistics computed based on the linear relationship between the JJA precipitation disorder pattern and the watershed slope strengthen the assumption of watershed topography influence on precipitation variability patterns at the watershed scale.

McLaughlin (1995) described a part of the Lower Colorado basin as characterized by several small and isolated ranges of mountains that sustain perennial and diversified

vegetation. These ranges of mountains are reported to be separated by plains with deserts and desert grasslands. Yet the spatial contrast reported in the vegetation may reflect local climatic responses. Through this study, the observed trends in precipitation variability in relation with terrain characteristics (flat or hilly) could be indirectly justified based on local vegetation structure. Furthermore, McLaughlin (1995) showed the existence of a positive and strong relationship between the flora diversity and the terrain elevation.

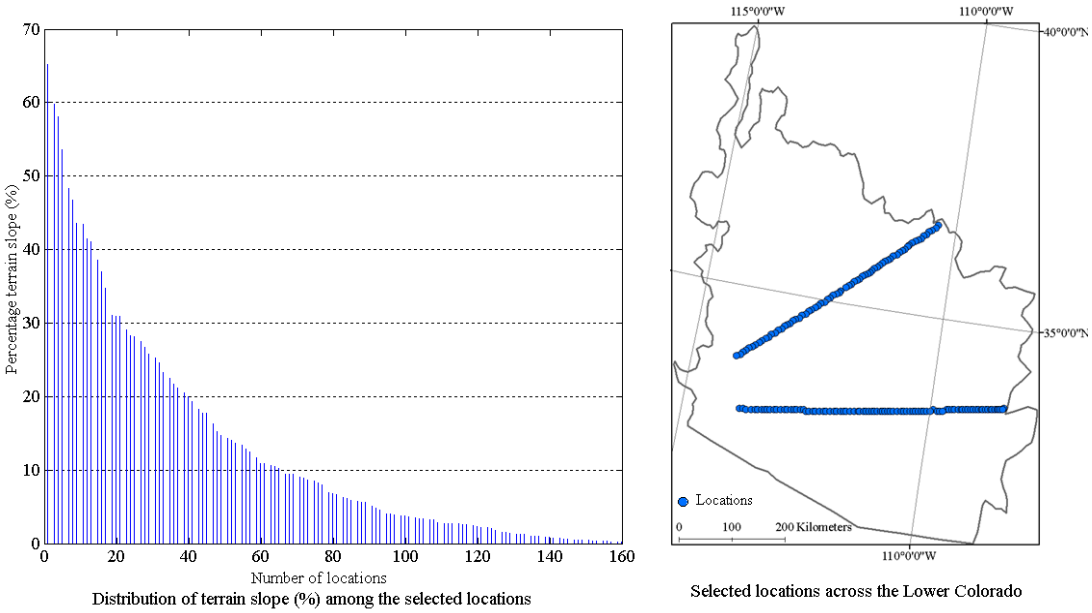

Figure 12 Locations selected across the Lower Colorado watershed (right) and the related distribution of percentage terrain slope (left)

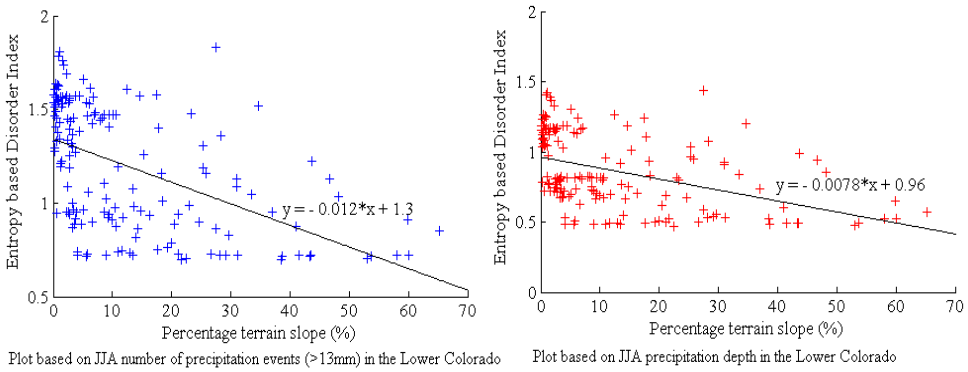

Figure 13 Scatter plot of the disorder index by the corresponding terrain slope (%) based on the 204 locations across the Lower Colorado watershed

Table 2 Summary statistics of the relationship between the entropy based Disorder Index and the percentage terrain slope

Statistics	Formula	JJA number of precipitation event	JJA Precipitation total
DI's Mean (μ)	$\mu = n^{-1} * \sum_{i=1}^{n} DI_i$	1.19	0.86
DI's Coefficient of variation (CV)	$CV = \sigma / \mu$	0.28	0.31
Linear regression	$DI_i^{'} = f(Slope)$	$DI_i^{'} =$ 1.3-0.012 *Slope	$DI_i^{'} =$ 0.96-0.0078 *Slope
Pearson Correlation (r)	$r = \frac{\sum_{i=1}^{n}(DI_i - \overline{DI})(Slope_i - \overline{Slope})}{\sqrt{\sum_{i=1}^{n}(DI_i - \overline{DI})^2 \sum_{i=1}^{n}(Slope_i - \overline{Slope})^2}}$	- 0.52*	- 0.44*
Spearman's rank correlation	$r_S = 1 - \frac{6\sum_{i=1}^{n} d_i^2}{n^3 - n}$	-0.59	-0.52
Root Mean Square Error ($RMSE$)	$RMSE = \left[n^{-1} \sum_{i=1}^{n} \left\| DI_i^{'} - DI_i \right\|^2 \right]^{1/2}$	0.29	0.24
Mean Absolute Error (MAE)	$MAE = \left[n^{-1} \sum_{i=1}^{n} \left\| DI_i^{'} - DI_i \right\| \right]$	0.25	0.21

*Coefficient of Correlation is significant at $p < 0.01$

2.5.3.2. Approach based on combined principal component and cluster analyses

In this part of the study, we focus on the Lower Colorado basin and its 74 precipitation stations. To examine precipitation anomalies across the watershed, we created boxplots on the z-scores of 50 stations randomly selected from the two regions: 25 stations in the hilly region and 25 in the plain region. For each station precipitation time series, outliers were defined based on the interquartile range (IQR). A threshold was defined around the first quartile (Q_1) and the third quartile (Q_3) where: $Minimum = Q_1 - 1.5 * IQR$, and $Maxmum = Q_1 + 1.5 * IQR$. All precipitation records falling outside this range are considered as outliers. Overall, we observe a much greater number of outliers (noted as "+" signs) in the plains region (Figure 14 and Figure 15).

Next, we used principal component analysis (PCA) with an oblique rotation. White et al. (1991) indicated that the oblique rotation is useful for loading of factor variance purposes, and creates a balance between the variance loaded in the PCs. At each station, the precipitation values were standardized into z-scores. Hence, PCA was performed on the 74 z-score time series. For the PC selection, we considered PCs with eigenvalues greater than one (Kaiser, 1958) and thus retained 4 PCs based also on the scree plots represented in Figure 16. Using the first 4 PCs in each case (JJA precipitation totals and number of rainy days), oblique rotation was performed. For the JJA period, the 4 PCs explained 75% and 59% of the variance in precipitation totals and number of rainy days, respectively (Figure 16). In PCA-based regionalization, the PC coefficients are commonly used for factor grouping. To identify similar regions, we performed cluster analysis on the PCs. The use of cluster analysis in PCA based spatial regionalization is well described

(Baeriswyl and Rebetez, 1997; Pecher et al., 2013). Of the existing cluster analysis types, the hierarchical clustering algorithm is best suited for this type of study. Hence, hierarchical clustering was performed to group stations into four homogenous regions, based on the PC loading factors. From each of the JJA precipitation variables we were able to identify four main regions (Figure 17). For both precipitation amount and number of rain event days, precipitation regions 1 and 3 are dominated by more hilly terrain (Figure 17). Meanwhile, precipitation region 2, in both cases of JJA precipitation variables, extends southeastward and corresponds in large part to the flat terrain. Similarly, precipitation region 4 is mainly characterized by flat terrain. Combining these two clustering results, we obtain an idealized classification of terrain as shown in Figure 18.

Results from the combined PC and cluster analyses show a general correspondence between terrain topography and rainfall patterns. We note from Figure 17 and Figure 18 that each cluster has grouped precipitation stations into regions with similar geographic characteristics (hilly versus plain). We also infer that the analysis performed on JJA precipitation series captures the variability and correspondence with the topography. In other words, these results indicate that the different regions identified based on the JJA precipitation anomalies are characterized by different topographies. We thus indirectly conclude that there is a topographic influence on the JJA precipitation anomalies. Consequently, it would be reasonable to consider the role of the watershed topography in global and regional climate model parameterizations.

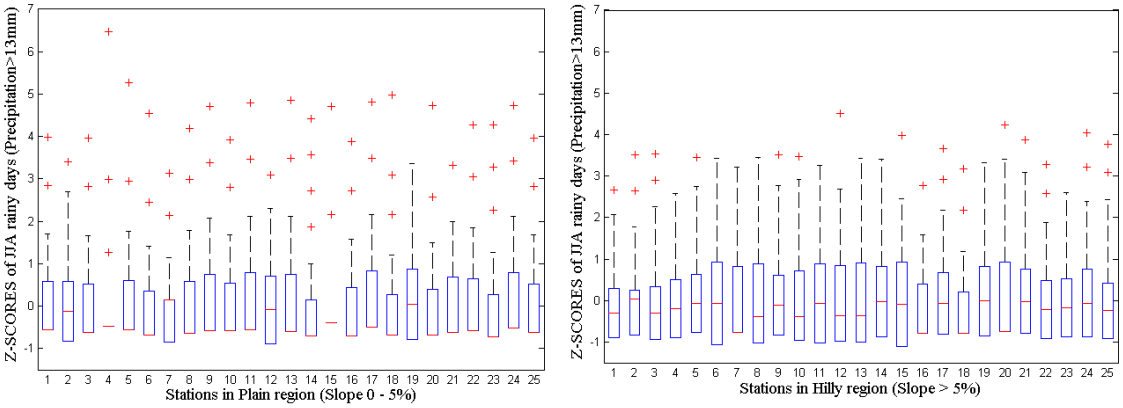

Figure 14 Boxplots of z-score time series of number of JJA precipitation events (>13 mm) for 50 stations randomly selected, 25 from the flat region (left) and 25 from the hilly region (right)

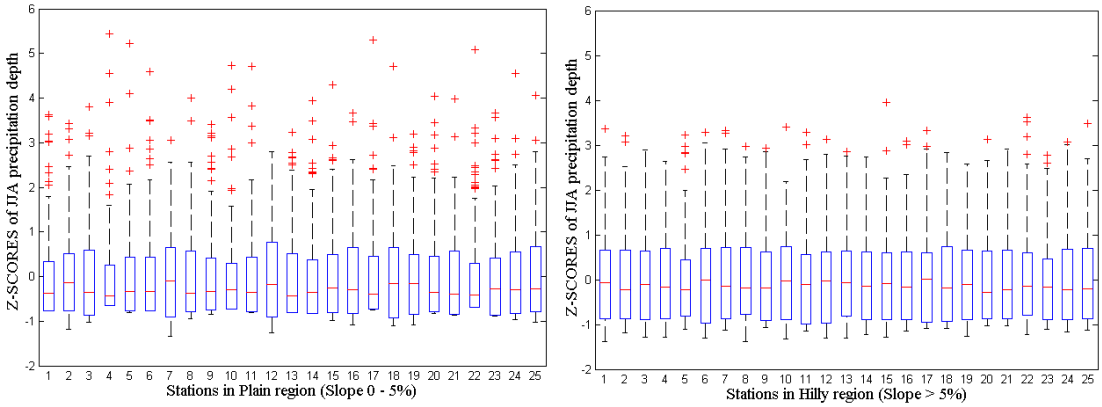

Figure 15 Boxplots of z-score time series of JJA precipitation depth for 50 stations randomly selected, 25 from the flat region (left) and 25 from the hilly region (right)

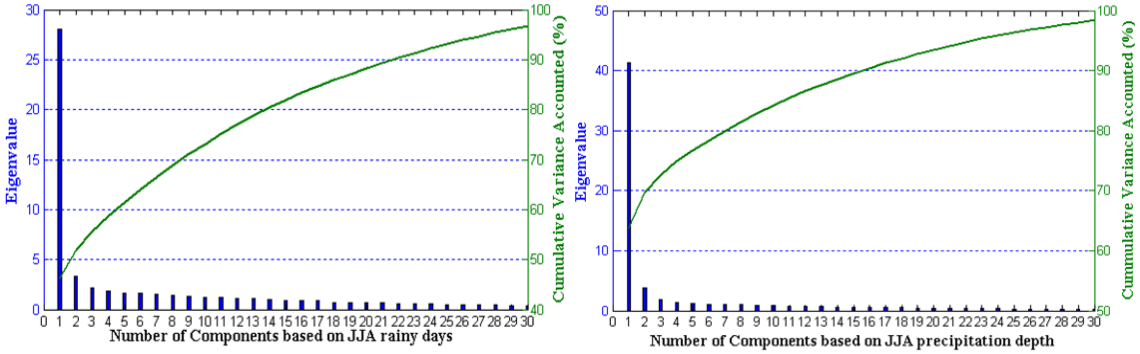

Figure 16 Scree plot used for selecting the PCs. The bars describe each of the first 30 PCs and their corresponding eigenvalues. The curve describes the percentage of cumulative variance accounted for by the PCs

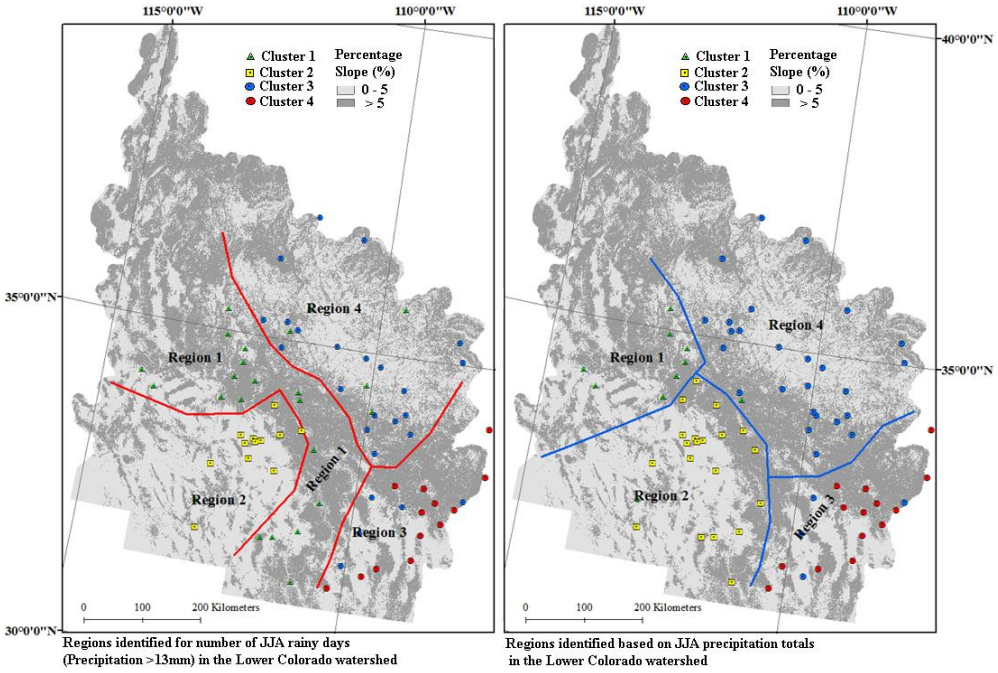

Figure 17 Spatial domains resulting from the cluster analysis performed on the selected PCs, identified based on JJA precipitation depth (right) and number (left) based on precipitation stations in the Lower Colorado watershed

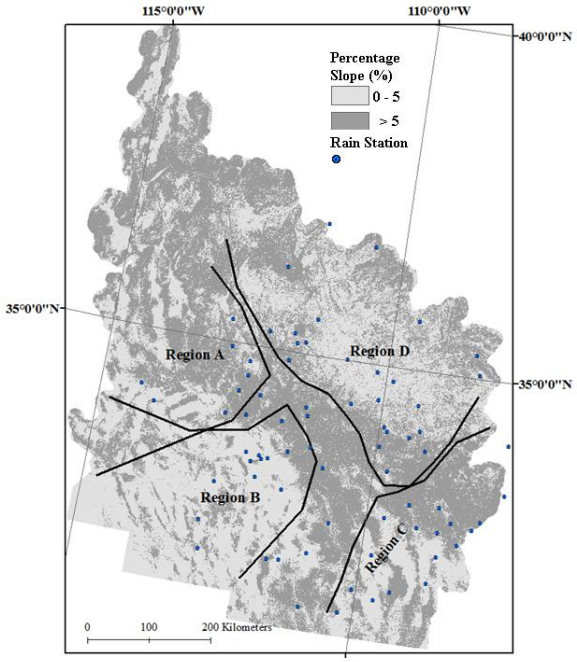

Figure 18 Regions identified based on JJA precipitation depth and number of rainy days. Region A is the intersection of the two Regions 1 in Figure 17. Region B is the intersection of the two Regions 2 in Figure 17. Region C is the intersection of the two Regions

2.6. Conclusions

The JJA period corresponds to the warm season and is important in the southwestern U.S. due to its contribution to annual precipitation. Most crops are grown during this period. The moisture during that period is highly influenced by the NAM. However, the variability in the summer precipitation characteristics (precipitation amount and number of events) may not be fully explained by the NAM.

From this study, we find that the entropy-based variability in seasonal precipitation records is not homogeneously distributed in space. Seasonal precipitation characteristics (number of events and precipitation amount) increase from east to west in the southwest

U.S. In the east and humid part of the region, the fluctuations in the summer precipitation characteristics are lower, while the same fluctuations increase in arid regions.

At the watershed level, the entropy-based variability indicates a potential influence of local watershed morphology characteristics on the JJA precipitation variability. While the orographic influence on precipitation generation is well documented in areas characterized by large mountain barriers, its more general effect on terrain variability, and its effect on precipitation disorder have not been previously shown. Leung et al. (2003) indicate how the interaction between atmospheric circulation and orography influences the climate regime in the western U.S. region. However, integrating that interaction in future climate simulations represents a real challenge for modelers.

In general, GCMs are designed to simulate future climate at resolutions of hundreds of kilometers. Because of that coarse spatial resolution, their outputs are not adequate at the local level (Oreskes et al., 2010). Furthermore, feedbacks associated with terrestrial processes are poorly represented in most GCMs (Knight and Harrison, 2012). This issue with GCMs is improved by regional climate models (RCMs), which project simulations at finer spatial and temporal resolutions. Even if RCMs embed some topographic influences (Sobolowski and Pavelsky, 2012), a better approach is to employ multi-model ensemble simulations. A typical example is the approach developed by the North American Regional Climate Change Assessment Program (NARCCAP), which developed a multi-model approach combining GCMs and RCMs for future precipitation and temperature projections.

Studies have indicated that the NARCCAP models perform well in representing extreme weather events (Wang et al. 2009; Wehner 2012). The idea of increased extreme events is consistent under climate change scenarios, nevertheless it may be relevant to evaluate and integrate the effects induced by hilly versus flat terrains on the precipitation regime, which may result in a relative reduction of extreme events. In fact, results from this study indicate that summer precipitation characteristics tend to show less disorder in complex terrain compared to plains regions. The magnitude of watersheds' effects on precipitation was assessed partially through the presented results by focusing on terrain slope. Although this study did not target all possible watershed physical characteristics for quantifying the effects on precipitation anomalies, it has established 1) that 19–27% of precipitation variability is related to slope, 2) clustered precipitation variability corresponds to terrain variations, and 3) there is a stabilizing effect of hilly relief on the JJA precipitation characteristics. It would also be relevant to extend such studies to quantify the watershed topography influence on other atmospheric factors.

CHAPTER III

VEGETATION RESPONSE TO PRECIPITATION ACROSS THE ARIDITY GRADIENT OF THE SOUTHWESTERN UNITED STATES

3.1. Synopsis

The atmospheric water demand significantly affects primary production, as well as the terrestrial water balance. However, the precipitation gradient from arid to humid regions extends beyond simple water balance and raises questions regarding the vegetation dynamic at large scales. For a 23-year period (1989–2011), we analyzed precipitation during the growing season in conjunction with the Normalized Difference Vegetation Index (NDVI) series for 21 satellite scenes spread across the southwestern United States. The satellite scenes were classified into three different groups based on the United Nations Aridity Index (AI). Group 1 was categorized as relatively humid, with AI≥0.65, group 2 was intermediate with 0.50≤AI<0.65, and group 3 was relatively dry with AI<0.50. Four types of vegetation covers were targeted: deciduous forest, shrubland, pasture, and grassland. On a long-term basis, significant positive trends in the NDVI series were evident for all types of vegetation in groups 1 and 2. However, neither the total precipitation nor the number of precipitation events (>3 mm and >13 mm) changed during this time. The magnitudes of trends in NDVI decreased with the aridity level. Cross-correlation analyses were used to track the lagged behavior of the four types of vegetation in relation to precipitation amount and number of events. The vegetation response was similar between precipitation amount and number of precipitation events. The general

behavior of vegetation depends on the region, precipitation, and the type of vegetation cover. In the arid region, we find distinct responses to precipitation for perennial vegetation versus annual vegetation types. The magnitude and significance of vegetation responses to precipitation patterns increase with environmental aridity.

3.2. Introduction

Ongoing climate change is being attributed to multiple factors, and evidence of climate change has been reported widely around the globe (Huntington, 2006). The increasing emission of greenhouse gases is recognized to be the main driver of climate warming. As a result, during the period of 1906 to 2005, a global increase in temperature of 0.74°C has been reported (IPCC, 2007). Furthermore, the atmospheric temperature is projected to increase by 2 to 4°C by the end of the current century (IPCC, 2007). Changes in climate are expected to alter arid ecosystems. However, the predicted changes in precipitation amount vary widely, depending on the models and their underlying assumptions (O'Gorman, 2012). Any potential benefit from an increase in precipitation amount would likely be cancelled by an increase in evapotranspiration due to climate warming (Maestre et al., 2012).

Water stress on vegetation is one of the ways of characterizing the level of available moisture. Based on simulations from different multi-model ensembles, Seager et al. (2007) projected a consistently drier climate in the southwest United States for the 21st century. In contrast, Maestre et al. (2012) reported several gaps in our knowledge regarding future impacts of climate change on drylands and highlighted the need to

consistently determine these impacts. Relying on model outputs to understand the future of climate and vegetation is clearly essential. However, no matter how sophisticated or robust any projection may appear, most models have uncertainties associated with their simulations. Therefore, it is necessary to first consider the observed trends, to improve our observational understanding and hence the interpretability of model simulations.

During the last two decades, the use of remote sensing has been essential for vegetation studies at large scales. The Normalized Differential Vegetation Index (NDVI) has been a successful and reliable tool in a variety of vegetation and precipitation studies (e.g., Rigge et al., 2013; Vicente-Serrano et al., 2006). Our study analytically investigates the influence of precipitation characteristics on the NDVI series during the vegetation growing season of May through September, as defined by Slayback et al. (2003). We cover a 23-year period from 1989 to 2011. Four different types of vegetation cover are considered, and their observational variability is investigated with particular focus on the southwestern U.S., which spans a wide range in terms of aridity. NDVI has been frequently employed to address the influence of climatological components, such as temperature and precipitation on vegetation cover. However, the long-term impacts of precipitation patterns are still unclear at regional scales because of the temporal limitation of satellite data.

It is generally recognized that climate change will bring about a decrease in precipitation across arid regions (Huntington, 2006; IPCC 2012). Furthermore, significant variability in precipitation patterns is reported, as is greater frequency of extreme events. A timely supply of water via precipitation is critical for rain-fed plants. The expected

future behavior of vegetation will be closely tied to the variability of precipitation, as driven by climate change. This study uses remotely sensed vegetation data during the vegetation growing season to address how precipitation characteristics (number of events and precipitation amount) may relate to the growth pattern of different types of vegetation. As part of this main objective, we also estimate vegetation and precipitation trends, potential temporal lags of the vegetation response, as well as the effects of seasonality on vegetation growth.

3.3. Climate classification across the study domain

The southwestern United States is relatively dry, compared to the rest of the country. Water availability is already a critical issue and will become of heighted importance due to climate change. Because of the crucial role of vegetation in hydrological processes, it is paramount to understand the future variability in the southwestern U.S. The study region encompasses the states of Louisiana, Arkansas, Oklahoma, Texas, New Mexico, and Arizona (Figure 19). We classify the study domain based on an aridity index, which is a useful indicator (Deniz et al., 2011) and describes the degree of dryness of the climate in a specific region.

Indeed, several indices have been developed and proposed for regional classification according to their aridity level (Sahin, 2012; Gao and Giorgi, 2008; Erinç, 1965; De Martonne, 1926). However, the best known aridity index is defined by the United Nations Environmental Program (UNEP; Maestre et al., 2012). This UNEP aridity index (AI) is the ratio of annual precipitation (P, mm) to the annual potential

evapotranspiration (PET, mm): AI = P/PET. This aridity index is widely accepted for characterizing dryland climatic boundaries (Maestre et al., 2012). The UNEP AI is employed here to characterize the degree of aridity across the spatial domain of our study. Based on AI, drylands are defined as regions where AI<0.65. An extended UNEP classification identified climate types (Maestre et al., 2012; Sahin, 2012) according to AI as: hyper-arid (AI<0.05), arid (0.05≤AI<0.20), semi-arid (0.20≤AI<0.50), sub-humid (0.50≤AI<0.65), semi-humid (0.65≤AI<0.80), humid (0.80≤AI<1.0), and very humid (1.0≤AI<2.0). We assessed the UNEP AI across the study domain using the long term average yearly Penman-Monteith PET (Vorosmarty et al., 1998) and precipitation, provided by the Earth Observation System (EOS)-EarthData at the University of New Hampshire (http://eos-earthdata.sr.unh.edu). The original PET and precipitation data were gridded at a 0.5 degree resolution. Figure 19 indicates that large parts of the domain have an AI<0.65 and can thus be classified as drylands. The dryness level gradually increases from east to west over the study region (Figure 19). The local vegetation follows that trend in that it is much denser in the more moist east and gets sparser westward (Homer et al., 2004).

For the vegetation dynamics analysis, we selected 21 Landsat satellite scenes (see details in methodology section) across the study domain. Each satellite scene has, on average, a footprint of 170 × 185 km. For purposes, of this study, the 21 satellite scenes were classified into three groups (Table 3) based on the dryness of the climate. The first group (group 1), here designated as “moist,” is comprised of scenes 1 to 7 which span the relatively humid regions with AI≥0.65. The second group (group 2), here designated

"intermediate," includes scenes 8 to 12, which span regions with 0.50≤AI<0.65. The third group (group 3), here designated as "dry," is composed of scenes 13 to 21, which span regions with AI<0.50. Group 2 (intermediate) can be considered to be a transitional climate zone, between the humid (group 1) and the arid (group 3) parts. For each group, the precipitation and vegetation data series were derived by averaging the data for the respective satellite scenes.

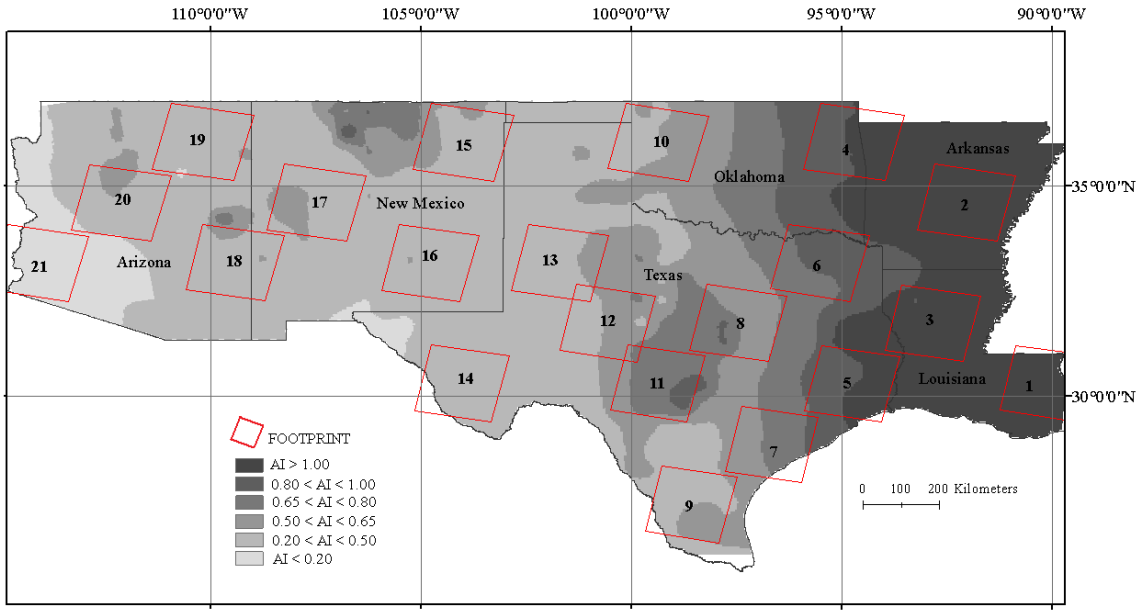

Figure 19 UNEP Aridity Index variability and selected satellite scene (footprint) locations across the study region

.

Table 3 Characteristics of selected satellite scenes across the study region; the Worldwide Reference System 2 (WRS-2) identifies the selected satellite scenes shown in Figure 19 . Group 1: moist region with AI≥0.65. Group 2: intermediate region with 0.50≤ AI<0

Climate grouping based on UNEP's AI	Scene	Aridity Index		WRS-2 Ref.		Scene center coordinates		Vegetation coverage (%)			
		Mean (AI)	CV (AI)	Path	Row	Lat. (°N)	Lon. (°W)	Deciduous Forest	Grassland	Pasture	Shrubland
Group 1 (humid)	1	1.45	0.06	22	39	30.3	-90.1	2.2	2.4	16.7	10.8
	2	1.17	0.02	24	36	34.6	-92.1	18.7	0.8	10.1	4.0
	3	1.09	0.04	24	38	31.7	-92.9	14.2	2.2	5.4	16.4
	4	1.02	0.1	26	35	36	-94.7	40.7	6.5	48.3	0.3
	5	1	0.1	25	39	30.3	-94.8	0.7	8.9	19.0	7.3
	6	0.82	0.08	26	37	33.2	-95.6	18.8	12.9	38.2	4.9
	7	0.69	0.12	26	40	28.9	-96.7	16.8	15.8	35.5	15.7
Group 2 (transitional)	8	0.64	0.13	27	38	31.7	-97.5	9.1	39.5	26.6	17.6
	9	0.52	0.12	27	41	27.4	-98.6	1.3	14.7	13.0	49.2
	10	0.51	0.07	29	35	36	-99.4	0.2	62.5	0.2	12.9
	11	0.62	0.12	28	39	30.3	-99.4	5.9	11.4	0.6	63.0
	12	0.53	0.13	29	38	31.7	-100.6	1.6	8.3	1.3	77.8
Group 3 (arid)	13	0.38	0.11	30	37	33.2	-101.7	0.2	32.2	0.4	24.5
	14	0.32	0.13	31	39	30.3	-104.1	0.1	11.1	0.0	76.7
	15	0.43	0.21	32	35	36	-104	0.0	75.4	0.1	18.1
	16	0.36	0.14	32	37	33.2	-104.8	0.0	36.4	0.1	52.4
	17	0.4	0.27	34	36	34.6	-107.5	0.0	21.9	0.6	56.1
	18	0.38	0.19	35	37	33.2	-109.5	0.1	1.8	0.2	67.9
	19	0.29	0.22	36	35	36	-110.2	0.0	20.1	0.0	78.7
	20	0.38	0.25	37	36	34.6	-112.2	0.1	3.4	0.1	63.5
	21	0.09	0.28	38	37	33.2	-114.1	0.1	2.4	5.4	91.8

3.4. Characteristics of vegetation types

In general, water availability is a key requirement for plant photosynthetic activity. In most ecosystems, the natural vegetation is a mixture of different species of plants. Based on their adaptability and survival under local conditions, species can be classified into two major plant types: perennial or annual. In arid ecosystems, this distinction is critical for vegetation dynamics. Hence, Salguero-Gomez et al. (2012) distinguished perennial species from annual ones, while describing the effect of precipitation on vegetation dynamics in drylands. Perennial species exhibit higher longevity and better resistance to droughts, while annual species conserve their population through high seed dormancy. The behavior of these two groups of plants in arid regions is more the result of a long-term adaptation process. Generally, during the cold season, the annual plant population decreases considerably and seeds remain on the ground. During the warm (plant growing) season, the combined effect of heat and moisture induce the germination of seeds.

The U.S. Geological Survey (USGS) distinguished a large variety of vegetation types in the southwestern United States (Lowry et al., 2007). Four of these vegetation types, including deciduous forest, shrubland, grassland, and pasture, were targeted in our study. The characteristics of each of these four vegetation covers are described by Homer et al. (2004, 2007), and more detailed descriptions are also available from the USGS Southwest Regional Gap Analysis Project (http://earth.gis.usu.edu/swgap). It should be noted that these vegetation covers are not equally represented across the study region. Table 4 presents the relative coverage of each of the selected vegetation types in the individual satellite scenes' spatial domain. In the southwestern United States, the

precipitation gradient decreases westward (Sohoulande Djebou et al., 2014) and seems to drive the land cover distribution. While the western and arid parts are less favorable for dense vegetation, some forest patches, including deciduous forests, are reported (Lowry et al., 2007). Indeed, some of these forest patches are part of riparian ecosystems and are sustained by perennial or ephemeral watercourses (Webb and Leake, 2006). In terms of percentage coverage, these forest formations are less represented in the arid region, but highly valued as they represent habitat for migratory animals and play an essential role in the local ecosystem (Webb and Leake, 2006; Ohmart and Anderson, 1982). Webb and Leake (2006) reported that the setting of such forest formations in the arid and semi-arid parts of the southwestern United States depends on the interaction between ground and surface water. Despite the low representativeness of deciduous forest and pasture in the arid and semi-arid region (Table 4), they play an important role in the local ecosystems and are therefore considered here, along with shrubland, pasture and grassland.

3.5. Methodology

3.5.1. Remote sensing and vegetation index data

A number of remotely sensed vegetation indices have been proposed and employed to address vegetation growth. Each of these indices presents both advantages and disadvantages. The Normalized Difference Vegetation Index (NDVI), the Enhanced Vegetation Index (EVI), and the Soil Adjusted Vegetation Index (SAVI) are three indices frequently employed in analyses of vegetation dynamics. NDVI is the most common, and has been applied to assess vegetation dynamics at large scales during the last two decades.

NDVI is sensitive to chlorophyll activity and changes in vegetation cover, which it can reproduce relatively well (Huete et al., 2002; Carlson and Ripley; 1997). However, NDVI has a saturation limitation when it is employed for leaf area index (LAI) estimates, particularly in high vegetation density regions (Huete et al., 2002). EVI is designed to improve vegetation monitoring in high biomass regions (Huete el al. 2002; Lobell et al., 2010), as it can better capture variations in canopy structure and LAI. However, the southwestern United States is characterized by sparser vegetation, which supports the use of NDVI. SAVI was proposed to minimize soil brightness noise on NDVI (Huete, 1988). However, Liu and Huete (1995) reported on the instability of SAVI regarding atmospheric variables, as soil brightness and atmospheric noise are not independent. Corrections have been proposed to improve NDVI by reducing the uncertainty related to soil brightness and atmospheric noise. The Landsat Ecosystem Disturbance Adaptive Processing System provides algorithms for calibration and atmospheric correction of satellite scenes (Masek et al., 2006). The USGS Earth Resources Observation and Science (USGS-EROS) center used such algorithms to correct the satellite bands such that the uncertainty of the final NDVI products is greatly reduced.

This study, thus, uses NDVI from USGS-EROS for assessing vegetation growth. The NDVI values span from −1 to 1; the positive values indicate vegetation cover, while the zero and negative values represent non-vegetated features. The original NDVI data are generated from Advanced Very High Resolution Radiometer (AVHRR) images through the USGS Greenness Mapping and Remote Sensing Phenology projects (Eidensshink, 2006; Reed, 2006). Aboard the National Oceanic and Atmospheric Administration

(NOAA) series of environmental satellites, AVHRR sensors collect images with a 1.1 km spatial resolution on a daily basis over the entire globe. The NDVI series were derived from biweekly cloud and haze free composite images. For individual vegetation types, the NDVI series were obtained by intersecting the NDVI composite images with the National Land Cover Database (NLCD). The USGSG-EROS used NLCD versions 1991 and 2001. The NLCD are 30 m spatial resolution raster layers generated from Landsat thematic mapper images for the whole conterminous U.S. (Homer et al., 2004; Vogelmann et al., 2001).

Landsat's sensors provide continuous scenes spanning approximately 170 km north-southward, 185 km east-westward and follow the worldwide Reference System 2 (WRS-2) which indicates, for each scene, the corresponding path and row. Using Landsat-derived land cover data as the interface, the AVHRR NDVI composites are resampled with respect to Landsat scene sizes. Hence, within each Landsat scene's footprint, the NDVI value for a specific land cover is the average value of all pixels corresponding to that land cover. The USGS-EROS has been consistently producing NDVI data since 1989 for the conterminous United States (Eidenshink, 2006; Wang et al., 2003). In this study we used 23 years of NDVI data (1989–2011) and focused on the warm period of approximately May through September (i.e., April 23–September 23 based on the biweekly time scale), which was defined as the vegetation growing season by Slayback et al. (2003).

3.5.2. Precipitation data

Daily precipitation data were acquired from the NOAA National Climatic Data Center (NCDC). A total of 92 ground-based precipitation stations were considered. All stations are located within the 21 selected Landsat satellite scenes, and each scene encompasses 3 to 6 precipitation stations. Based on the time scale of bi-weekly remotely sensed vegetation data, the yearly period from April 23 to September 23 (Julian days 113 to 266) was considered over the entire available record from 1989 to 2011. Daily precipitation data were aggregated into the biweekly time scale. The specific precipitation variables used here are the number of precipitation events and the total precipitation amount. To derive the number of precipitation events, we considered two thresholds: the number of days with precipitation greater than 3 mm (0.1 in), and those greater than 13 mm (0.5 in). For both the precipitation and vegetation time series, the Mann-Kendall test was performed to detect monotonic trends, and Kendall's tau (τ) coefficients were evaluated to estimate seasonality effects. Specifically, we used Kendall's tau-b because, unlike Kendall's tau-a, it adjusts for potential ties in the ranked correlations. The purpose of evaluating seasonality is to identify potential cumulative trends (i.e. season-to-season dependence) in the vegetation growth cycles.

3.5.3. Vegetation dynamics metrics

Plant photosynthesis results in primary production, which indicates vegetation growth and the level of photosynthetic activity (Wang et al., 2003; Di et al., 1994). NDVI series have been consistently employed as an indicator for addressing vegetation growth (Fang et al. 2005; Wang et al., 2003). Fang et al. (2005) utilized NDVI to assess grassland

and deciduous forest growth in temperate biomes of China. Carlson and Ripley (1997) emphasized that NDVI captures the dynamics of vegetation cover. Focusing on sparse vegetation coverage during the growing season, Carlson and Ripley (1997) reported that NDVI is sensitive to vegetation density until full coverage is reached. This characteristic of NDVI is used particularly for LAI estimates (Huete et al., 2002; Carlson and Ripley, 1997). Besides the direct application of NDVI, several metrics have been successfully employed to assess the impact of precipitation on vegetation dynamics. The $NDVI_{Ratio}$ is a metric that describes biological green-up events (Clinton et al., 2010; White et al., 1997). For a specific time *t*, the $NDVI_{Ratio}$ is defined as:

$$NDVI_{Ratio} = \frac{\left(NDVI_{t} - NDVI_{Min} \right)}{\left(NDVI_{Max} - NDVI_{Min} \right)} \tag{3}$$

Explicitly, the $NDVI_{Ratio}$ does not incorporate any precipitation component. Instead, cross-correlation allows for the analysis of relationship between vegetation growth and precipitation. Based on the approach of Clinton et al. (2010), we applied cross-correlation to investigate vegetation dynamics in relation to precipitation.

Over the course of a 5-month growing season (Julian days 113–266), the biweekly time step allows for only 11 data points of NDVI and precipitation. For the entire 23-year period (1989–2011) this resulted in a sample size of only 253, which is too few for the cross-correlation analysis (Clinton et al., 2010). To overcome this time-scale issue, previous authors have suggested the use of spline methods (Hermance et al., 2007; Rozhenko, 2010). Cubic spline interpolation has been reported as an efficient, stable, and powerful approach (Duan et al., 1998). Therefore we applied a cubic spline interpolation,

which also minimizes the residual and provided us with data at a finer temporal resolution for subsequent cross-correlation analysis.

Following the approach of Clinton et al. (2010), we defined the time scale (t) to be a hundredth of the growing season. Then, for each year, the 11 biweekly NDVI and precipitation points were used to derive 100 values. For the 23-year period, each satellite scene was thus represented by a series of 2300 points. For the cross-correlation analysis we selected a lag (l) such that $l \in \{0, t, 2t, ..., 100t\}$ and 100 cross-correlation values were computed. If the precipitation and NDVI series are indexed with time factor t, the NDVI series can be identified as $\{NDVI_t : t = 1, ..., 2300\}$ and the precipitation series by $\{P_t : 1, ..., 2300\}$. Finally, the cross-correlation between the vegetation (NDVI) and precipitation (P) series was defined as:

$$\rho(l,t) = \frac{\sum_{t=1}^{2300}\left[(NDVI_t - \mu_{NDVI}) * (P_{t-l} - \mu_P)\right]}{\sqrt{\sum_{t=1}^{2300}(NDVI_t - \mu_{NDVI})^2}\sqrt{\sum_{t=1}^{2300}(P_{t-l} - \mu_P)^2}} \quad (4)$$

where $\mu_{NDVI} = 1/2300 * \sum_{t=1}^{2300} NDVI_t$ and $\mu_P = 1/2300 * \sum_{t=1}^{2300} P_{t-l}$

The resulting cross-correlation provided the timing (lag) and magnitude at which NDVI and precipitation co-varied during the 23-year period.

3.6. Results

3.6.1. Analysis of trends in NDVI series

The NDVI series for each of the four types of vegetation cover in different aridity groups is presented in Figure 20. The seasonal Kendall rank correlation (Hirsch et al., 1982) analysis was performed to estimate the effect of seasonality on the overall trend. The seasonality in the NDVI series based on Kendall's τ is presented in Figure 21. The red lines in Figure 21 indicate the upper and lower limits of Kendall's τ values at the 95% confidence level. The significance of trend lines in Figure 20 is indicated by Kendall's τ values corresponding to the 0-year seasonality in Figure 21. A joint interpretation of Figure 20 and Figure 21 illustrates that there are significant positive trends, for all four types of vegetation cover in the moist (group 1) and intermediate (group 2) climate regions during the 1989–2011 period. In the dry region (group 3), except for the deciduous forests, there are no significant trends in the NDVI series (Figure 20a and Figure 21a). Overall, the trends are very similar for all four types of vegetation. The trends in the NDVI series decrease with the aridity level of the region. Kendall's τ increases with the seasonality effect (Figure 21). This seasonality analysis suggests that the primary production increases yearly in the humid ecosystems, while in the arid region there are no significant changes in primary production, except for deciduous forests.

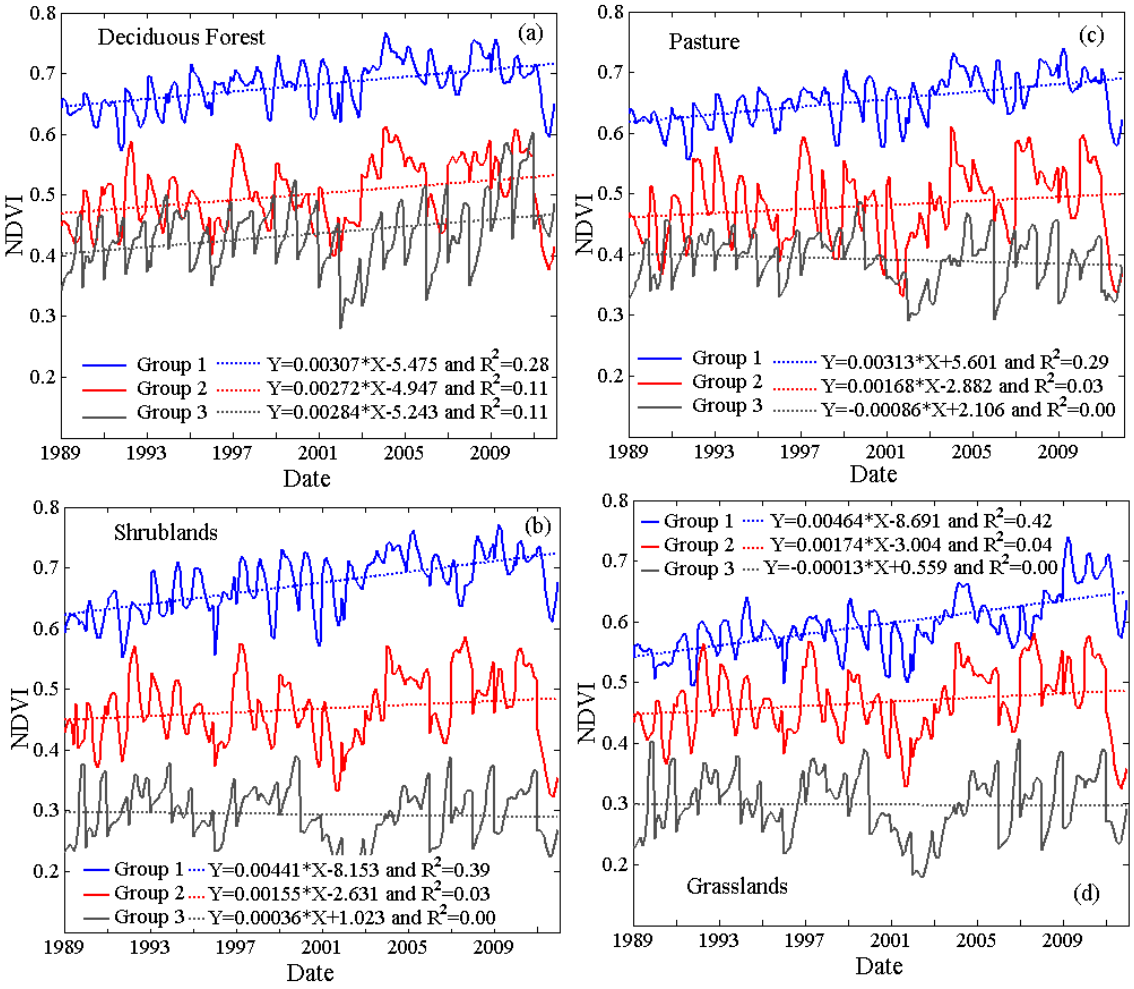

Figure 20 Trends in vegetation greenness as an indicator of primary productivity. (a) Deciduous forests, (b) shrublands, (c) pastures, and (d) grasslands. Group 1: moist region with AI≥0.65. Group 2: intermediate region with 0.50≤AI<0.65. Group 3: dry region with

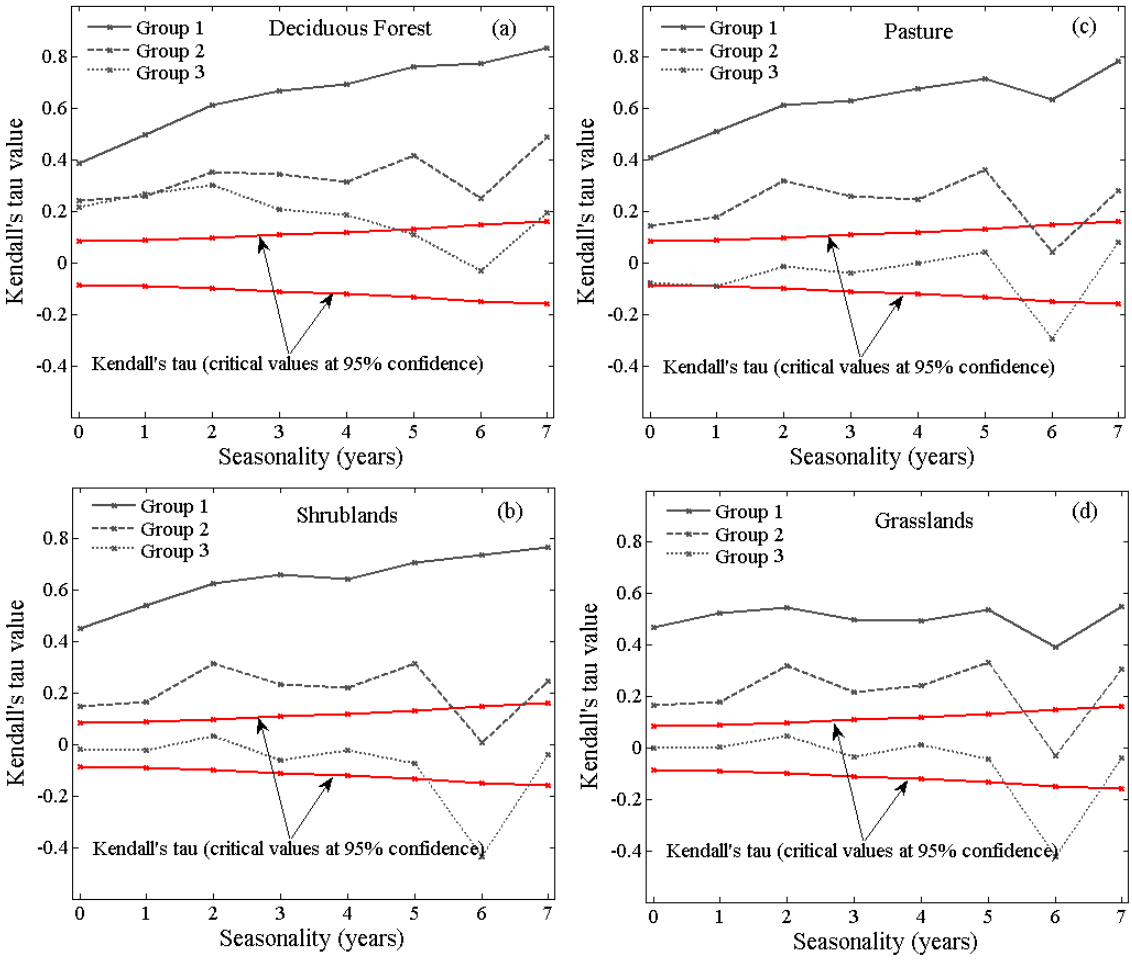

Figure 21 Seasonality effect on Kendall's τ for four types of vegetation. Red lines represent 95% upper and lower significance limits for Kendall's τ. Group 1: moist region with AI≥0.65. Group 2: intermediate with 0.50≤AI<0.65. Group 3: dry with AI<0.50

3.6.2. Analysis of trends in precipitation series

The Mann-Kendall test (95% confidence level) was performed on the precipitation time series for each of the three climate regions (Table 4). The precipitation variables are total biweekly precipitation amount and number of biweekly precipitation events. The precipitation events greater than 3 mm and 13 mm were considered separately. For the NDVI analysis, only the growing seasons over the period 1989-2011 were considered. The

Mann-Kendall test indicated no significant trends in the annual growing seasons' precipitation variables (Table 4). However, the analysis computed by partitioning biweekly the growing season, revealed some cases of significant negative trends (Table 4). These significant trends were consistently observed in the biweekly periods 141–154 (May 21–June 3) and 169–182 (June 18–July 1) for the moist and intermediate regions, respectively. For these two biweekly periods, the precipitation variables (total precipitation, number of events) showed a gradual decrease over the 23-year period. This finding suggests that during the early part of the growing season, drying may be occurring. In addition, most of the Kendall τ values indicate negative trends, although they are not significant (p-value < 5%). However, this trend analysis in precipitation needs to be considered in the context of the relatively short time frame used in this study (only 23 years).

Table 4 Summary of the Mann-Kendall test performed on the 23-year precipitation variables for each of the groups. Group 1: moist region with AI≥0.65, group 2: intermediate region with 0.50≤AI<0.65, and group 3: dry region with AI<0.50. The significant Kendall's τ values (95% level) are in bold.

Precipitation variables		Annual	Biweekly period (Julian days)										
			113-126	127-140	141-154	155-168	169-182	183-196	197-210	211-224	225-238	239-252	253-266
Event > 3mm	Group1	-0.22	**-0.27**	-0.16	**-0.30**	-0.24	-0.15	-0.15	0.07	-0.03	-0.14	0.19	0.00
	Group2	-0.13	-0.07	-0.11	-0.15	-0.15	**-0.34**	0.08	0.17	0.04	**-0.28**	0.04	0.13
	Group3	-0.10	0.01	-0.15	0.02	-0.15	-0.19	0.19	0.11	0.10	-0.02	-0.20	-0.18
Event > 13mm	Group1	-0.26	-0.18	-0.11	**-0.30**	-0.24	-0.23	-0.10	0.12	0.00	0.05	0.11	0.13
	Group2	-0.05	0.01	-0.07	-0.13	-0.11	**-0.39**	0.11	0.15	-0.03	-0.22	0.13	0.08
	Group3	-0.07	0.16	-0.10	0.03	-0.19	-0.19	0.17	-0.01	0.03	0.08	-0.22	-0.21
Total (mm)	Group1	-0.18	-0.19	-0.07	**-0.34**	-0.15	-0.19	-0.16	0.10	0.03	-0.02	0.10	0.23
	Group2	-0.11	-0.15	-0.04	-0.19	-0.09	**-0.37**	0.09	0.10	0.00	**-0.27**	0.11	0.14
	Group3	-0.10	0.04	-0.07	0.04	-0.17	-0.19	0.15	0.08	0.08	-0.08	-0.16	-0.19

3.6.3. Cross-correlation analysis between vegetation growth and precipitation

For each vegetation type, we calculated cross-correlations with precipitation at various lags (Figure 22). The lags spanned from 0 to 100*t* with a time step $t = 1/100$ of the growing season. Positive cross-correlations are of primary interest in this analysis as we are tracking the positive response of vegetation. However, we might also expect a potential negative response of vegetation under some circumstances. For each set of cross-correlations the maximum value and its corresponding lag (converted to days) are indicated in Table 5. Comparison of cross-correlation curves for all four vegetation types shows many similarities, with moisture availability (aridity) primarily defining the response. The response of vegetation to total precipitation increases with the aridity level. In the moist region (group 1) the maximum positive cross-correlations are very low, and the intermediate (group 2) and dry regions (group 3) exhibit much higher positive correlations, peaking at lags between 6 and 12 days. This suggests that vegetation growth during the warm season in the moist region (group 1) does not depend strongly on precipitation forcing. This could be explained by the fact that, under water stress, plants react positively to any amount of water. Vegetation cover in arid regions is more likely under constant water stress compared to that in humid regions, and therefore its response to precipitation varies. In all cases the lags corresponding to the maximum cross-correlation values are approximately 7 days, which is below the biweekly time step of the original NDVI and precipitation series.

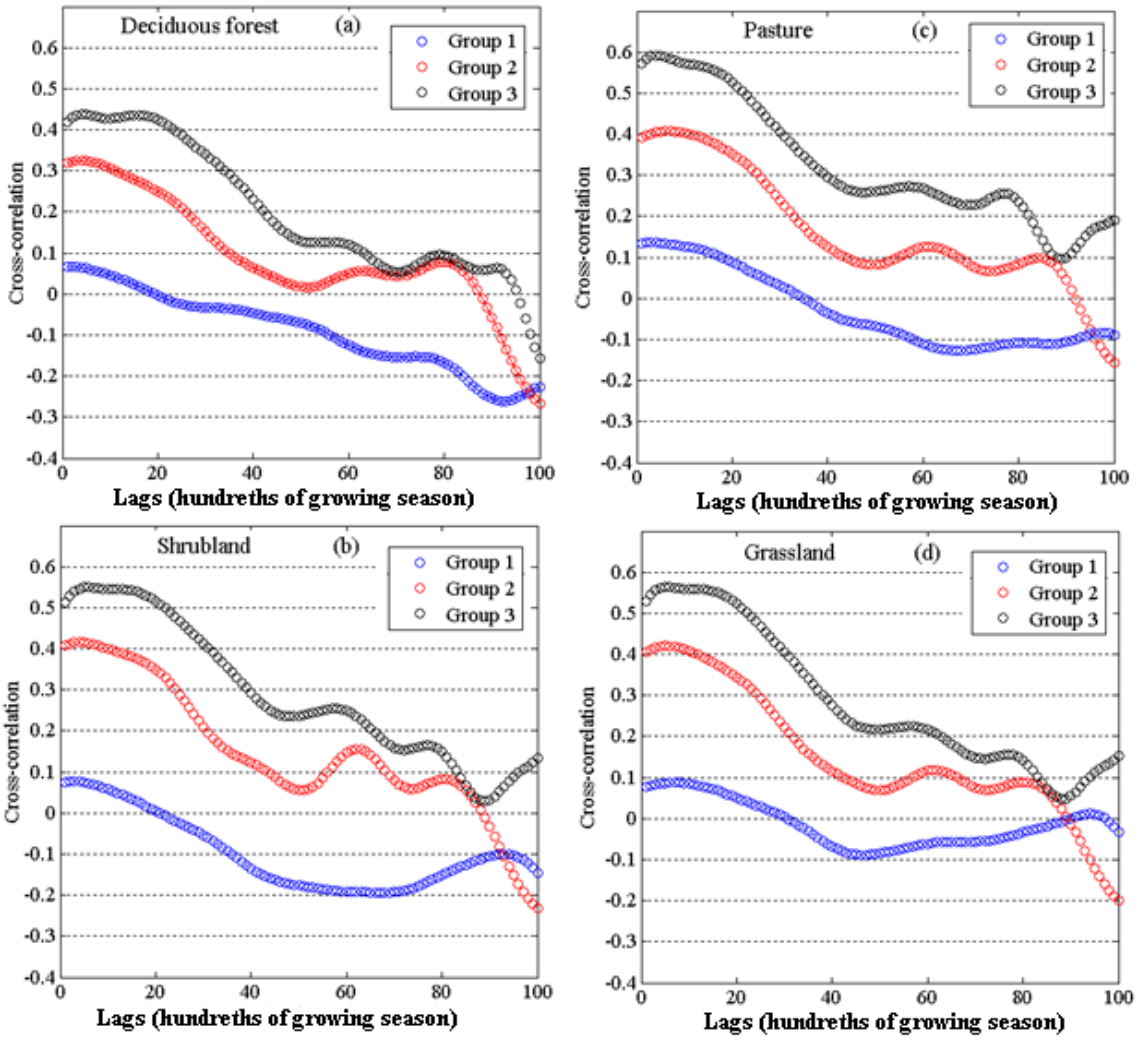

Figure 22 Cross-correlations between NDVI for different types of vegetation and precipitation amounts. Correlations exceeding ±0.05 are statistically significant (95%-level). Group 1: moist region with AI≥0.65. Group 2: intermediate region with 0.50≤AI<0.65. Group 3: dry region with AI<0.50.

Table 5 Temporal lags of vegetation response based on cross-correlation analysis; maximum correlation ρ(l,t) indicates the highest positive response of vegetation at lag l. Note that only the maximum values of positive cross-correlations are provided. Group 1: moist region with AI≥0.65, group 2: intermediate region with 0.50≤AI<0.65, and group 3: dry region with AI<0.50. The significant correlations (95% level) are in bold.

Type of vegetation	Climate type (group)	Total precipitation		Precipitation events (>13mm)		Precipitation events (>3mm)	
		Max. $\rho(l,t)$	Lag (days)	Max. $\rho(l,t)$	Lag (days)	Max. $\rho(l,t)$	Lag (days)
Deciduous Forest	Group 1	**0.07**	3	**0.09**	1	0.00	1
	Group 2	**0.33**	**6**	**0.35**	**7**	**0.35**	**9**
	Group 3	**0.44**	**6**	**0.42**	**6**	**0.44**	**6**
Grassland	Group 1	**0.09**	10	**0.12**	7	0.04	10
	Group 2	**0.42**	**7**	**0.44**	**9**	**0.44**	**10**
	Group 3	**0.56**	**9**	**0.54**	**7**	**0.54**	**7**
Pasture	Group 1	**0.14**	4	**0.16**	6	**0.07**	9
	Group 2	**0.41**	**10**	**0.43**	**10**	**0.44**	**12**
	Group 3	**0.59**	**6**	**0.57**	**6**	**0.60**	**6**
Shrubland	Group 1	**0.08**	4	**0.11**	6	0.03	4
	Group 2	**0.42**	**6**	**0.44**	**7**	**0.44**	**9**
	Group 3	**0.55**	**9**	**0.52**	**7**	**0.55**	**9**

3.6.4. Comparative analysis of vegetation response to precipitation characteristics

One of the main goals in this study was to understand which of the precipitation characteristics (total precipitation and number of precipitation events) impact vegetation dynamics the most. The preceding section indicates that precipitation amount and vegetation growth during the growing season co-vary in dry and intermediate regions (group 3 and group 2), but not in moist areas (group 1). To explore the impact of precipitation events, we target just the dry region (group 3) and present the cross-

correlation analysis by considering two types of vegetation cover: deciduous forests (Figure 23a) and shrublands (Figure 23b). Note that these two vegetation types are selected as examples only, and the results for the other two vegetation types (grassland and pasture) are described in Table 6. Table 6 presents the statistical relationships between the cross-correlation series of precipitation variables and each of the four vegetation types. Overall, the cross-correlations performed based on each of the three precipitation variables and NDVI's series are highly correlated ($0.87 \leq R^2 \leq 0.99$). Although correlation cannot establish cause and effect, it is nonetheless apparent that the number of precipitation events has a similar relationship with vegetation as precipitation amount does.

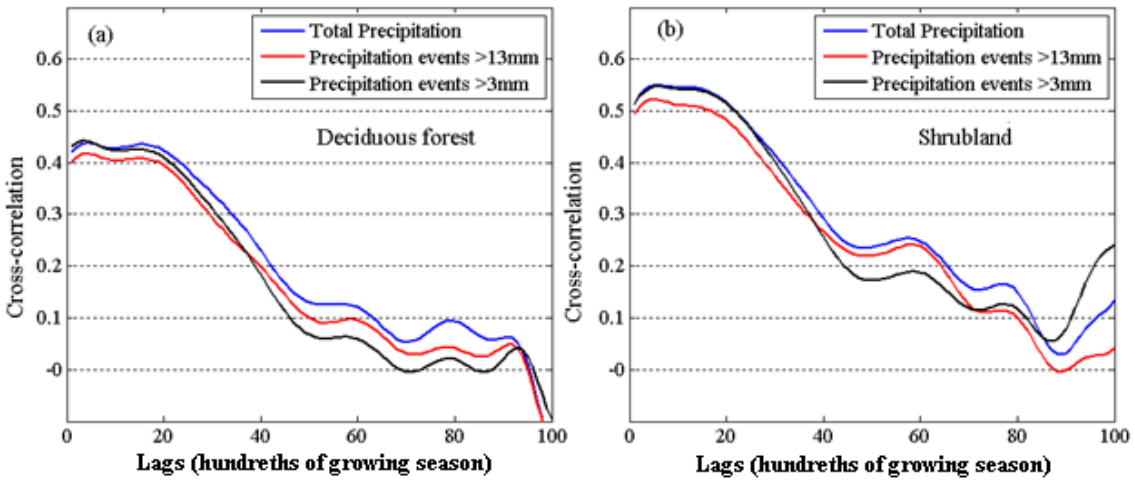

Figure 23 Cross-correlation between NDVI as a measure of vegetation growth, and different precipitation variables: total precipitation, number of precipitation events > 13 mm, number of precipitation events > 3 mm. The dry region (group 3 with AI<0.50) was target as an example for this plot

Table 6 Coefficients of determination based on the Pearson correlations computed pair-wise between cross-correlation series. The cross correlation series are computed between NDVI and precipitation variables (number of precipitation events >3 mm, events >13 mm) and total precipitation cross-correlation series. Group 1: moist region with AI≥0.65. Group 2: intermediate region with 0.50≤AI<0.65. Group 3: dry region with AI<0.50.

Precipitation variables	Climate classes	Deciduous Forest	Grassland	Pasture	Shrubland
Events >3mm	Group1	0.93*	0.97*	0.96*	0.98*
	Group2	0.98*	0.98*	0.97*	0.99*
	Group3	0.97*	0.92*	0.97*	0.93*
Events >13mm	Group1	0.99*	0.92*	0.99*	0.87*
	Group2	0.98*	0.99*	0.99*	0.99*
	Group3	0.99*	0.99*	0.99*	0.99*

*P-value <0.001

3.7. Discussion

The Mann-Kendall test indicated significant positive trends in the NDVI series representing grassland, pasture, shrublands, and deciduous forest. At the same time the precipitation variables (number of precipitation events and total precipitation) did not show any significant trends. This discrepancy between precipitation and vegetation trends indicates that the vegetation dynamics are not a direct consequence of precipitation in the southwestern United States. In the moist and intermediate regions (groups 1 and 2) the increasing trends observed in vegetation growth seem consistent with prior studies on NDVI trends (e.g., Los, 2013). Slayback et al. (2003) also reported an overall consistent positive trend in AVHRR's NDVI series in the North American region.

According to Los (2013), 40% of the positive NDVI trend observed in North America during the period 1982 to 2006 is related to CO_2 fertilization. Los (2013) also

related 40% of the trends to climate variation. However, the spatial trend patterns were not homogeneous. Hence, the difference in trends we observed for the moist and intermediate regions (groups 1 and 2) compared to the dry region (group 3) may warrant a different explanation. The discrepancies could be due to farming activities as well as the plants' adaptive responses in each of the regions. The arid environments of the U.S. southwest are often used for livestock production. The effect of grazing pressure on vegetation reduction has been reported for some locations in the western U.S. to the degree that mitigation strategies were even developed (Pellant et al., 2004). The primary productivity differs in humid and arid regions because of plant regeneration processes. In humid regions, there is a cumulative effect in the primary production over the years. However, in arid regions, particularly where annual vegetation dries up and mostly dies back during winter, it mostly regenerates during the growing season. Therefore, in arid regions there is no significant cumulative effect in the prior primary productivity on vegetation cover. This is also supported by the fact that only deciduous forests have a significant positive trend in the dry region (group 3). Indeed, the NDVI fluctuations indicate vegetation photosynthetic activity (Fang et al., 2005) and specific algorithms can be used to estimate LAI (Bresloff et al., 2013). Therefore, the observed trends in the NDVI series can be shown to be consistently associated with LAI and consequently related to the land cover dynamics.

Vegetation growth in arid environments should be considered as the result of various interactions. In the western U.S., Riggie et al. (2013) assert that grazing intensity, fire, and weather variability (i.e. temperature and precipitation) affect land cover

regeneration and therefore disturb biomass production. The inter-annual changes in primary production depend on these factors (Riggie et al., 2013). Therefore, the magnitude of primary productivity for a particular vegetation type may also be seen as a result of the long-term growth pattern.

Cross-correlation analysis suggests that the response of vegetation to precipitation increases with environmental aridity. This is consistent with the results obtained by Fang et al. (2005) who also reported that the vegetation cover response to precipitation became less significant with high precipitation frequency. Vegetation cover responses to different precipitation characteristics (frequencies of events versus total precipitation) are very similar.

One of the limitations of this research is that the period of study spans only 23 years, which is somewhat short for climate analysis. While precipitation data are available for almost a century in the southwestern U.S., consistent remotely sensed vegetation data are only available for less than three decades.

3.8. Conclusions

The southwestern United States is characterized by a strong gradient in aridity that affects the vegetation cover. A large part of the study region is arid and the aridity level increases westward. During the growing seasons, the responses of vegetation cover to precipitation are very similar in the three aridity classes targeted in the study. However, in the arid region, the perennial vegetation (deciduous forests) behaves differently from shrublands and the annual vegetation types (grasslands, pastures). We find that the

magnitude and significance of vegetation responses to precipitation patterns increase with the environmental aridity. Further, frequencies of precipitation events can be used similarly as precipitation amounts for vegetation monitoring in arid ecosystems. Regarding climate change, an increase in precipitation disorder should be considered a threat for rain-fed vegetation the same way as a decrease in total precipitation. However, another important component to consider in vegetation growth studies is soil moisture. Compared to precipitation, soil moisture data are poorly monitored and are not commonly available in time and space. Further research on the topic should involve soil moisture and investigate the role on large scale vegetation dynamics.

CHAPTER IV

RETRIEVING VEGETATION GROWTH PATTERNS FROM SOIL MOISTURE, PRECIPITATION AND TEMPERATURE USING ENTROPY

4.1. Synopsis

This study employed entropy theory to evaluate the relation of vegetation cover to soil moisture, precipitation and temperature patterns in the Texas Gulf watershed. Over a 12 year period, the Normalized Differential Vegetation Index (NDVI) of the growing season (May to September) for deciduous forest and grasslands, as well as precipitation, temperature and soil moisture data at a biweekly time scale were considered. Using three different vegetation growth metrics, we analyzed patterns in vegetation responses. An entropy scaling of the system of vegetation-soil moisture-precipitation-temperature reveals trends toward maximum entropy and shows the relevance of coupling these atmospheric variables in vegetation dynamic analysis. Our analysis indicates that soil moisture is potentially more efficient to use for vegetation dynamics monitoring at finer time scales compared to precipitation. However, the near-surface (5 cm) soil moisture series seems to better explain vegetation growth compared to 25 cm depth soil moisture series. This seems interesting as the recent satellite soil moisture monitoring projects are designed for estimating near-surface moisture. Month-wise, the vegetation response to atmospheric variables showed important dissimilarities. Therefore, we used an entropy-based clustering approach to discriminate the growing season. Later, a nested statistical model was employed for retrieving an estimate of NDVI. Meanwhile the best fit of

vegetation growth was obtained by coupling soil moisture and mean temperature. We found that the inclusion of soil moisture and temperature explained up to 68% and 62% of the variation of NDVI, respectively, for deciduous forest and grassland during June and July. However these relationships appeared weaker during the end of the growing season (August and September). Results of the study contribute to the debate on the relevance of soil moisture measurements, and may help large scale vegetation monitoring. Nevertheless, further studies on the topic are necessary and should involve diversified ecosystems and remote sensed products.

4.2. Introduction

The climate system is governed by complex interactions between the atmosphere, the hydroshepere, the lithosphere, the biosphere and the cryosphere (Peixoto et al., 1991). Changes in vegetation cover are merely a response resulting from both environmental and biological conditions. However, it is a conundrum to accurately incorporate into vegetation and climate models all the interactions emanating from the biophysical components of the climate. Consequently, the real vegetation and ecosystem functionalities are commonly simplified (Reich et al., 2007; Sitch et al., 2003).

Several authors have reported significant relationships between precipitation, temperature and remotely sensed vegetation indices (Brunsell and Young 2008; Pettorelli et al, 2006, Kawabata et al., 2001). The choice of focusing on individual factors rather than all of them at the same time is guided by the aim to depict their influence separately. However, attempts at using solely precipitation or temperature for vegetation dynamics

estimates have resulted in low efficiency, i.e., low overall correlation coefficients between Normalized Differential Vegetation Index (NDVI) and precipitation series (Liu et al., 2013; Nicholson et al., 1990). Ichii et al. (2001) found significant but weak relationships between vegetation growth and precipitation and pointed out insufficient long-term data. Outside of certain precipitation thresholds, Nicholson et al. (1990) reported weaker relationships between NDVI and precipitation, indicating non-linear overall relationships. At a global level, Kawabata et al. (2001) reported different scenarios of NDVI trends in relation to temperature and precipitation according to the location. However, efforts in retrieving NDVI from climate components poorly involved observed soil moisture data. Brunsell and Young (2008) emphasized the role of soil moisture in the short-term land surface response. Unfortunately, real observed soil moisture data are not consistently available in time and space (Seneviratne et al, 2006) and this has limited their use in large-scale vegetation dynamic studies.

Soil moisture is the water stored in the soil pores. Originally this water is replenished by atmospheric water through infiltration but can also be recharged through capillary rise (Legates et al., 2011). The rate of each of these two processes of soil water recharge depends on environmental and geophysical factors (Wang et al., 2013; Legates et al., 2011). In contrast to precipitation, the water in the soil is the one directly available for plant roots. Compared to precipitation and temperature, land-based soil moisture measuring instruments are relatively more expensive and costly in terms of monitoring and maintenance. For that reason, historical land-based soil moisture measurements are not consistently available in time and space explaining why several studies have been

conducted using model-generated soil moisture data (Seneviratne et al, 2006). Such an approach has led to model dependent conclusions which clearly affect the uncertainty in model results. Meanwhile, moisture sensitivity to microwave represents a crucial alternative for deriving soil moisture using satellite images (Pellarin et al., 2009; Wagner et al., 2003). Hence, remote sensing of soil moisture has made possible the quantification of near-surface moisture by combining infrared remote sensing and vegetation index, i.e., the Advanced Microwave Scanning Radiometer of the Earth Observing System (AMSR-E) uses passive microwave signals to generate mean term soil moisture estimates at a 25 km spatial resolution (Njoku et al., 2003). Lately the National Aeronautics and Space Administration NASA's Soil Moisture Active Passive (SMAP) mission (Entekhabi et al., 2010) is proposing a high resolution (spatial = 9 km, temporal = 3 days) global soil moisture measurement (Das et al., 2011). Although the SMAP project offers promising application perspectives, the algorithm proposed for retrieving soil moisture from remote sensed signals imbeds a vegetation water content correction (Das et al., 2011).

A potential weakness of using remote sensed vegetation index in the algorithm utilized for deriving remote sensed soil moisture estimation is that once estimated in such a way it becomes questionable to reuse the estimated soil moisture in a vegetation growth model. Doing this may cause redundant information which may lead to conflicting conclusions. Recently, Chen et al. (2014) used remote sensed soil moisture and concluded a significant relationship with NDVI. Note that both variables involved in Chen et al. (2014)'s analysis are derived from satellite images. That is a typical case of the concern regarding possible redundant information. Our approach departs from Chen et al. (2014)

as we used land-based measurements of soil moisture. Indeed, our study aims to contribute to the understanding of relationships between vegetation growth patterns, soil moisture, precipitation, and temperature. A main point is to explore the relevance of coupling land-based records of soil moisture, temperature and precipitation for vegetation growth analysis. However, further studies may be necessary to compare the inclusion of remote sensed and land-based soil moisture in vegetation growth estimate.

Specifically in this study, we applied different statistical tools as well as entropy theory. Along with remotely sensed vegetation index series; land-based historical records of precipitation, temperature and soil moisture were considered to appraise patterns of vegetation growth in the Texas Gulf watershed. The effectiveness of coupling soil moisture, precipitation, and temperature was addressed by performing an entropy scaling analysis on two types of vegetation cover: deciduous forest and grassland. Month-wise analysis of vegetation growth was conducted. We applied an entropy-based clustering method to the growing season and the result was employed in a nested statistical model.

4.3. Data and theory

4.3.1. Data and study domain

The spatial domain studied is the Texas Gulf watershed (Figure 24) which spans approximately over 468,000 km^2. The watershed sustains important socioeconomic activities and encompasses diversified ecosystems (Jayakrishnan et al., 2004; Sohoulande Djebou et al., 2014). In this study, the period of 2000-2011 was considered and only the yearly vegetation-growing months of May, June, July, August and September (MJJAS)

were targeted (Slayback et al., 2003). The NDVI data used are developed and released vegetation type wise with a biweekly temporal resolution by the United States Geological Survey's Earth Resources Observation and Science USGS-EROS. Daily land-based measured soil moisture series (5 cm and 25 cm depth) were obtained from the North American Soil Moisture Database NASMD (Ford and Quiring, 2013). Daily precipitation and temperature (maximum and minimum) data were obtained from the National Oceanic and Atmospheric Administration's National Climatic Data Center NOAA-NCDC. For consistency regarding the NDVI series, daily precipitation, temperature and soil moisture series were rescaled to a biweekly temporal resolution. Finally, the study targeted height Landsat satellite scenes and their spatial domains (Figure 24 and Table 7). Two types of vegetation covers, deciduous forest and grassland, were considered. These two vegetation covers are heterogeneously represented across the study domain and their specific futures are described through the USGS Southwest Regional Gap Analysis Project (http://earth.gis.usu.edu/swgap). Additional information on the vegetation covers classification are reported by Homer et al. (2004, 2007) and Lowry et al. (2007).

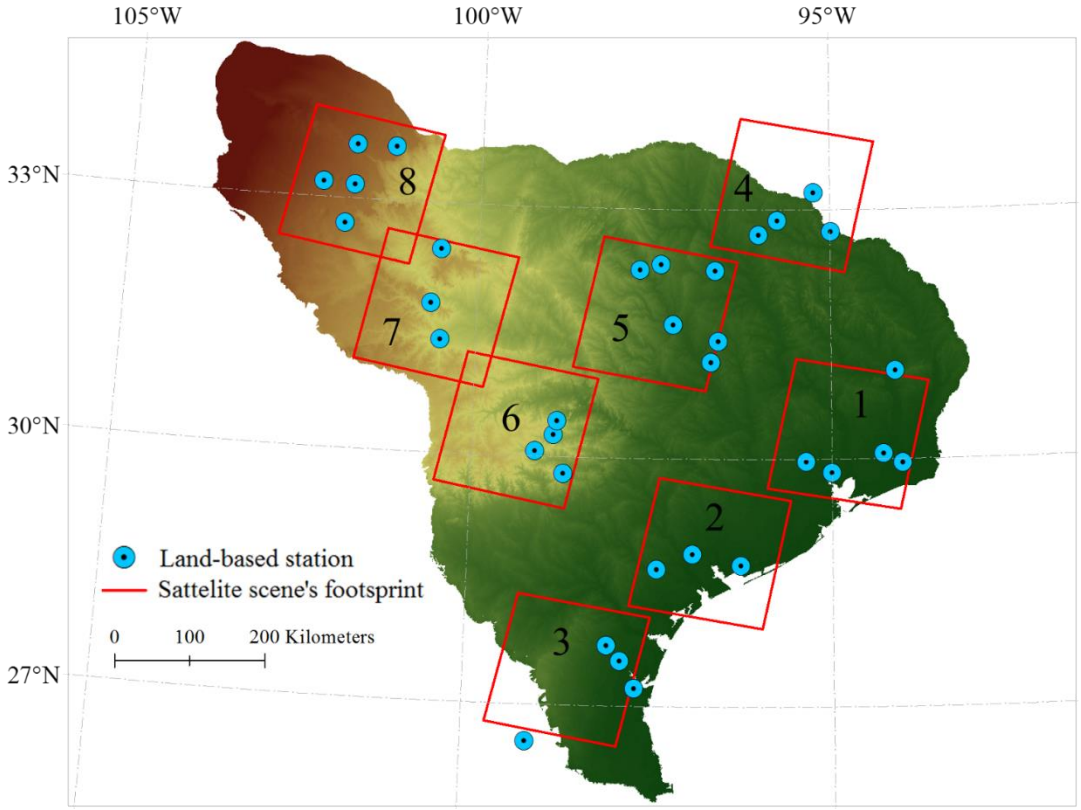

Figure 24 The Texas Gulf watershed showing the location for the land-based stations considered for the study. The location of each satellite scene considered is represented by the corresponding footprint

Table 7 Spatial characteristics of satellite scenes selected across the Texas Gulf watershed; the Worldwide Reference System 2 (WRS-2) identifies the selected satellite scenes shown in Figure 24. The geographic coordinates indicate the central point of each scene

Scene	WRS-2 References		Scene center's coordinates	
	Path	Row	Latitude (°N)	Longitude (°W)
1	25	39	30.3	-94.8
2	26	40	28.9	-96.7
3	27	41	27.4	-98.6
4	26	37	33.2	-95.6
5	27	38	31.7	-97.5
6	28	39	30.3	-99.4
7	29	38	31.7	-100.6
8	30	37	33.2	-101.7

4.3.2. Vegetation growth metrics

NDVI successfully captures plants photosynthesis activities as well as changes in canopy (Huete et al., 2002; Carlson and Ripley, 1997). These attributes made NDVI a reliable tool for quantifying vegetation growth. Besides the vegetation index series (NDVI), we considered two additional vegetation growth metrics, the $NDVI_{Ratio}$ and the $NDVI_{Slope}$ (Clinton et al., 2010; White et al., 1997). The objective was to identify a suitable metric for analysis. Based on the NDVI time-series, the $NDVI_{Ratio}$ at a specific time *t* can be defined as:

$$NDVI_{Ratio} = \frac{(NDVI_t - NDVI_{Min})}{(NDVI_{Max} - NDVI_{Min})} \quad (5)$$

$NDVI_t$ is the vegetation index at a time *t* while $NDVI_{Min}$ and $NDVI_{Max}$ are the minimum and maximum vegetation indices of the season, respectively. On the other side, $NDVI_{Slope}$ is computed as the difference between two consecutive vegetation index values divided by the time difference. Note that our methodology did not address vegetation dynamic in order to appraise any lag time influence. Yet the results obtained in the chapter 3 indicated that the optimum lags range from 6 to 12 days. Meanwhile the biweekly temporal resolution considered in this chapter, overlaps the optimum time lags, which therefore should not be a major concern.

4.3.3. Description of joint entropy

We employed joint entropy to address vegetation behavior based on precipitation, temperature and soil moisture. The joint entropy expresses the dependence between two or more variables. The relevance of entropy is its applicability to both linear and non-

linear systems (Singh, 2013). The joint entropy was applied to address the probabilistic relation between vegetation growth and the atmospheric variables (soil moisture, precipitation and temperature). Given the probability distribution of a variable X, the entropy $H(X)$ is expressed by:

$$H(X) = -\sum_{i=1}^{n} p\ (X_i) \log_2 [\ p\ (X_i)] \tag{6}$$

where $p(X_i)$ is the probability of event X_i; n is the number of possible events. The Probability Density Function PDF of variable X is addressed using discrete intervals for the values of X. In that approach, the discrete PDF is defined for n equal-width bins defined for the range of X. The entropy $H(X)$ is a measurement of information or uncertainty (Sohoulande Djebou et al., 2014; Singh, 2013), contained in the distribution of variable X. Similarly, entropy can be computed for a joint probability distribution of two or more variables. With three variables, the process for inferring the joint probability distribution is based on a three-way contingency analysis which we illustrated in Table 8. For each variable, events are categorized using n equal-width bins. The joint discrete PDF inferred from the three-way contingency analysis is utilized for the joint entropy estimate. Considering the three variables: (i) Precipitation (P), (ii) Soil moisture (SM) and (iii) Vegetation growth index (VI), the process generates a discrete PDF made of n^3 discrete probabilities such that:

$$\sum_{i=1}^{n}\sum_{j=1}^{n}\sum_{k=1}^{n} p(P = P_i,\ SM = SM_j,\ VI = VI_k) = 1 \tag{7}$$

The magnitude of information contained in the joint probability distribution can be determined by:

$$H(P, SM, VI) = -\sum_{i}^{n}\sum_{j}^{n}\sum_{k}^{n} p(P_i, SM_j, VI_k)\log_2[p(P_i, SM_j, VI_k)] \quad (8)$$

The joint entropy $\boldsymbol{H(P, SM, VI)}$ is the total information contained in the three variables. The maximum entropy occurs when the uncertainty is maximum and it corresponds to a scenario of uniform probability distribution $p(P_i, SM_j, VI_k) = \frac{1}{n^3}$. Singh (1997, 2011, 2013) discussed the relevance of entropy theory in environmental and water engineering. In the scheme of our study, Figure 25 illustrates the information shared within the coupled variables (*SM*, *P*) and *VI*. Moreover the same methodology was applied using the couplings of temperature and soil moisture (*T*, *SM*), temperature and precipitation (*T*, *P*) along with *VI*.

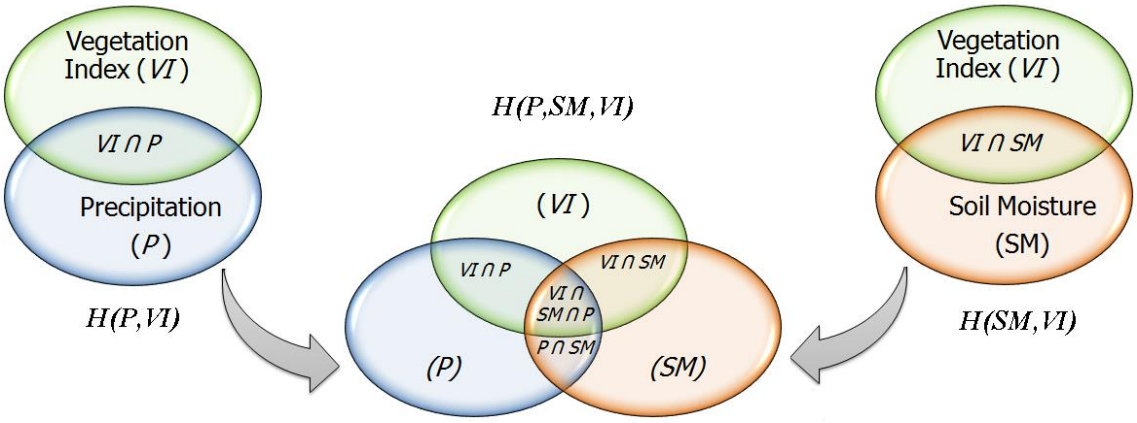

Figure 25 Schematic illustration of the joint entropy approach. H(P, SM, VI) stands for the three dimensional joint entropy including soil moisture and precipitation (P, SM) and vegetation growth index (VI). H(P, VI) and H(SM, VI) represent two dimensional joint entropies

Table 8 Illustration of a three-way contingency table employed to infer joint probability distribution. In this example we consider series X, Y and Z. Each variable is categorized into 2 classes (n=2). Observations are cross-classified and the discrete PDF is estimated

Variables			Discrete Probabilities
$X = \{X_1, X_2\}$	$Y = \{Y_1, Y_2\}$	$Z = \{Z_1, Z_2\}$	
$X = X_1$	$Y = Y_1$	$Z = Z_1$	$p\ (X=X_1, Y=Y_1, Z=Z_1)$
		$Z = Z_2$	$p\ (X=X_1, Y=Y_1, Z=Z_2)$
	$Y = Y_2$	$Z = Z_1$	$p\ (X=X_1, Y=Y_2, Z=Z_1)$
		$Z = Z_2$	$p\ (X=X_1, Y=Y_2, Z=Z_2)$
$X = X_2$	$Y = Y_1$	$Z = Z_1$	$p\ (X=X_2, Y=Y_1, Z=Z_1)$
		$Z = Z_2$	$p\ (X=X_2, Y=Y_1, Z=Z_2)$
	$Y = Y_2$	$Z = Z_1$	$p\ (X=X_2, Y=Y_2, Z=Z_1)$
		$Z = Z_2$	$p\ (X=X_2, Y=Y_2, Z=Z_2)$

4.4. Results and discussion

4.4.1. Entropy scaling of system vegetation, soil moisture, precipitation and temperature

In accordance with the objective stated earlier regarding the use of entropy scaling, this section presents the relationship between the probability distribution of vegetation index, soil moisture, temperature, and precipitation. NDVI series and each couple of the atmospheric variables were rescaled accordingly by using different time intervals. Hence, NDVI, temperature and soil moisture values were averaged to derive the value corresponding to each discrete time interval. The precipitation values were totalized for each time interval. Lotsch et al. (2003) and Liu et al. (2013) used similar approaches for identifying appropriate time scales for a vegetation and precipitation study. However, their methods were based on linear correlation analysis which requires a normality assumption on the variables in contrast with entropy theory which is applicable to any type of distribution (Singh, 1997, 2013). Prior to entropy computation, a spline interpolation (Rozhenko, 2010) was applied to the variables. Such an approach minimizes residuals (Duan et al., 1998) and allowed us to employ finer increments of time interval. The three dimensional relationships between NDVI and each couple of the atmospheric variables (soil moisture, precipitation, temperature) were evaluated independently for both grassland and deciduous forest at different time intervals. Graphs a and b, in Figure 26, present the entropy scaling for deciduous forest and grassland respectively. The fitted curves depict the trend and give an estimate of the entropy values with a coefficient of determination ($R^2 \geq 0.84$). The overall paradigms are very similar for deciduous forest and

grassland. Both entropy curves tend to converge gradually toward a maximum entropy state H_{Max}. These trends corroborate with the second law of entropy which states on the moving toward entropy maximization (Swenson, 1989). Therefore, coupling soil moisture, precipitation, and temperature is quite consistent for vegetation dynamic analysis in regard to the entropy law. Indeed, Dewar (2010) emphasized that the carbon balance of the ecosystems can be approximated to a steady state at a large time scale. Implicitly the steady state can be interpreted as the state of maximum entropy. From Figure 26, the computed actual entropy increases remarkably within 0 and 2 months-time intervals. Beyond 2 months, the increasing rate is moderate and becomes smoother toward 6 months. This overall trend indicates that finer time intervals provide more incremental information for studying vegetation dynamics. The analysis presented in the next sections considered a biweekly time scale which is more informative than the monthly time scale recently considered by Liu et al. (2013) for vegetation dynamic analysis.

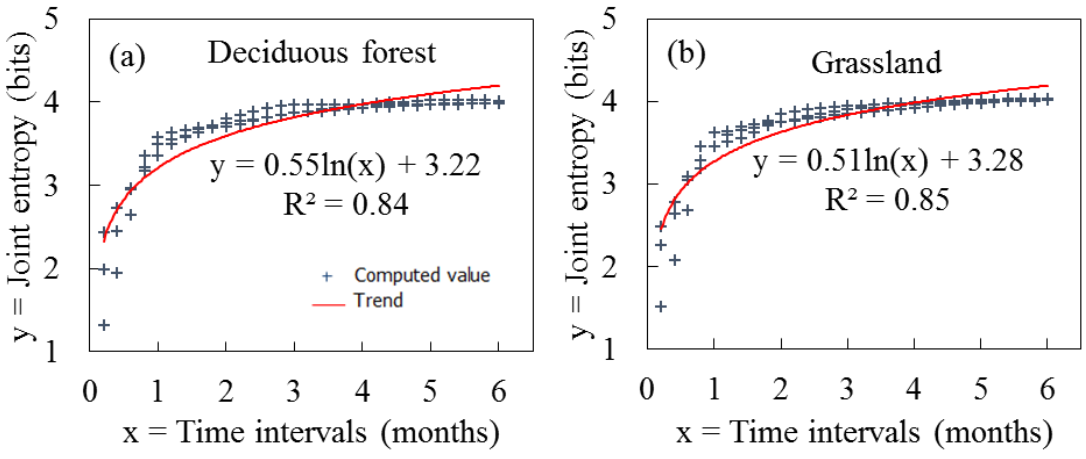

Figure 26 Three dimensional entropy scaling of vegetation index VI, precipitation P, temperature T and soil moisture SM. Approach based on joint entropy computation

4.4.2. Month-wise analysis of vegetation response to soil moisture, temperature and precipitation during the vegetation growth period

In this section, biweekly soil moisture, temperature, and precipitation series were analyzed to primarily identify the goodness of using each of the three vegetation metrics (NDVI, $NDVI_{Ratio}$, $NDVI_{Slope}$) indicated earlier in the methodology. Hence, we derived the biweekly vegetation metrics series and analyzed the correlation along with each of the atmospheric data series. The results are presented in Figure 27. Soil moisture series at 5 cm and 25 cm were highly correlated (R2>64). However, soil moisture at 5 cm showed higher correlation with vegetation growth in the case studied. The relationships presented in Figure 27 seems to depend on the month and the vegetation metric rather than on the vegetation type. The signals obtained indicated the capacity of NDVI to better depict the impact of each of the atmospheric variables (temperature, precipitation, soil moisture) on vegetation growth. However $NDVI_{Ratio}$ and $NDVI_{Slope}$ may be consistently involved in the vegetation dynamic in relation to temperature for particular months of the growing season, i.e., May for $NDVI_{Ratio}$ (R=-0.67) and July for $NDVI_{Slope}$ (R=-0.72). Compared to the entire growing season (Table 9), the month of May shows a lower mean daily temperature (23.22˚C) with a high variability (CV=0.09). Paradoxically, the month of July is characterized by a relative low temperature variability (CV=0.04). Indeed, Joseph et al. (2014) reported that high soil water content increases the temperature sensitivity of photosynthesis. From their results, we could infer the difficulty of explaining vegetation growth by focusing marginally on a single atmospheric variable. Figure 28 presents the

probability distribution of each of the variables considered in the study. With a 95% confidence interval, soil moisture and NDVI follow a truncated normal probability distribution, which is not the case for cumulative precipitation and temperature. This observation is relevant to highlight the use of entropy theory in our study. However, results obtained at this stage need to be considered with the climatic context of ecosystems in the Texas Gulf Watershed. In sum, one can infer from Figure 27 and Figure 28 that the vegetation growth patterns seem heterogeneous within the growing season months. This leads to the next section where we performed a clustering analysis in order to discriminate the growing season.

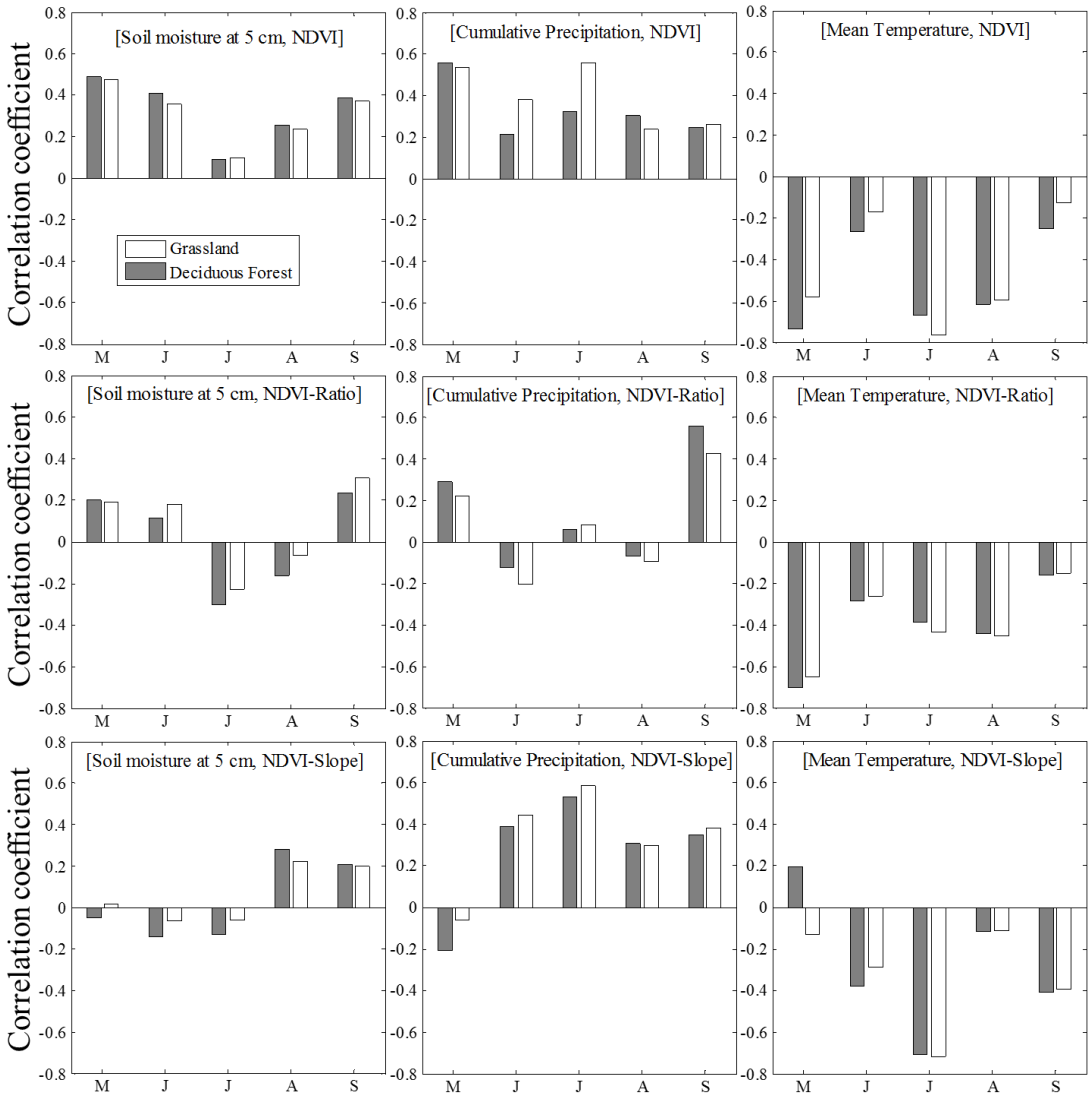

Figure 27 Analysis of NDVI, NDVIRatio, NDVISlope responses to soil moisture, precipitation and temperature for each month of the vegetation growing season (May, June, July, August and September).

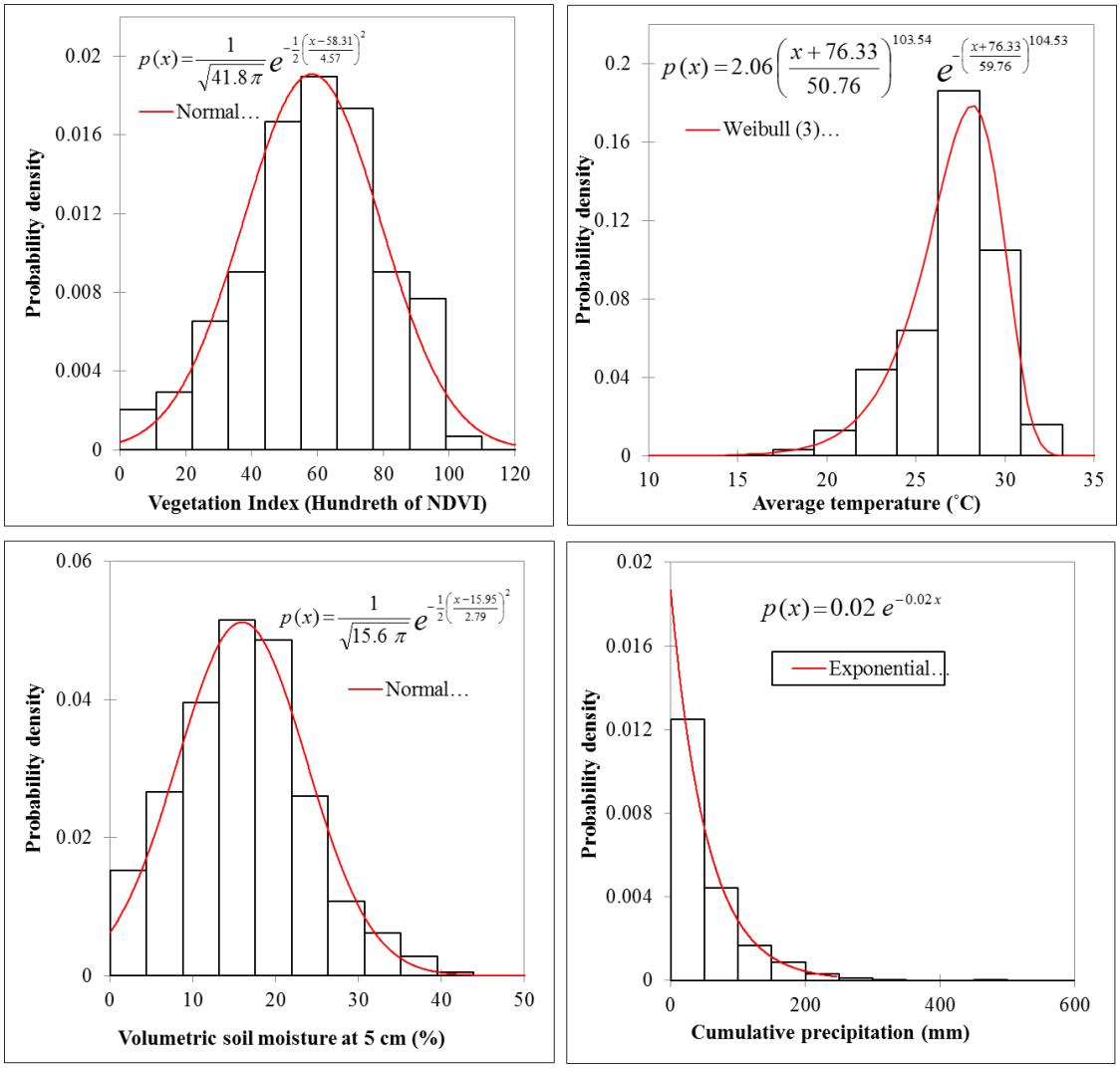

Figure 28 Probability Distribution of NDVI, soil moisture, temperature and cumulative precipitation.

Table 9 Summary of temperature series during the growing season; CV=coefficient of variation

	May	June	July	August	September
Average	23.22˚C	27.31˚C	29.02˚C	29.73˚C	27.27˚C
CV	0.094	0.061	0.040	0.043	0.056

4.4.3. Entropy-based clustering of vegetation growing seasons

In the previous section, the month-wise analysis showed different patterns of vegetation response to atmospheric variables during the growing season (May, June, July, August and September). Attempts to retrieve NDVI pooling all the months together led to poor statistical relationships. In this section we apply an entropy-based clustering method to discriminate the growing season. Our clustering method is derived from Ratkowsky (1984) and Krasovskaia (1997). Despite their usefulness, conventional hierarchical clustering methods are not designed to indicate the optimum number of clusters. To obtain the optimum number of clusters, Mojena (1977) described a statistical stopping rule for selecting partitions. However, Mojena's process was designed particularly for hierarchical clustering. Later, Ratkowsky (1984) proposed a stopping rule with wider application to hierarchical and nonhierarchical clustering methods. In his process, Ratkowsky (1984) employed the Jaccard similarity coefficient which measures the matching between two individuals X and Y by $J(X,Y)=\frac{|X \cap Y|}{|X \cup Y|}$. Ratkowsky (1984) proposed a criterion whose maximization indicated the optimum number of clusters. Krasovskaia (1997) used entropy theory and developed a clustering method which was somehow inspired from Ratkowsky's approach. However, the method proposed by Krasovskaia (1997) was typically designed for river flow regime classification. In this section, we emphasized Ratkowsky's method by using entropy theory. Compared with Krasovskaia (1997), our method seems simple and may have wider usage. Indeed, we employed the joint entropy to measure relationships between groups of variables. As mentioned in previous sections,

the entropy method provided consistent results regardless of the distribution patterns of variables (Krasovskaia, 1997).

Our entropy-based clustering has three steps. The first step consists of the computation of a *p* by *p* matrix of entropy-based similarity index. Note that *p* is the number of variables and in our case *p* is the number of months during the growing season (*p*=5). We present here our similarity index by using the example of mean temperature denoted as *T*. Given T_x and T_y, two mean temperature series for months *x* and *y* of the vegetation growing season, $x \text{ and } y \in \{May, June, July, August, September\}$, the corresponding similarity index $\rho_T(x, y)$ is defined as the ratio of the trans-entropy by the joint entropy:

$$\rho_T(x, y) = \frac{H(T_x) + H(T_y) - H(T_x, T_y)}{H(T_x, T_y)} \tag{9}$$

where $H(T_x)$ and $H(T_y)$ are the marginal entropy values for *x* and *y*, respectively. For *x*=*y*, $H(T_x, T_x) = H(T_x)$ as the joint distribution of two identical series is invariant. The numerator term stands for the trans-entropy. Our similarity index is probabilistic and inferred from the Jaccard similarity coefficient (Ratkowsky, 1984). The other two steps of our method can be referred at as within-group and inter-group steps. The clustering aimed to minimize the within-group dissimilarity while the inter-group's one should be higher. The within-group step leads to a pooled mean index value ρ_1. This step has only one stage where all the elements of the matrix obtained from the first step are averaged. The third step consists in clustering the growing season into *n* groups ($1 \le n \le p$). At each level of *n* groups, months in the same group and having the same average similarity index are

considered similar and assigned a unit similarity index for the inter-group similarity calculation, otherwise the initial index is conserved. A corresponding similarity index ρ_n is computed. Like Ratkowsky (1984), the stopping rule criterion $(\rho_n - \rho_1)/n^{1/2}$ is computed at each stage of this clustering process. Indeed the optimum number of groups is reached when the criterion attains a maximum value.

Table 10 presents the method and its application to the growing season based on each of the atmospheric variables (soil moisture, precipitation, temperature). The results indicate different clustering patterns depending on the atmospheric variable. Based on soil moisture or precipitation, the growing season can be optimally clustered in two groups, whereas the optimum number of clusters is three with temperature. The months of June and July appeared in the same clusters regardless of the atmospheric variable. However, the discriminating criteria is still maximum when we move from two to three clusters in both cases of soil moisture and precipitation. With this trade-off we could retain three clusters for all the three atmospheric variables: cluster M (month of May), cluster JJ (months of June and July), and cluster AS (months of August and September).

Table 10 Clustering the growing season month using an entropy based stopping rule process. The number of group at each stage of the process is n. *Optimum value of the discriminating criteria indicating the optimum number of clusters.

Soil moisture

	M	**J**	**J**	**A**	**S**
M	1	0.73	0.76	0.80	0.80
J	0.73	1	0.73	0.74	0.76
J	0.76	0.73	1	0.73	0.74
A	0.80	0.74	0.73	1	0.77
S	0.80	0.76	0.74	0.77	1
$\overline{\rho}$	0.82	0.79	0.79	0.81	0.81

n	ρ_n	$\rho_n - \rho_1$	$(\rho_n - \rho_1)/n^{1/2}$	Clusters
1	0.81	0	0	MJJAS
2	0.96	0.16	0.11*	MAS, JJ
3	1	0.19	0.11	M, JJ, AS
4	1	0.19	0.10	M,JJ, A, S
5	1	0.19	0.09	M, J, J, A,S

Cumulative biweekly precipitation

	M	**J**	**J**	**A**	**S**
M	1	0.75	0.76	0.77	0.70
J	0.75	1	0.81	0.80	0.76
J	0.76	0.81	1	0.80	0.78
A	0.77	0.80	0.80	1	0.76
S	0.70	0.76	0.78	0.76	1
$\overline{\rho}$	0.80	0.82	0.83	0.83	0.80

n	ρ_n	$\rho_n - \rho_1$	$(\rho_n - \rho_1)/n^{1/2}$	Clusters
1	0.81	0	0	MJJAS
2	0.96	0.15	0.11*	MS, JJA
3	1	0.19	0.11	M, JJ, AS
4	1	0.19	0.09	M, JJ, A,S
5	1	0.19	0.08	M, J, J, A,S

Temperature

	M	**J**	**J**	**A**	**S**
M	1	0.71	0.71	0.77	0.67
J	0.71	1	0.71	0.76	0.70
J	0.71	0.71	1	0.77	0.69
A	0.77	0.76	0.77	1	0.68
S	0.67	0.70	0.69	0.68	1
$\overline{\rho}$	0.77	0.78	0.78	0.80	0.75

n	ρ_n	$\rho_n - \rho_1$	$(\rho_n - \rho_1)/n^{1/2}$	Clusters
1	0.77	0	0	MJJAS
2	0.91	0.13	0.09	MJJ, AS
3	0.96	0.18	0.11*	M, JJ, AS
4	1	0.23	0.11	M,JJ, A, S
5	1	0.23	0.10	M, J, J, A,S

4.4.4. Estimate of vegetation growth from soil moisture, temperature and precipitation

Using monthly cumulative precipitation, mean temperature, and soil moisture series as independent variables, we first derived bivariate statistical models for *VI* estimate. Analyses were performed using each of the three clusters identified in section 3.3. In most cases, linear fitting of the NDVI series to precipitation, temperature or soil moisture series resulted in poor correlation coefficients and high root mean square errors which indicate weak accuracy. To comprehend such results, it is necessary to recall plant physiology sustaining primary production. In fact, the vegetation growth can be summarized by the simple balance between leaf transpiration and photosynthesis. However, this flux describing plant growth depends on stomatal conductance and may not be monotonic in relation to atmospheric variables (Duursma et al., 2014). For example, the temperature sensitivity of photosynthesis increases up to an optimum and later decreases when the temperature gets higher (Duursma et al., 2014). Cluster-wise, we attempted a two dimensional fitting using NDVI as predictand and each of the atmospheric variables as predictor. We noted that a simple logarithmic transformation on precipitation series gave a better relationship with vegetation index for both deciduous forest and grassland. With soil moisture and temperature, a quadratic model exhibited a better fitting. However a power transformation revealed a stronger relationship between NDVI and soil moisture particularly for cluster AS. Results, for both deciduous forest and grassland, are presented in Table 11. The overall patterns are similar for both vegetation types. In contrast, discrepancies are more notable from one cluster to another. Later, we proposed a nested statistical model (Figure 29) for retrieving NDVI by coupling atmospheric

variables. Different candidate equations were tested to fit Vegetation Index (*VI*) by coupling pair-wise soil moisture (*SM*), Temperature (*T*) and Precipitation (P). The fitting procedure aimed to minimize the sum of squared residuals. The ensemble *E* of candidate equations can be summarized as:

$$E = \{VI_{SM,P} = f(SM,P);\ VI_{SM,T} = f(SM,T);\ VI_{T,P} = f(T,P)\} \quad (10)$$

Likewise, analysis was performed with each cluster (M, JJ, AS). For both deciduous forest and grassland, we obtained the best fitting by combining pair-wise logarithmically transformed precipitation with a second degree polynomial of soil moisture and temperature (Table 12). In particular, during the months of June and July (cluster JJ), the coupling of soil moisture and temperature provided an estimate of NDVI with R^2=0.68 for deciduous forest and R^2=0.62 for grassland. However, the relation was weaker during August and September (cluster AS). The nested model proposed is explicitly presented in Figure 29. Table 12 reports the performance of the model. The RMSE values indicate an overall better accuracy for the estimates during the months of May, June and July. The three dimension scatter-plots of the couplings are presented in Figure 30. Compared to the coupling (*SM, T*) or (*P, T*), the coupling (*SM, P*) seems to underestimate high values of *VI*. In fact, plant growth is naturally regulated by certain limiting factors. Hence, a minimum temperature, solar energy, and water content are required to stimulate the growth of most plants (Duursma et al., 2014; Joseph et al., 2014; Szeicz, 1974). While the solar energy flux may not be a limiting factor during the growing season (Szeicz, 1974), the condition on temperature and soil water content may play a determinant role by affecting photosynthesis. Therefore, the biophysical interpretation of

our results requires an understanding of the continuum of soil, water and plant. Indeed, the fraction of soil water available for plants is the difference between the water content at field capacity and the one at the permanent wilting point. However, plants ability to uptake water is related to the pressure at which the water is attached to the soil particles. Richards and Weaver (1943) determined the permanent wilting point as 15 bar for most of plants, while the field capacity was 0.33 bar (Ritchie, 1981; Slatyer, 1957). The corresponding volumetric soil moisture varies depending on the soil type (Richards and Weaver, 1943), i.e., a clay soil compared to sandy soil. Soil type characterization may be a critical component which could be used along with soil moisture in models for describing and simulating vegetation growth. Therefore, future research on the topic may consider the spatial variability of soil type.

Table 11 Bivariate fitting of deciduous forest and grassland's NDVI series. Analyses are conducted cluster-wise for each type of vegetation with each of the atmospheric variables (soil moisture SM, cumulative precipitation P, mean temperature T). Quadr.= quadratic, Corr.=correlation., Equ. = equation

	Deciduous Forest								
	VI=f(SM)			**VI=f(P)**			**VI=f(T)**		
Cluster	M	JJ	AS	M	JJ	AS	M	JJ	AS
Equ.	Quadr.	Quadr.	Power	Log	Log	Log	Linear	Quadr.	Quadr.
Corr.	0.54	0.73	0.69	0.65	0.35	0.30	0.73	0.63	0.36
P value	<0.01	<0.01	<0.01	<0.01	<0.05	<0.05	<0.01	<0.01	<0.05
	Grassland								
	VI=f(SM)			**VI=f(P)**			**VI=f(T)**		
Cluster	M	JJ	AS	M	JJ	AS	M	JJ	AS
Equ.	Quadr.	Quadr.	Power	Log	Log	Log	Linear	Quadr.	Quadr.
Corr.	0.50	0.64	0.55	0.55	0.52	0.32	0.58	0.66	0.40
P value	<0.05	<0.01	<0.01	<0.01	<0.01	<0.05	<0.01	<0.01	<0.01

Table 12 Summarizing the results of the nested model. VI = Vegetation Index; P = Precipitation; T=Temperature; SM = Soil Moisture; Corr. = correlation coefficient; RMSE = Root Mean Square Errors.

	Deciduous Forest					
	Cluster M		Cluster JJ		Cluster AS	
	Correlation	RMSE	Correlation	RMSE	Correlation	RMSE
VI = f (SM, P)	0.71	0.13	0.73	0.12	0.39	0.21
VI = f (P, T)	0.78	0.11	0.63	0.14	0.38	0.21
VI = f (SM, T)	0.88	0.09	0.83	0.10	0.44	0.20
	Grassland					
VI = f (SM, P)	0.63	0.14	0.71	0.14	0.38	0.26
VI = f (P, T)	0.63	0.14	0.70	0.14	0.41	0.26
VI = f (SM, T)	0.76	0.12	0.79	0.12	0.46	0.25

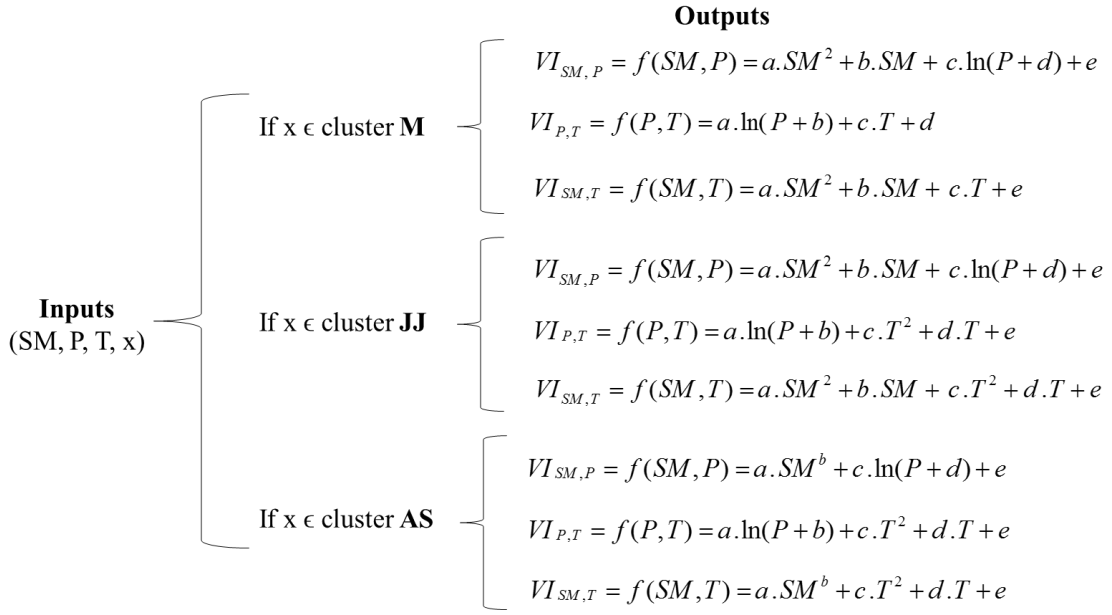

Figure 29 Diagram presenting the nested statistical model used for vegetation index VI estimate. SM = Soil Moisture a 5 cm, P=Cumulative Precipitation, T=Mean Temperature, x=month of the growing season; a, b, c, d, e are the parameters identified base on a least square errors approach

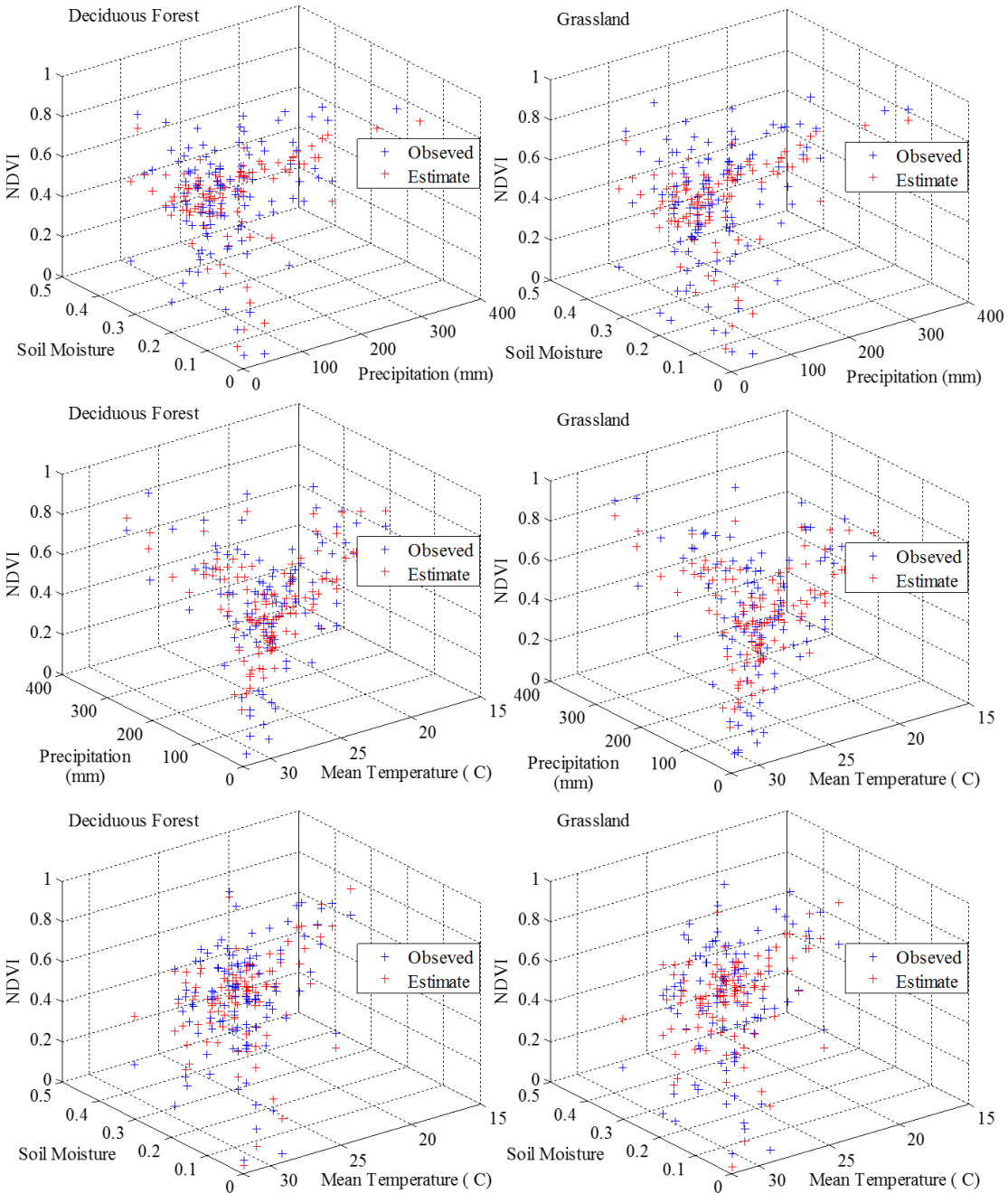

Figure 30 Three dimensional scatter-plots of Vegetation Index (NDVI) as a function of coupled atmospheric variables [soil moisture (SM), precipitation (P) and temperature (T)].

4.5. Synthesis and conclusions

Application of entropy illustrates the consistency of coupling soil moisture, temperature and precipitation for vegetation growth analysis. The three dimensional joint entropy analysis reveals that finer temporal scales are more informative. Interestingly, the overall relationships with both deciduous forest and grassland NDVI series show similarity confirming a conclusion recently reported by Liu et al. (2013). Indeed, Liu et al. (2013) indicated similitude in NDVI response to climate variables regardless of the vegetation type. However, the three vegetation metrics tested in our study, exhibit interesting vegetation growth patterns which significantly differ according to the growing season's month and the atmospheric variable. Despite the overall relevance of the raw NDVI series, the $NDVI_{Ratio}$ gave interesting signals with temperature series during the month of May while $NDVI_{Slope}$ had its highest signal with July's temperature series. Note that for the location considered, May has the lower mean daily temperature of the growing season. In addition, the temperature during May seems very unstable (highest variability), while July is warmer with the lowest variability. Such an observation seems interesting and could be fully addressed through further studies.

Although the consistency of coupling atmospheric variables is demonstrated, attempts to retrieve vegetation growth pattern by assuming a total exchangeability of the growing season months lead to poor relationships. The entropy-based clustering method proposed, discriminate the growing season into three clusters. We distinguish cluster M (May), cluster JJ (June and July) and cluster AS (August and September).

Marginally, each of the atmospheric variables studied shows a relatively poor linear relationship with NDVI. In biophysical processes, it is common to observe non-linear relationships between factors even if they appear to interact. Through variable transformation, we are able to extract significant relationships which lead to statistical models employed for retrieving vegetation growth patterns. Coupling the atmospheric variables, we propose a nested statistical model for retrieving vegetation growth patterns. However, there is a discrepancy of RMSE depending on the cluster, coupled atmospheric variables and vegetation types. The coupling of soil moisture and temperature is able to explain up to 68% and 62% of vegetation index variation for deciduous forest and grassland, respectively. Although our study is constrained by the environmental and climate conditions of the ecosystems in the Texas Gulf watershed, results can be extended in order to improve the use of soil moisture measurement in land-atmosphere models. However, the models established using the coupling of atmospheric variable may also be relevant for downscaling remote sensed vegetation growth patterns. Despite this general remark, it is important to recall the discrepancies mentioned earlier regarding the magnitudes of the statistical relationships obtained suggesting more research efforts on the topic. In summary, we highlight the following conclusions:

(i) The entropy scaling of NDVI, soil moisture, temperature and precipitation reveal common patterns, showing the goodness of coupling atmospheric variables for vegetation dynamic.

(ii) Vegetation response to atmospheric variables varies very much during the growing season period. Therefore, it may be wise to cluster the growing season while conducting a vegetation dynamic study.

(iii) Soil moisture and temperature seem consistently coupled for vegetation dynamic studies at finer temporal resolution. i.e, soil moisture and temperature series could be relevant for vegetation growth appraisal at finer time scales, while precipitation may be interesting to address vegetation patterns at seasonal and inter-seasonal scales (Ichii et al., 2002; Kawabata et al., 2001; Knapp and Smith, 2001).

The results obtained, using the spatial domain of the Texas Gulf watershed, are supported by previous studies conducted in similar climatic regions of the globe. The scope of our conclusions may be extended at a regional level and considered wisely in vegetation dynamics as well as water resources studies. However, a transition toward continental and global stage may require additional research efforts. Therefore, further study on this topic are encouraged and should address diversified ecosystems, vegetation types and involve as well long-term remote sensed and land-based measurement data.

CHAPTER V

IMPACT OF CLIMATE CHANGE ON PRECIPITATION PATTERNS: A COMPARATIVE APPROACH

5.1. Synopsis

Impacts of climate change on precipitation are usually reported in time and space but seem insufficiently described for use in water resources management and planning. Although customary trend and extreme event analyses are essential, they may not be sufficient to determine the ampleness of changes due to climate change. Our study addresses the effect of climate change on precipitation patterns. Specifically, we employ parsimonious methods to examine changes over the entire ranges of monthly precipitation total and number of events (>3mm). We consider a regional climate model simulation of historical (1971-2000) and future (2041-2070) precipitation series across the Texas Gulf watershed. The precipitation series are bias corrected. We explore different technics frequently involved in impact analysis and resorted limitations. We then propose and use a probabilistic approach to depict the magnitudes of plausible effects of climate change. Finally, we infer temporal changes in seasonal precipitation regimes. The temporal variability of changes is remarkable across the watershed, suggesting important spatial weights. Whereas it is not a substitute for other approaches, our probabilistic method is useful for a better understanding of critical changes in precipitation amounts and occurrences under climate change spectra.

5.2. Introduction

Climate factors are often characterized by cyclic patterns and it is common to associate the range of precipitation events with seasonality. In most of terrestrial biomes, this seasonality plays a critical role and determines the dynamics of plants and animal populations (Sillett et al., 2000). Precipitation characteristics, such as amount, duration, intensity and frequency, vary from year to year and are driven by climatic factors at the regional and continental scales (Cai et al., 2014; Wehner, 2013). That is the case with the North American Monsoon (NAM) that controls summer precipitation in North America (Higgins and Shi 2001). Similar schemes are noticeable across the globe, as precipitation regimes are characterized, to some extent, by cyclic variations with certain return periods. However, non-cyclic anomalies are becoming more evident these days, perhaps due to climate change (Cai et al., 2014; Huntington, 2006; Dore, 2005). Therefore, it is important that the cyclic patterns do not mask the influence of climate change (e.g. Cai et al., 2014; raised such concern regarding the millennium drought recently experienced in Australia).

The climate change signals have started to receive increasing attention in recent years. Even though studies on climate change impact have been increasingly reported worldwide, the approaches employed in the assessment have mainly focused on extreme events and risk analyses (Tohver et al., 2014; Ahmed et al., 2013; Haylock et al., 2006; Dore, 2005). Further, long-term statistics, including trend analyses and jump detection, are applied to precipitation series (Kalra and Ahmad, 2011; Hamed, 2008; Haylock et al., 2006). However, the future effects of climate change on water resources are still being debated (Lespinas et al., 2014; Groves et al., 2008). Several authors emphasize the scheme

of climate change with higher occurrences of extreme events (Chiew et al., 2009; Dore, 2005). Likewise, shifts in the precipitation seasonality are observed in different parts of the globe (Regonda et al., 2005). It seems therefore logical to partition the effects that are attributable to climate change under the circumstances where regular cyclic patterns are known to embed variability as well. Meanwhile, model simulations are useful for addressing the effects of climate change on water resources (Butcher et al., 2014).

For water resource management, it is essential to address the impacts of climate change by considering the watershed as a functional unit. At the watershed scale, local characteristics, such as basin topography and vegetation cover, are reported to have significant effects on precipitation distribution (Sohoulande Djebou et al., 2014). In addition, some of these characteristics are interactive, compounding the complexity of factors driving changes in precipitation regimes. This makes the inclusion of plausible climate change effects in water resources management, challenging (Groves et al., 2008). Usually, the approaches employed to quantify the impact of climate change focus on extreme precipitation events, often neglecting other events. Recently, Ntegeka et al. (2014) employed a quartile change analysis to address climate change impact on precipitation series. Their method of analysis is interesting as it sheds light on different aspects of future perturbations based on individual quartile range. This suggests that it may be necessary to employ more diversified approaches in climate change impact assessment. Our study expounds technics regularly used in climate change impact assessment, then we highlight limitations. Upon these technics, we propose a probabilistic impact analysis. Specifically, we report a probabilistic assessment of climate change

impact on precipitation. We examine alterations of precipitation characteristics across the Texas Gulf watershed. The study describes an explanatory approach for addressing changes in seasonal precipitation patterns. The analysis is done within the realm of climate change based on regional climate model simulations. We also employ a bias correction for the precipitation series (Ahmed et al., 2013; Wood et al., 2002).

5.3. Methodology

The methodology consists of the following steps: (1) Data and study region, (2) bias correction, (3) pooled analysis of changes in precipitation patterns, (4) non-parametric analysis of changes in precipitation across precipitation ranges, and (5) probabilistic estimates of changes in precipitation patterns. Each of these steps is now discussed.

5.3.1. Data and study region

The study area considers the Texas Gulf watershed that is characterized by a wide range of ecosystem and climatic features. We employ model generated precipitation series for two time periods: 1971-2000 (historical) and 2041-2070 (future). We obtain the precipitation data from the North American Regional Climate Change Assessment Program NARCCAP. The NARCCAP releases a number of regional climate model (RCM) simulations over the conterminous United States for historical and future periods (Wehner, 2013). Specifically, RCM's future climate simulations are driven by the Special Report on Emissions Scenario SRES-A2 (Nakicenovic et al., 2000). The SRES-A2 scenario is based on the assumptions that include a world population reaching ten billions by 2050, a regionally oriented economic development, a projected CO_2 concentration of

575 ppm by 2050 and of 870 ppm by 2100 (Nakicenovic et al., 2000). The RCM's historical and future simulations of the NARCCAP have been frequently employed to address the impact of climate change on water resources in the North American region (Mearns et al, 2012; Bürger et al., 2011).

We utilize the NARCCAP RCM3-GFDL ensemble model simulations which revealed consistency for precipitation studies in the various regions of North America (Ahmed et al., 2013). The ensemble RCM3-GFDL encompasses uncertainties related to boundary conditions defined by the Geophysical Fluid Dynamics Laboratory (GFDL) (Mearns et al, 2012). The RCM3-GFDL precipitation series are gridded data, available for historical (1971-2000) and future (2041-2070) periods with a 50 km spatial resolution. The time slices for RCM3-GFDL products are predefined. The data are available for transient runs which is a limitation for exploring a wider period. Mearns et al. (2012) analyzed the goodness of the NARCCAP's ensemble outputs based on individual grid cells and addressed seasonality by distinguishing winter DJF (December-January-February), spring MAM (March-April-May), summer JJA (June-July-August), and autumn SON (September-October-November) precipitation. Likewise, we selected and addressed 25 grid cells across the Texas Gulf watershed (Figure 31 and Table 13). For ease of presentation, we find it convenient to select representative grid cells. Hence, we apply a k-means clustering to the precipitation series of the 25 grid cells (Hartigan and Wong, 1979) and identify two clusters (Table 13). The clustering displays a clear spatial pattern as we could note from Figure 31 that the cluster 1 encompasses isohyets of mean annual precipitation varying within 700 and 1400 mm, while the isohyets corresponding

to cluster 2 vary within 500 and 700 mm. From clusters 1 and 2 we retain grid cells A and H, Q and X. Meanwhile, bias correction was critical to improve the accuracy of the RCM3-GFDL precipitation series (Bürger et al., 2011). To set the parameters of the bias correction algorithm, we use land-based precipitation series obtained from the National Oceanic and Atmospheric Administration's Global Historical Climatological Network database NOAA-GCHN. We identify 25 precipitation stations with respect to each of the grid cells. However, by pairing the RCM3-GFDL's daily precipitation series with the selected land-based station, we note discrepancies in the occurrence sequences. This is inherent in model simulations in general (Weichert and Bürger, 1998). To remedy this problem and get a better fitting, we consider daily average values for the months. We now discuss the bias correction procedure in the next section.

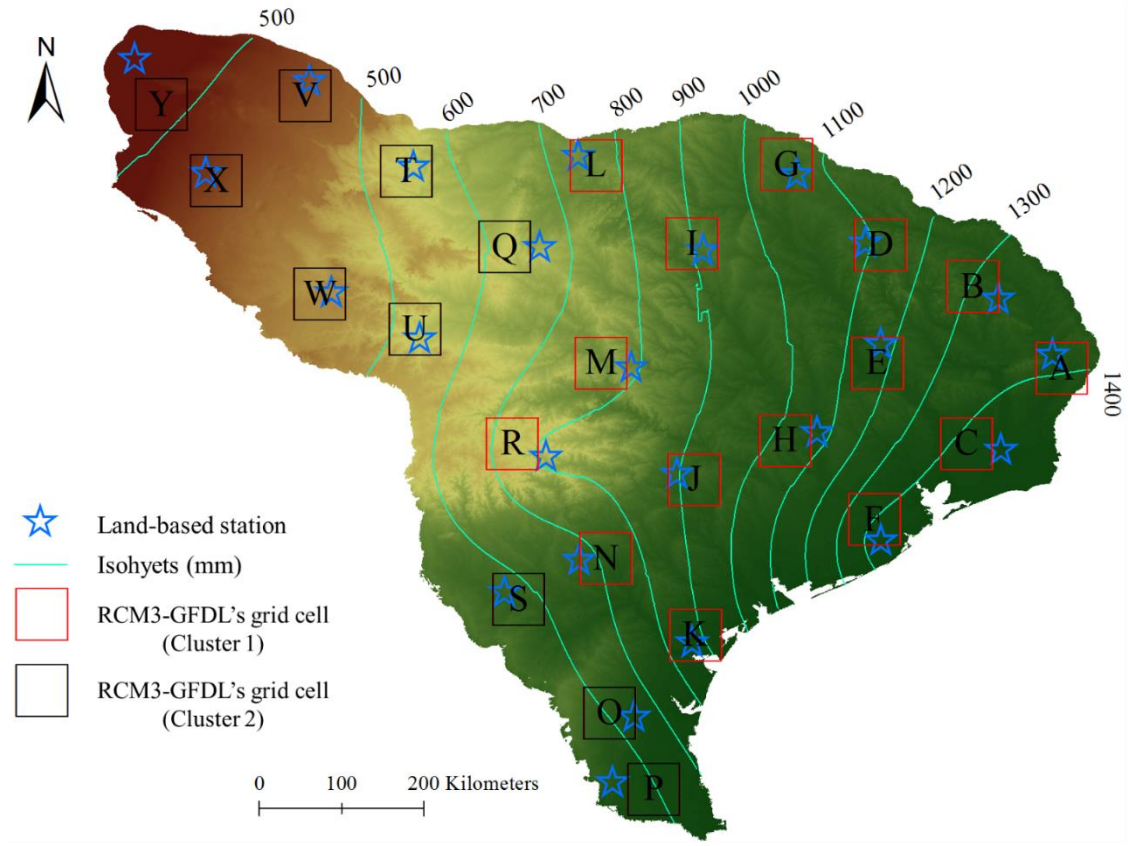

Figure 31 Map of the Texas Gulf watershed showing the selected RCM3-GFDL grid cells (referred to by letters), the land-based precipitation stations considered for the bias correction and the annual precipitation gradient

Table 13 References corresponding to the selected grids in the Texas Gulf watershed

GRID	Lat	Long	RCM3 Ref.		Cluster	GRID	Lat	Long	RCM3 Ref.		Cluster
			yc	xc					yc	xc	
A	31.02	266.52	14	73	1	N	28.94	261.54	9	63	1
B	31.92	265.55	16	71	1	O	27.24	261.58	5	63	2
C	30.20	265.48	12	71	1	P	26.40	262.06	3	64	2
D	32.38	264.54	17	69	1	Q	32.35	260.43	17	61	2
E	31.08	264.51	14	69	1	R	30.20	260.52	12	61	1
F	29.36	264.47	10	69	1	S	28.49	260.58	8	61	2
G	33.26	263.52	19	67	1	T	33.19	259.35	19	59	2
H	30.23	263.50	12	67	1	U	31.45	259.45	15	59	2
I	32.39	262.49	17	65	1	V	34.01	258.25	21	57	2
J	29.80	262.51	11	65	1	W	31.84	258.41	16	57	2
K	28.10	262.52	7	65	1	X	33.08	257.28	19	55	2
L	33.25	261.44	19	63	1	Y	33.91	256.67	21	54	2
M	31.08	261.49	14	63	1						

5.3.2. Bias correction procedure

Systematic bias is often associated with climate model outputs. In some cases, bias can mislead to conclusions regarding climate impact analysis (Ahmed et al., 2013; Piani et al., 2010). For that reason, bias correction becomes essential in climate modeling. A wide range of algorithms have been used for bias correction. Piani et al. (2010) proposed a histogram equalization method for bias correction of precipitation series that has shown potential for application in water resources for several regions of the globe. We chose to remove the bias from the RCM3-GFDL series by applying the algorithm suggested by Piani et al. (2010). Considering the model simulated and corrected precipitation series as P_{mod} and P_{cor}, respectively, the algorithm used is defined by:

$$P_{cor} = a + b P_{\mathrm{mod}} \tag{11}$$

$$P_{cor} = (a + b\,P_{\mathrm{mod}})\,[1 - Exp\,(-(P_{\mathrm{mod}} - P_0)/\tau)] \qquad (12)$$

where *a, b, P_0,* and τ are the parameters. In equation (11), *a* and *b* simply represent the intercept and the coefficient for a linear regression. In equation (12), τ is a rate factor, and *a* and *b* are related to P_0 through the relation $P_0 = -a/b$ which is known as the dry day correction factor. Whereas both equations (11) and (12) are valuable for bias correction for daily precipitation series, equation (12) is less parsimonious. At individual grid cells and for each month of the year, we apply equation (11) or (12) by preferring the one providing lower root mean squared errors (RMSE). In equation (12), we estimate the parameters by addressing the objective function that aims to minimize the RMSE; results for grids A, H, Q and X are recapitulated in Table 14. The parameters in the algorithm are set month-wise by fitting land-based precipitation series and the RCM3-GFDL historical simulation. Finally, at each grid cell, we utilize the set parameters and correct the historical and future precipitation series.

Table 14 Estimated parameters for the bias correction algorithm [equation (5.2)]; example with grid cells A, H, Q and X are presented.

	Parameter	JAN	FEB	MAR	APR	MAY	JUN	JUL	AUG	SEP	OCT	NOV	DEC
	a	-0.22	-0.48	-0.49	-0.48	-0.47	0.5	-0.48	-0.49	-0.47	-0.47	-0.46	-0.47
	b	0.01	0.01	0.01	0.01	0.01	0.5	0.01	0.01	0.01	0.01	0.01	0.01
A	P_0	22.00	48.00	49.00	48.00	47.00	-1.00	48.00	49.00	47.00	47.00	46.00	47.00
	τ	6	20	20	20	18	2	22	24	22	22	18	18
	RMSE	2.68	2.51	1.79	2.13	2.37	2.95	1.77	2.02	1.83	2.54	2.89	2.31
	a	-0.45	-0.47	-0.49	0.5	-0.47	-0.49	-0.49	-0.49	-0.49	-0.48	-0.48	-0.39
	b	0.03	0.01	0.01	0.41	0.01	0.01	0.01	0.01	0.01	0.01	0.01	0.02
H	P_0	15.00	47.00	49.00	-1.22	47.00	49.00	49.00	49.00	49.00	48.00	48.00	19.50
	τ	6	24	24	2	18	20	30	28	22	22	22	8
	RMSE	1.92	1.80	1.52	1.62	2.03	2.59	1.47	1.63	1.99	3.57	2.17	1.46
	a	0.28	0.32	0.5	-0.31	0.5	-0.48	-0.48	-0.48	-0.49	-0.48	-0.37	-0.06
	b	0.07	0.06	0.03	0.01	0.25	0.01	0.01	0.01	0.01	0.01	0.02	0.01
Q	P_0	-4.00	-5.33	-16.67	31.00	-2.00	48.00	48.00	48.00	49.00	48.00	18.50	6.00
	τ	2	2	2	20	2	28	28	24	34	34	18	2
	RMSE	0.31	0.46	0.51	0.80	1.05	1.33	1.53	1.53	1.17	1.65	0.48	0.53
	a	-0.49	-0.39	-0.32	-0.48	-0.46	-0.48	-0.32	-0.48	-0.49	-0.44	-0.48	-0.42
	b	0.01	0.03	0.02	0.01	0.01	0.01	0.01	0.01	0.01	0.01	0.01	0.04
X	P_0	49.00	13.00	16.00	48.00	46.00	48.00	32.00	48.00	49.00	44.00	48.00	10.50
	τ	52	8	10	34	22	26	24	34	28	24	42	8
	RMSE	0.57	1.19	0.64	1.12	1.88	1.25	0.84	1.31	2.18	1.73	0.83	0.91

5.3.3. Pooled analysis of changes in precipitation pattern

Very often, the effect of climate change on precipitation series is inferred, based on mean and variance (Dore, 2005). However, these two statistics are not sufficient to represent some critical features that are attributable to climate change. Table 15 resumes a comparative analysis of future and past precipitation series for seasons of DJF, MAM, JJA and SON. The pooled averages show changes which we evaluated by performing a Student's t test of independence of means. Indeed, previous authors explored changes using the t test. E.g. Cai et al. (2014) employed the t test to evaluate the significance of seasonal precipitation decrease in Australian regions. Our results show significant differences between past and future monthly precipitation totals and monthly numbers of events (>3mm) during seasons MAM, JJA and SON. Paradoxically, the changes during DJF are not significant. As stated earlier, analysis in Table 15 is informative but may not be strong enough to conclude the changes observed. A boxplot analysis may be useful to clear potential weighing factors shaded in the analysis. In Figure 32, we present boxplots of monthly precipitation totals for the 25 grid cells series. Due to the high discrepancies between precipitation ranges across the Texas Gulf watershed (Figure 31), data transformation is necessary for a standard comparative analysis. Therefore, we employ the percentage precipitation changes, which quantify the departure from the long term mean (Tebaldi et al., 2004) defined as:

$$\Delta_{P_i} = 100.\frac{P_i - \mu_P}{\mu_P} \tag{13}$$

P_i is a given precipitation value, μ_P is the long term mean and Δ_{P_i} is the corresponding percentage precipitation change.

Figure 32 shows some clustering of outliers foreshadowing the existing changes between past and future precipitation series. Particularly, these clustering patterns are remarkable during the DJF season (Figure 32) which we previously presented with no significant changes through the analysis of mean values. Such configuration is frequent in precipitation data analysis and points to further appraisal.

Table 15 Comparison of RCM3-GFDL's historical and future precipitation series in the Texas Gulf watershed. The monthly precipitation total and number of events (>3mm) are considered for seasons DJF, MAM, JJA and SON. μ=monthly mean, σ=standard deviation, and CV=coefficient of variation

		Monthly PREC (mm)		Number of events (PREC>3mm)	
		1971-2000	2041-2070	1971-2000	2041-2070
μ	DJF	56.85[a]	57.48[a]	4.47[a]	4.41[a]
	MAM	109.96[a]	103.41[b]	8.88[a]	8.09[b]
	JJA	104.08[a]	96.35[b]	9.67[a]	8.45[b]
	SON	66.32[a]	75.29[b]	5.18[a]	5.45[b]
$CV = \frac{\sigma}{\mu}$	DJF	0.69	0.73	0.60	0.58
	MAM	0.66	0.76	0.55	0.62
	JJA	0.93	1.02	0.77	0.85
	SON	1.07	1.13	0.73	0.77

Student's t-test for independent means, performed to compare the historical mean and the future mean of monthly precipitation total, monthly number of precipitation events>3mm; (a, b) indicates the rejection of the null hypothesis of mean equality with 95% confidence, otherwise both means are labeled with (a, a).

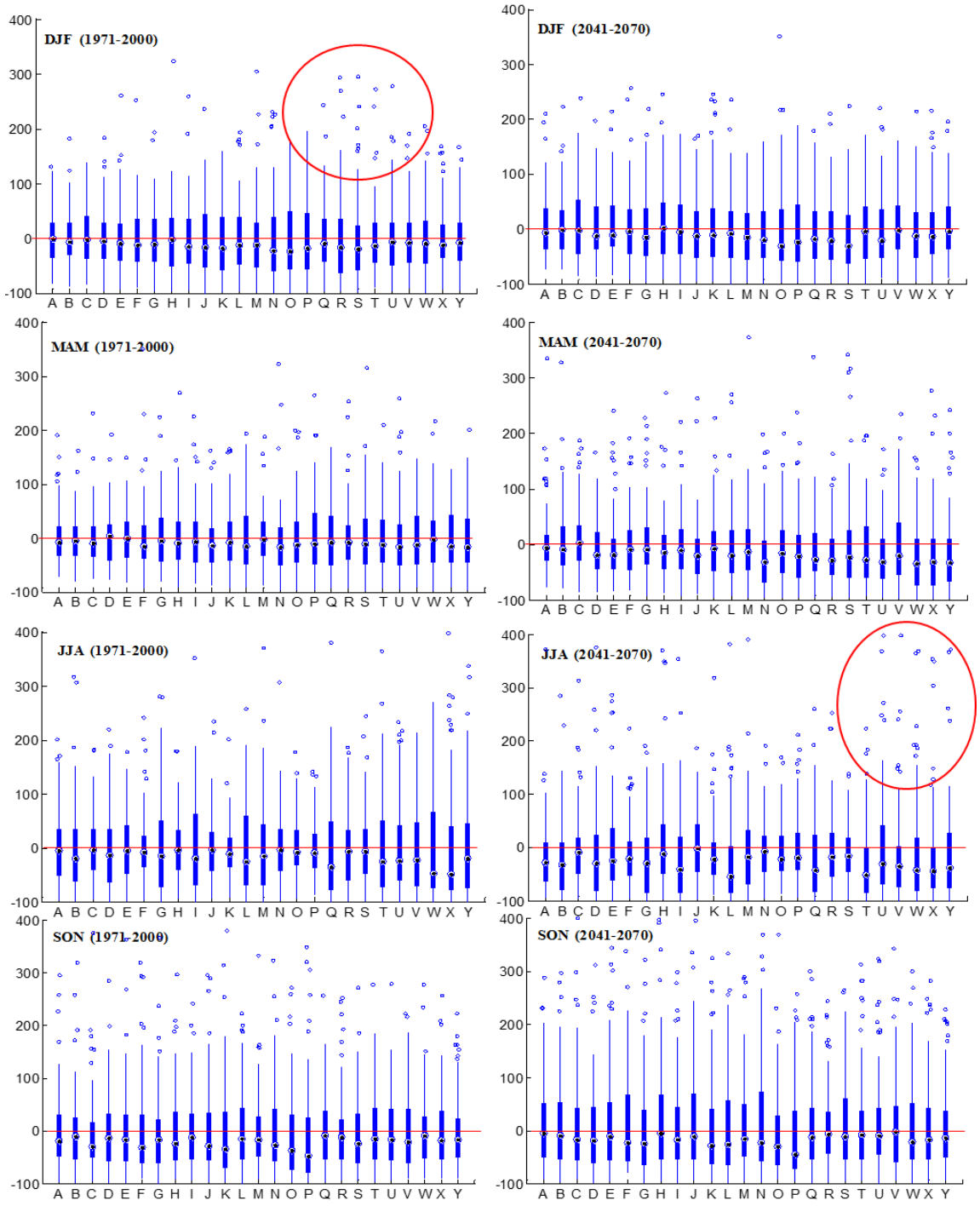

Figure 32 Boxplots of the percentage of changes in monthly precipitation series. Comparing the RCM3-GFDL precipitation series for historical (1971-2000) and future periods (2041-2070).

5.3.4. Non-parametric analysis of changes across precipitation ranges

5.3.4.1. Kernel estimate

In this section, we examine the magnitude of changes in the precipitation ranges. We considered the probability density functions PDFs derived from the past and the future precipitation series. In our approach, we applied a Gaussian kernel (Jann, 2007; Seaman and Powell, 1996; Silverman, 1986) to estimate and plot the density function of the monthly precipitation characteristics. The kernel estimator $\hat{f}(.)$ is defined by:

$$\hat{f}(p) = \frac{1}{nh}\sum_{i=1}^{n} K\left(\frac{p - P_i}{h}\right) \tag{14a}$$

$$K(p) = \frac{1}{\sqrt{2\pi}} Exp\left(-\frac{p^2}{2}\right) \tag{14b}$$

$$\int K(p)\, dp = 1 \tag{14c}$$

where h is the band width or smoothing parameter; $K(.)$ is the Gaussian kernel; n is the series size; P_i is any random value within the range of precipitation series; p denotes the center of any bin with the h width. The choice of band width h is critical for the kernel estimation, as it determines the degree of smoothness. Silverman (1986) proposed a simple calculus for the identification of the optimum band width h_{opt}. In the case of Gaussian kernel, the formula (equation 14d) proposed by Silverman (1986) depends on the series size n and its standard deviation σ:

$$h_{opt} = 1.06\,\sigma\, n^{-1/5} \tag{14d}$$

For each grid cell, the kernel estimates were analyzed by distinguishing the four seasons DJF, MAM, JJA and SON. Results were comparable and the overall paradigm is

described here by spotting grid cells A, H, Q and X, represented in Figure 33 and Figure 34.

At the first glance, curves for the kernel density estimates in Figure 33 and Figure 34 exhibit discrepancies between the past and future precipitation series. However, an analytical insight shows notable patterns spread differently along the precipitation ranges. Explicitly, the differences between past and future precipitation series are not just tied to extreme events part of the curves suggesting the need to revise prior conceptions on climate change impact. This observation motivates the importance of addressing climate change pattern not by focusing only on extreme events but the entire range of precipitation values. In support of this assertion, we performed a binary bivariate analysis. The approach begins with a binary transformation of past P and future P' precipitation series. We considered different percentiles (1st, 2nd and 3rd quartiles) as thresholds and performed the binary transformation as:

$$P = \begin{cases} 1 \; if \;\; P > percentile \;\; (P) \\ 0 \; otherwise \end{cases} \quad and \quad P' = \begin{cases} 1 \; if \;\; P' > percentile \;\; (P') \\ 0 \; otherwise \end{cases} \tag{15}$$

Pairing both past and future precipitation series, we derived contingency tables (Table 16) and later estimated the degree of association by calculating Pearson's ϕ values as:

$$\phi = \frac{N11N00 - N01N10}{\sqrt{N.1\ N.0\ N.1\ N0.}} \tag{16}$$

Symbols in equation (16) are defined in Table 16. Guilford (1941) demonstrated that Pearson's ϕ is related to the critical χ^2 statistic that is addressed with 1 degree of freedom and an arbitrary *p-value* as:

$$\chi^2 = N\phi^2 \tag{17}$$

Results of testing the match between historical and future precipitation series are presented in Table 17 and Table 18. Significant values in the tables indicate strong similarity or match between the past and future precipitation series. However, there are only a few cases of significant similarities with monthly precipitation total (Table 17) and number of precipitation events (Table 18). The binary bivariate analysis confirms and shows the significance of the changes resorted earlier in Figure 33 and Figure 34.

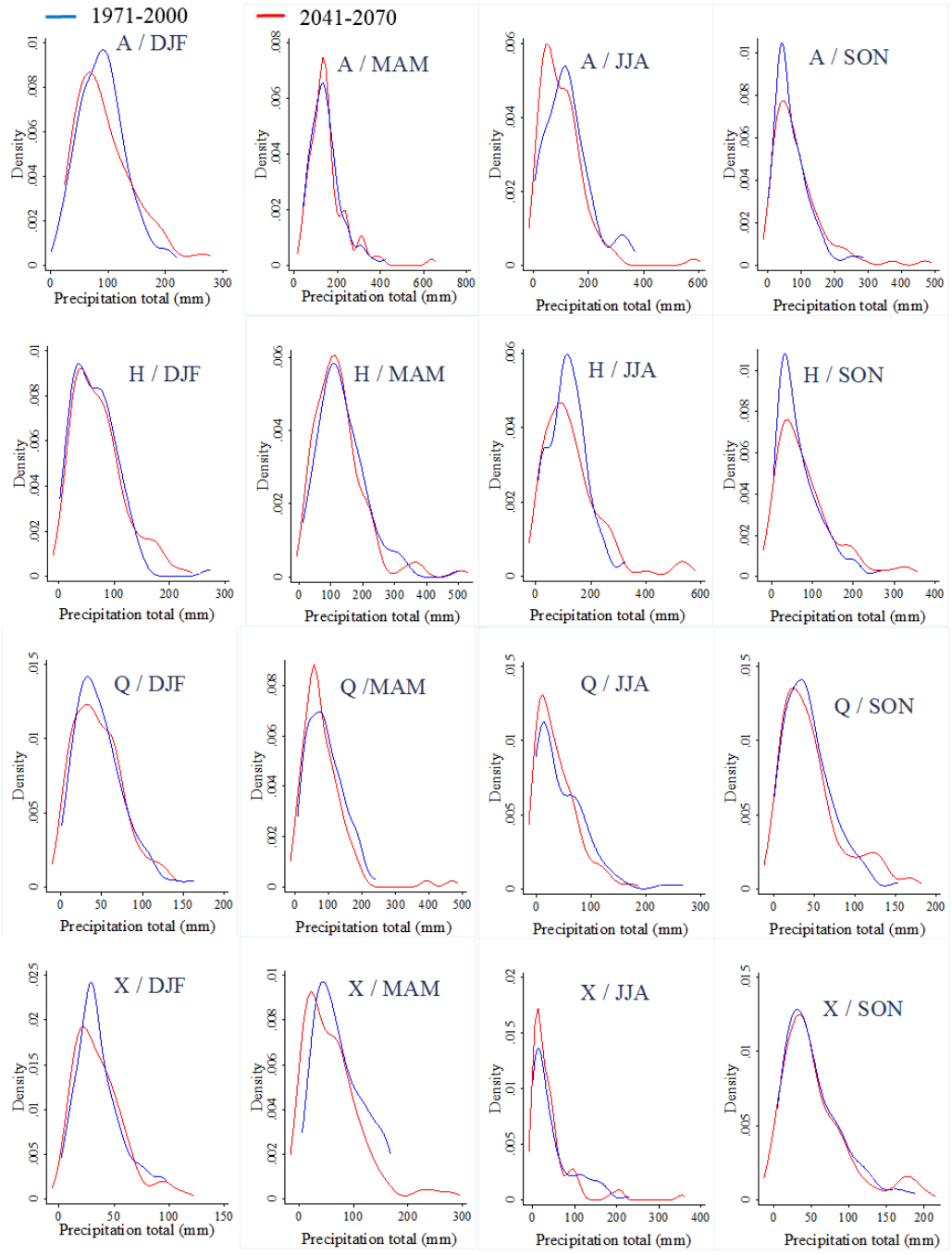

Figure 33 Comparing the probability density estimates for past (blue curve) and future (red curve) monthly precipitation during the seasons of DJF (December-January-February), MAM (March-April-May), JJA (June-July-August) and SON (September-October-November). We estimated the probability density using a Gaussian kernel. Example based on grids A, H, Q and X (figure 31).

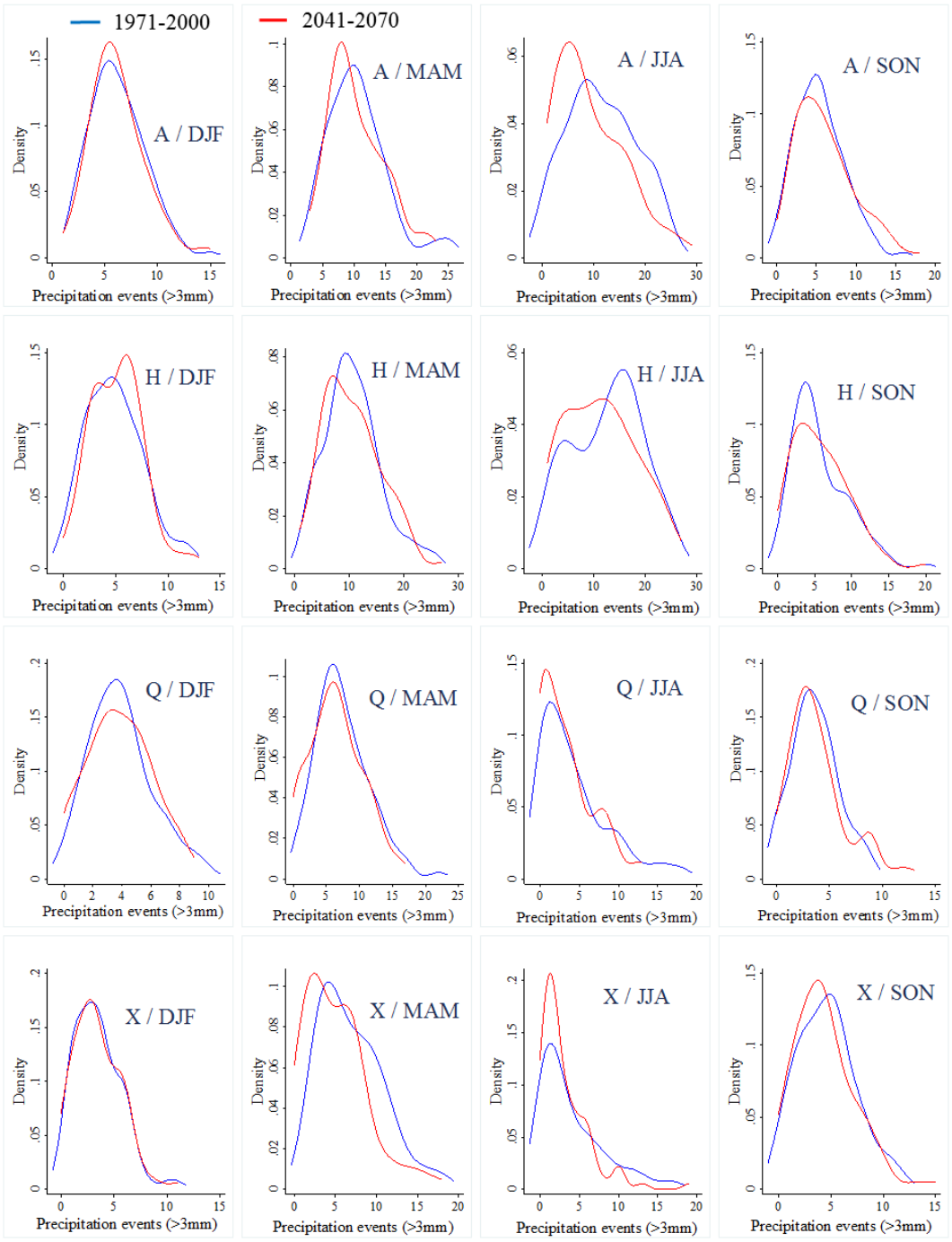

Figure 34 Comparing the probability density estimates for past (blue curve) and future (red curve) monthly number of precipitation events (>3mm) during the seasons of DJF (December-January-February), MAM (March-April-May), JJA (June-July-August) and SON (September-October-November). We estimated the probability density using a Gaussian kernel. Example based on grids A, H, Q and X (figure 31).

Table 16 Binary bivariate contingency table obtained by pairing past P and future P' precipitation series.

	P'=1	*P'=0*	*Total*
P=1	*N11*	*N10*	*N1.*
P=0	*N01*	*N00*	*N0.*
Total	*N.1*	*N.0*	*N*

Table 17 Values of $\chi^2 = N\phi^2$; estimating the degree of association between past *P* and future *P'* monthly precipitation total using RCM3-GFDL ensemble model simulations. The critical χ^2 for 1 degree of freedom and a p-value = 0.05 is 3.84 and the significant values are marked with "*". Q1, Q2 and Q3 represent the 1st, 2nd and 3rd quartiles. Example based on grids A, H, Q and X (figure 31).

Thresholds		< Q1	Q1 – Q2	Q2 – Q3	> Q3
A	DJF	0.02	0.14	1.48	1.66
	MAM	0.52	1.69	0.07	0.07
	JJA	1.22	0.01	0.37	0.48
	SON	4.43*	0.52	0.52	0.22
H	DJF	3.11	0.13	0.12	6.41*
	MAM	0.98	0.50	0.18	0.02
	JJA	1.20	2.77	0.00	0.03
	SON	1.17	0.59	0.02	0.94
Q	DJF	2.21	0.00	1.70	0.45
	MAM	0.59	1.75	0.12	0.00
	JJA	7.72*	0.27	0.25	0.30
	SON	0.39	0.89	0.98	2.81
X	DJF	1.00	0.44	4.09*	0.74
	MAM	0.10	0.63	0.02	0.08
	JJA	8.22*	3.24	3.29	4.08
	SON	0.11	0.00	1.18	0.53

Table 18 Values of $\chi^2 = N\phi^2$ estimating the degree of association between past P and future P' monthly number of precipitation events (>3mm) using RCM3-GFDL ensemble model simulations. The critical χ^2 for 1 degree of freedom and a p-value = 0.05 is 3.84 and the significant values are marked with "*". Q1, Q2 and Q3 represent the 1st, 2nd and 3rd quartiles, respectively. Example based on grids A, H, Q and X (figure 31).

Thresholds		< Q1	Q1 – Q2	Q2 – Q3	> Q3
A	DJF	1.03	0.34	1.59	15.16*
	MAM	2.53	0.31	3.04	5.00*
	JJA	5.22*	0.69	2.26	0.49
	SON	0.88	0.16	0.22	0.00
H	DJF	0.98	1.77	1.51	23.04*
	MAM	0.47	0.18	1.76	0.45
	JJA	2.06	0.01	0.87	1.51
	SON	2.67	0.65	0.00	0.00
Q	DJF	0.00	1.28	0.13	1.95
	MAM	5.56*	0.07	0.77	0.85
	JJA	0.10	1.90	0.23	1.18
	SON	1.59	6.15*	0.12	0.00
X	DJF	0.10	0.00	3.91	0.44
	MAM	4.55*	0.44	0.07	0.71
	JJA	0.11	0.19	2.73	3.63
	SON	2.21	0.45	0.46	0.00

5.3.4.2. Trends analysis

This section examines and compares monotonic trends in the precipitation series. The time series of the seasonal precipitation values are presented in the Figure 35. We observe an alternation of peaks particularly in the precipitation series corresponding to the future climate scenario. These peaks account for extreme precipitation events and their presence is noticeable during each of the four seasons. However, their magnitude and pace in time and space seem very irregular. Upon the pattern observed in Figure 35, we estimate trends in the seasonal precipitation series by performing the Mann-Kendall test

with a p-value =0.05 (Hamed 2008; Yue et al., 2002). In accordance with the Figure 35, we consider precipitation series for the grids A, H, Q and X; then we evaluate the Kendall's tau values. This computation begins by ranking the precipitation series. Let's suppose (P_i, T_i) and (P_j, T_j) a pair in the precipitation series of size *n*, such that $1 \leq i < j \leq n$. $P_.$ is the precipitation value at the date $T_.$. If P_i-P_j and T_i-T_j have the same sign, the pair is said *concordant* otherwise *discordant*. In case a difference is zero, the pair is considered as tied. The formula for the Kendall's tau is given by the equation (18):

$$Kendall''s\ tau = \frac{n_c - n_d}{\sqrt{[n(n-1)/2 - \sum t_i(t_i - 1)/2][n(n-1)/2 - \sum u_i(u_i - 1)/2]}} \quad (18)$$

Where n_c and n_d are the number of *concordant* and *discordant* pairs respectively; t_i is the number of tied values at a particular rank for P. and u_i is the number of tied for T.

We resume the results in Table 19. For both case of monthly precipitation total and number of events, there is no significant trends in the future precipitation series except with the grid Q during MAM, which seems to be exceptional. However, with the past precipitation series, we report positive and significant trends with the grid cells A, H and Q during JJA season and the grid X during MAM. This observation is consistent with both precipitation total and number of events. From a joint analysis of Figure 35 and Table 19, we may assert that the future scenario does not embed significant trends whilst the presence of peaks is notable. Yet, the statistically non-significant does not necessary mean that the trends are not practically meaningful (Yue et al., 2002). Rather, it seem reasonable to understand that the irregularity of the events in the future precipitation series is likely to shade meaningful information in time and space. Therefore, we are noting the

insufficiency of the monotonic trend analysis to expound adequately information on changes in precipitation patterns. This fact explain the essence of the probabilistic impact analysis presented in the next section.

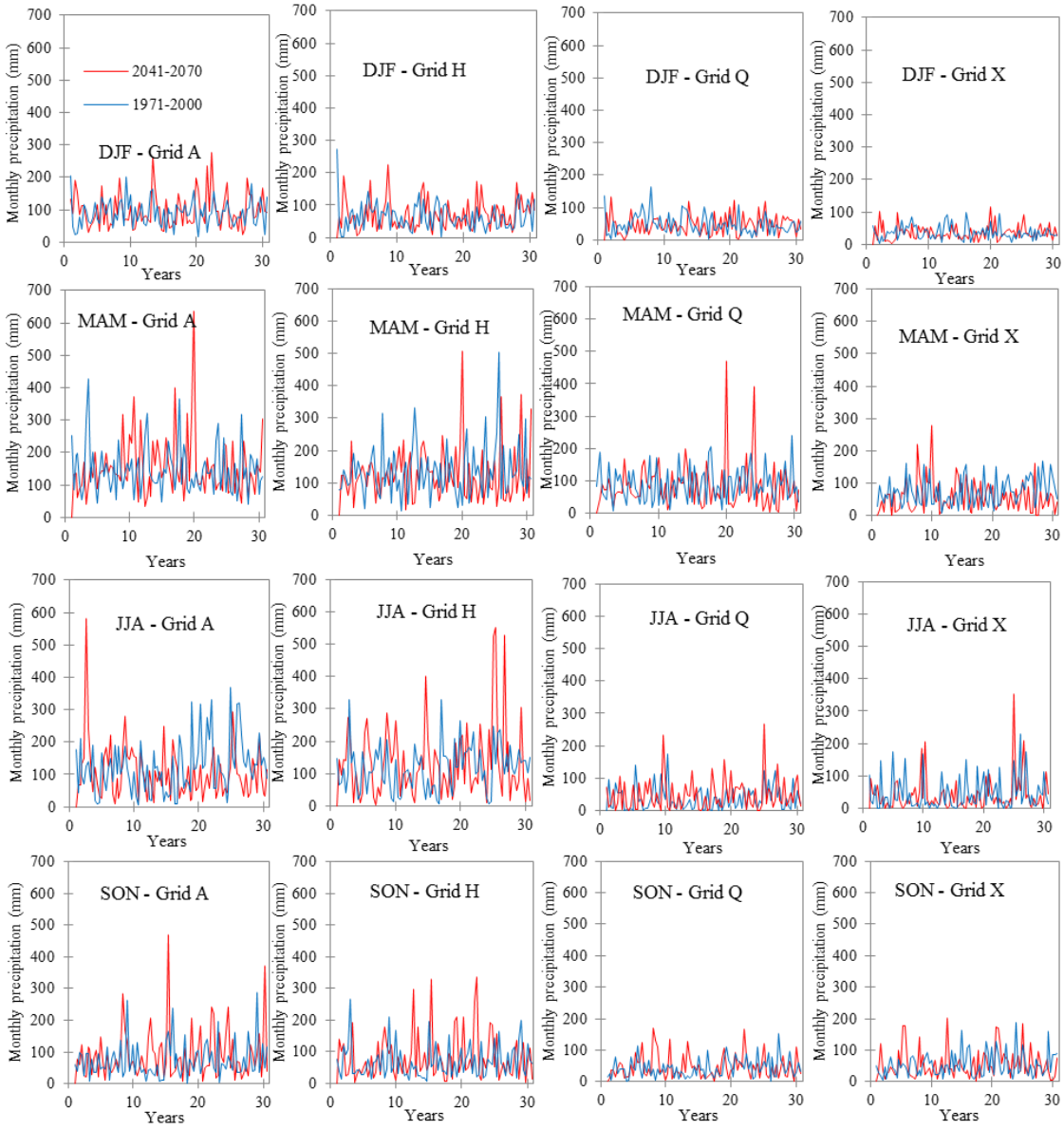

Figure 35 Comparing the seasonal precipitation series between historical (1971-2000) and future (2041-2070) climate.

Table 19 Report of Mann-Kendall's non-parametric trend test. The table presents the Kendall's tau values computed with the seasonal precipitation series.

Season	Grids	Precipitation total		Number of events (>3mm)	
		1971-2000	2041-2070	1971-2000	2041-2070
DJF	A	0.01	0.03	-0.02	0.06
	H	-0.05	0.09	-0.12	0.04
	Q	-0.11	0.03	-0.04	0.03
	X	-0.06	0.05	-0.01	0.02
MAM	A	-0.06	-0.03	0.00	0.09
	H	0.03	-0.05	0.13	-0.04
	Q	0.06	-0.13	0.12	**-0.17**
	X	**0.16***	-0.04	**0.16***	-0.09
JJA	A	**0.18***	-0.08	**0.24***	-0.07
	H	**0.17***	0.01	**0.14***	-0.03
	Q	**0.13***	0.05	**0.14***	-0.02
	X	0.10	0.03	0.10	0.00
SON	A	0.10	0.02	0.11	0.06
	H	0.05	0.04	0.09	0.03
	Q	0.12	0.04	**0.16***	0.02
	X	0.09	0.07	0.11	0.08

*Significant trend with 95% CI.

5.3.5. Probabilistic estimate of changes in precipitation patterns

Deterministic projections of climate scenario are customary inferred from a 'best guess'. However, such projections do not reflect the range of uncertainties contain in the scenario simulation. Palmer and Raisanen (2002) asserted that probabilistic projections are more useful as they provide wider view on plausible impacts. Previous studies attempted to address climate change impacts using a probabilistic framework (Pierce et al., 2013; News et al., 20107; Palmer and Ralsanen, 2002). The methods developed vary more or less among authors. E.g. Under climate change frame, Pierce et al. (2013)

evaluated mean precipitation changes and retrieved the probability distributions by fitting climate models simulations. Their probabilistic method is more oriented toward a downscaling and it did not expound effectively the probabilistic impacts. However, Crosbie et al. (2013) reported a typical case study in which they presented a clear probabilistic assessment of climate change impact on water resources. Specifically, Crosbie et al. (2013) resorted probability of exceedances by targeting plausible future scenario. In a different style, Palmer and Raisanen (2002) considered climate change effects as binary responses and conducted a probabilistic impact study. All these methods enable a larger understanding of plausible future changes. However, the probabilistic assessment of climate change remains less explored and efforts toward a diversified method should likely be beneficial in water resource planning (News et al., 2007; Palmer and Raisanen, 2002). The approach developed here is a contribution to this general need.

The aim of this section is twofold. The analysis reported here addresses changes in precipitation seasonality but also evaluates the changes in the probabilities of occurrence within precipitation ranges. The focus is more on the inner variations of precipitation within seasons. The method employed is probabilistic. Specifically, we applied a probit model to the historical and future RCM3-GFDL simulations separately, and evaluated the probabilities of precipitation events within the seasons. For this purpose, we restructured values in the future and present precipitation series by assigning four dichotomous dependent variables. For instance, the first dependent variable, named DJF, takes on the value 1 when the precipitation value in the series belongs to the DJF season, otherwise 0. Likewise, we derived the remaining three dependent variables by considering

seasons MAM, JJA and SON separately. Palmer and Raisanen (2002) reported similar proceeding in climate impact analysis. Indeed, they considered effects as a dichotomous response and successfully addressed climate change impact through a probabilistic framework. In our case, the four binary responses were associated with individual precipitation series. The binary transformation enables a probabilistic analysis of changes in seasonal patterns across the ranges of precipitation values. The explanatory variables were monthly precipitation characteristics (total and number of events >3mm). Subsequently, we applied a bivariate probit model to the future and present precipitation series by focusing on individual seasons separately. The bivariate probit model with predictor *P* (monthly precipitation) is defined by the link function:

$$\Phi^{-1}(P) = \beta_0 + \beta_1 P + \varepsilon \quad with \quad \varepsilon \sim N(0, \sigma^2) \tag{19a}$$

$$\Phi(.) = \int \frac{1}{\sqrt{2\pi}} Exp\left(-\frac{1}{2}u^2\right) du \tag{19b}$$

$$prob\ (Y = 1/P) = \Phi(\beta_0 + \beta_1 P + \varepsilon) \tag{19c}$$

where *Y* is the outcome of the probit model; Φ (.) is a cumulative distribution for a standard normal random variable; and Φ^{-1} (.) is the inverse normal distribution. Details of the probit model are explicitly presented in Table 20 and Table 21.

The marginal response of changing variable *P* is given by the derivative:

$$\frac{\partial Y}{\partial P} = \beta_1 \Phi(\beta_0 + \beta_1 P) \tag{19d}$$

In equation (19d), we note that the change depends not only on the value of β_1 but also on *P*. This relation is interesting, as it permits to capture continuous changes within

the entire range of precipitation series. The demarche allows evaluating the probability that any value within the precipitation range occurs during a particular season of the year. By estimating separately these probabilities for past and future series, we consistently quantified the changes in precipitation regimes. Figure 36 and Figure 37 present the probability curves for the monthly precipitation total and the number of precipitation events, respectively. Clearly, we notice that the probability of occurrence of any precipitation value varies consistently within the precipitation ranges. Moreover, the changes between the past and future precipitation scenarios seem to display notable spatial characteristics. The amplitude of these changes depends on the season. Interestingly, we are able to address the magnitudes of these changes across the entire Texas Gulf watershed by estimating the future and past probabilities associated with each of the first (Q1), second (Q2) and third (Q3) quartiles of the 25 grid cells. Later we estimate the changes in terms of percentage using equation (20):

$$\Delta'(\%) = \frac{prob'(.) - prob(.)}{prob(.)} \times 100 \tag{20}$$

where Δ' is the percentage of change, and *prob* (.) and *prob'* (.) are, respectively, the probability estimates based on the past and future precipitation series.

We summarize the results of this analysis in terms of maps presented in Figure 38 and Figure 39. For illustration, we utilize a color scale to feature the extent of changes. Between seasons, changes prevail differently exhibiting a relationship with seasonality. In addition to this overall seasonal trend, we can see from Figure 38 and Figure 39 spatial patterns associated with the changes. For both monthly precipitation total and number of

events (>3 mm) the contrast of probability changes are similar for the seasons DJF and SON on one hand, and MAM and JJA on the other hand. During DJF and SON, the changes are slightly erratic over the watershed, particularly at Q2 and Q3. However, the gradient of changes during MAM and JJA tend to vary westward. We can establish a relationship with the westward decreasing precipitation gradient displayed earlier by the isohyets in Figure 31. A large part of the watershed is associated with positive changes of probabilities at Q1 and Q2 during MAM and JJA, while the changes are negative during DJF and SON. Paradoxically, the trends are inversed with Q3.

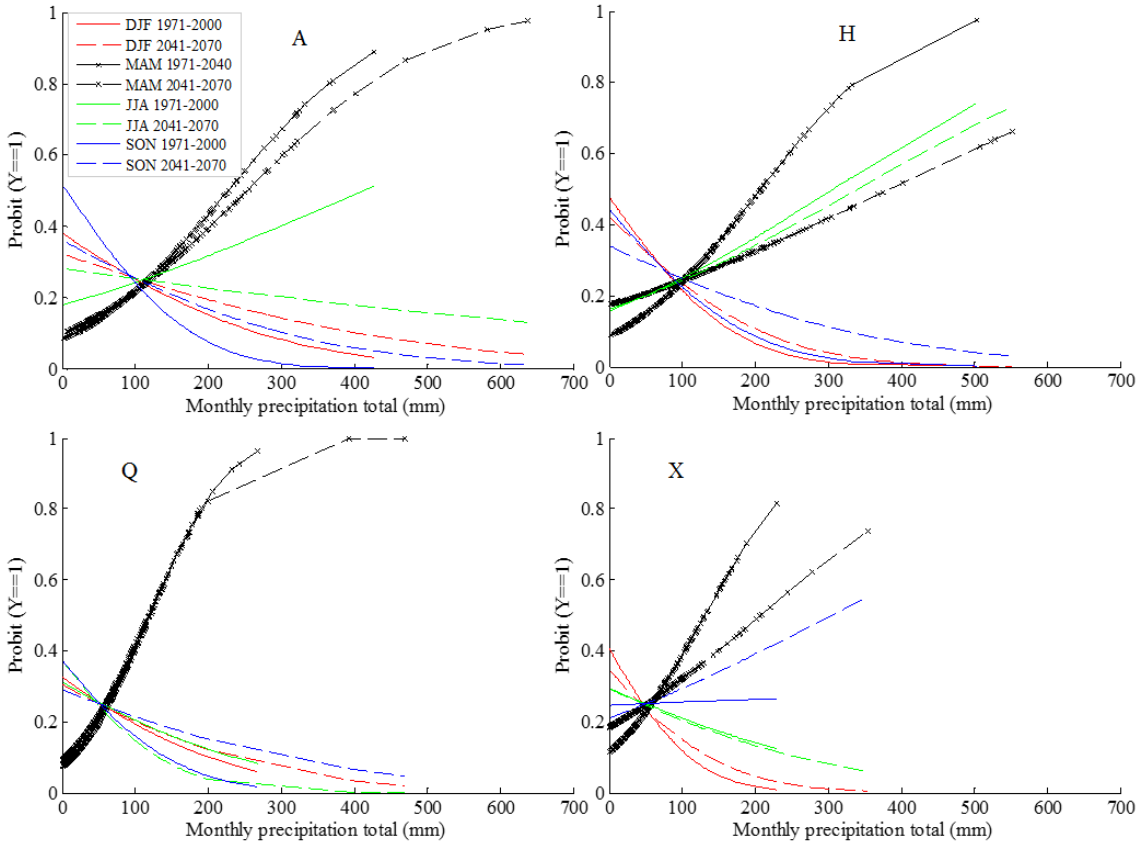

Figure 36 Probit estimate of monthly precipitation total (mm). A seasonal comparison of historical and future trends.

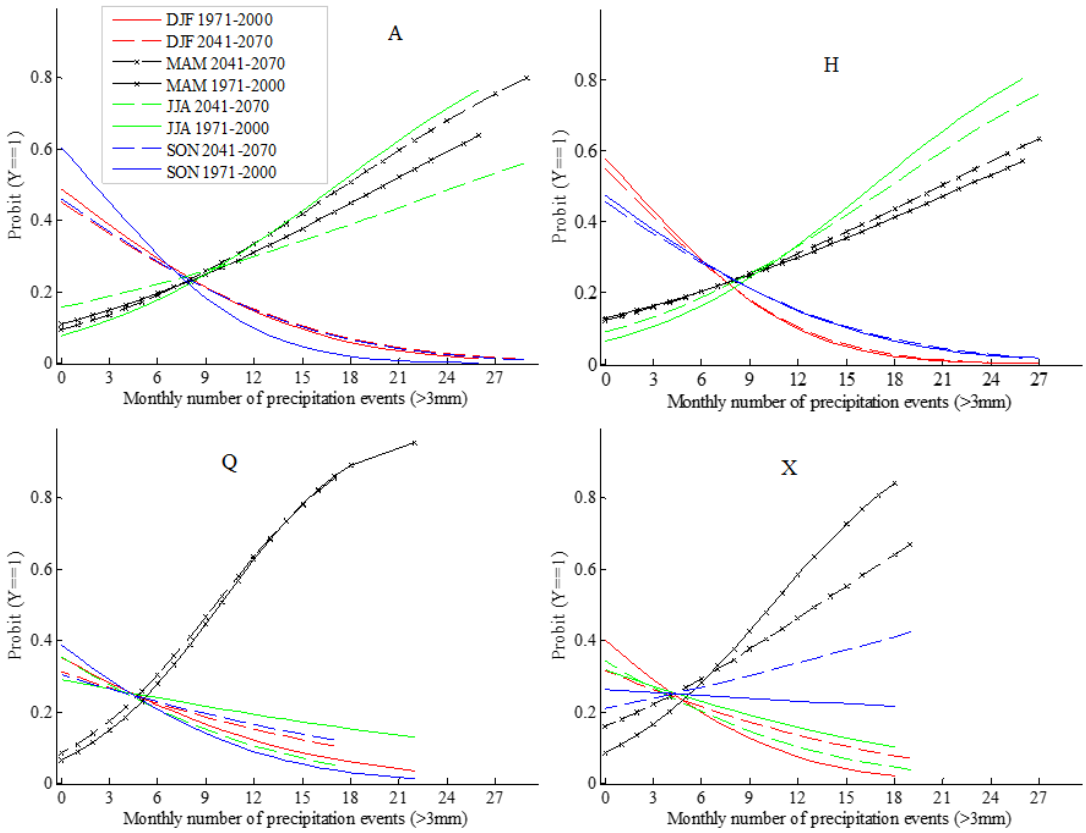

Figure 37 Probit estimate of monthly number of precipitation events (>3mm). A seasonal comparison of historical and future trends.

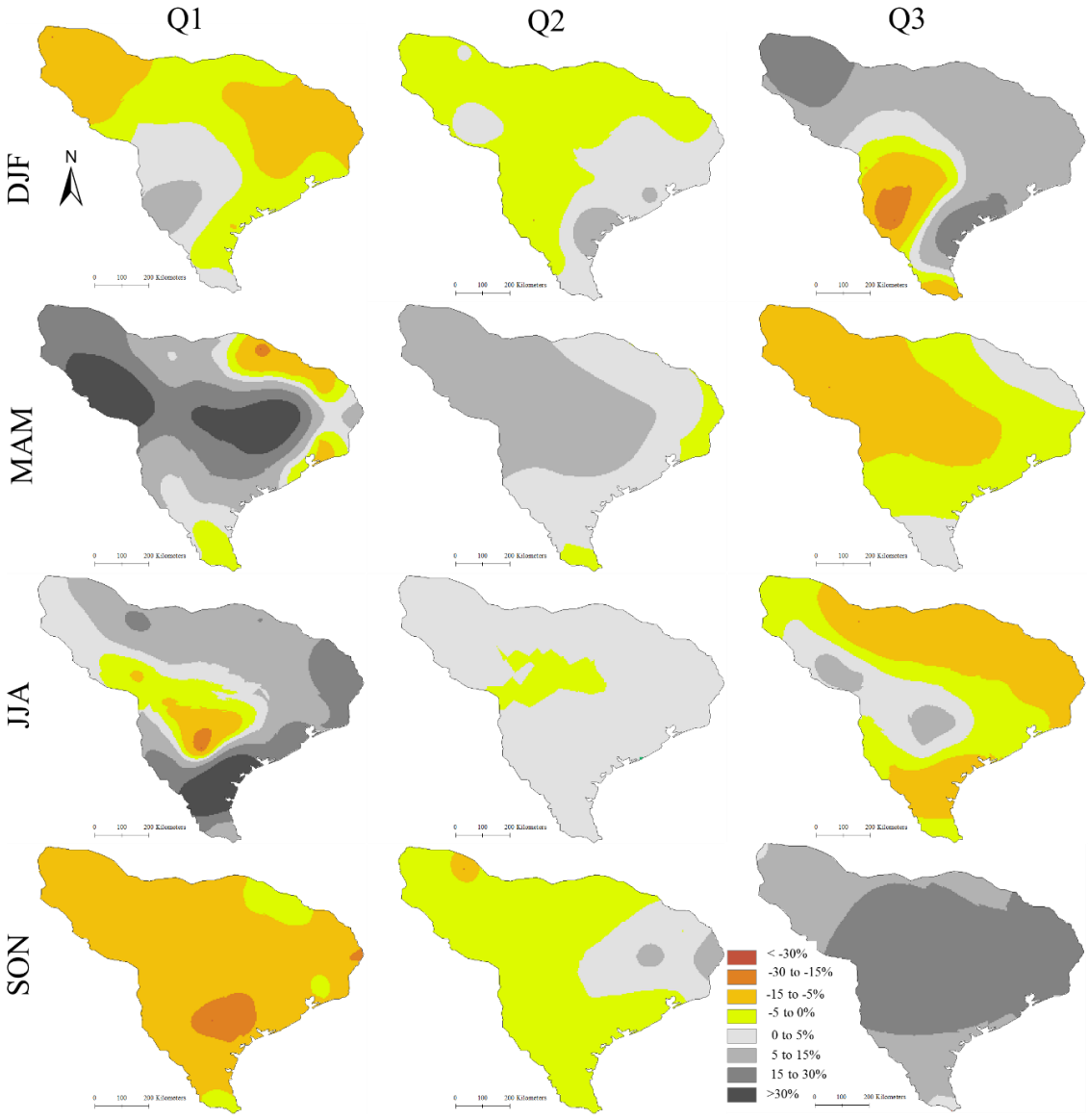

Figure 38 Estimate of seasonal changes in the probability of occurrence for the quartiles of monthly precipitation total. Q1, Q2 and Q3 represent the 1st, 2nd and 3rd quartiles, respectively

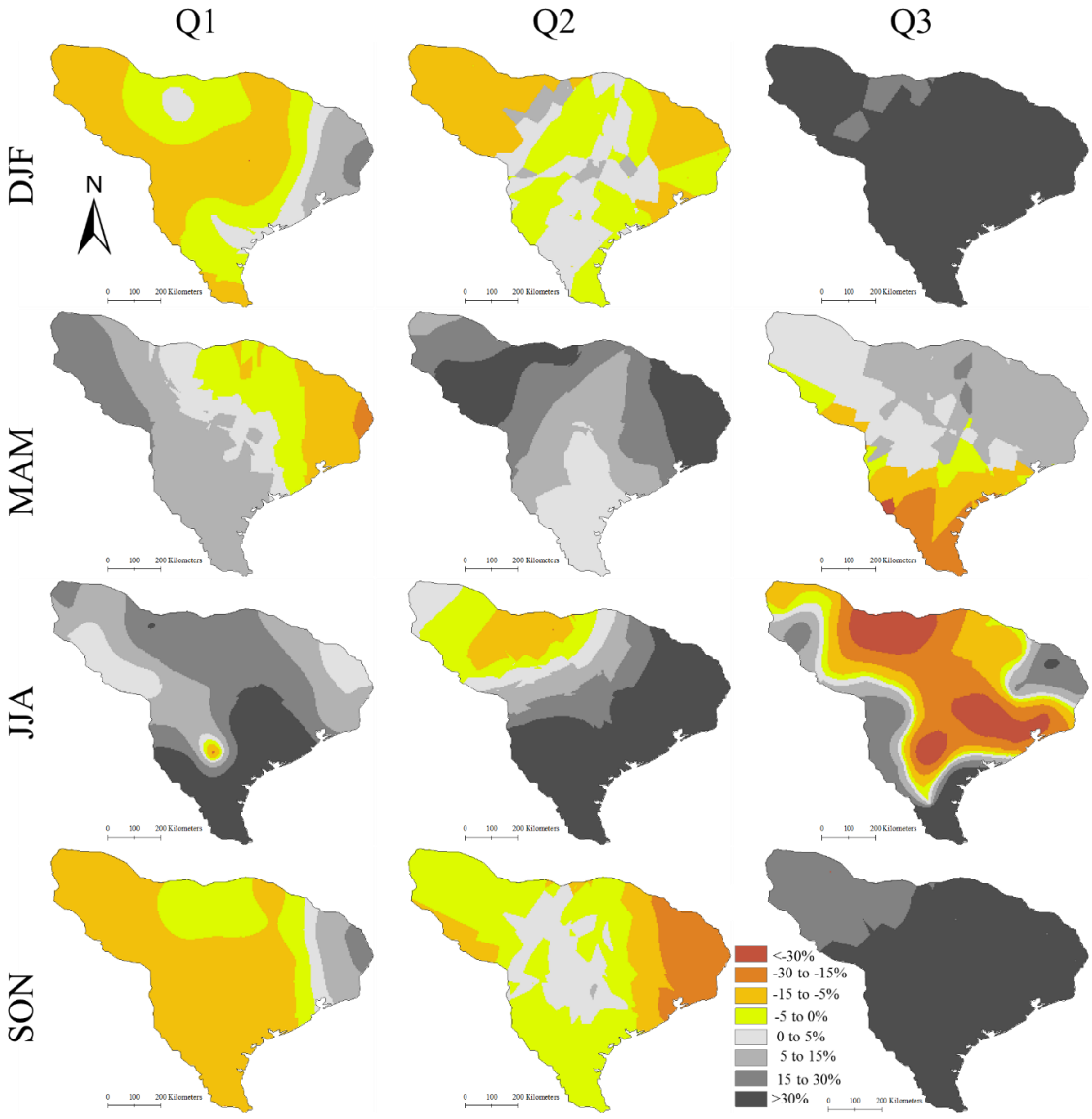

Figure 39 Estimates of seasonal changes in the probability of occurrence for the quartiles of monthly number of precipitation events (>3mm). Q1, Q2 and Q3 represent the 1st, 2nd and 3rd quartiles, respectively.

Table 20 Probit estimates of monthly precipitation total for grid cells. The table reports the probit parameters β0 and β1, as well as the model significance p. ** indicates a p-value <0.01; *indicates p-value <0.05.

GRID		DJF			MAM			JJA			SON		
		β_1	β_0	p	β_1	β_0	p	β_1	β_0	p	β_1	β_0	p
A	Past	-0.004	-0.31	**	0.006	-1.39	**	0.002	-0.92	*	-0.007	0.04	**
	Future	-0.002	-0.46	*	0.005	-1.28	**	-0.001	-0.58	*	-0.003	-0.36	**
B	Past	-0.003	-0.37	**	0.007	-1.40	**	0.001	-0.81	*	-0.008	-0.01	**
	Future	-0.001	-0.55		0.007	-1.41	**	-0.002	-0.49		-0.005	-0.27	**
C	Past	-0.005	-0.17	**	0.004	-1.17	**	0.003	-0.96	**	-0.004	-0.32	**
	Future	-0.004	-0.28	**	0.004	-1.21	**	0.001	-0.79	*	-0.003	-0.39	**
D	Past	-0.003	-0.39	**	0.007	-1.36	**	0.000	-0.65	**	-0.007	-0.14	**
	Future	-0.002	-0.51		0.007	-1.39	**	-0.001	-0.55		-0.005	-0.26	**
E	Past	-0.005	-0.23	**	0.009	-1.59	**	0.002	-0.86		-0.007	-0.05	**
	Future	-0.003	-0.39	**	0.004	-1.15	**	0.001	-0.75		-0.004	-0.35	**
F	Past	-0.008	0.10	**	0.002	-0.90	*	0.004	-1.24	**	-0.002	-0.42	**
	Future	-0.006	-0.04	**	0.002	-0.87	*	0.003	-1.02	**	0.000	-0.62	
G	Past	-0.004	-0.39	**	0.008	-1.41	**	-0.001	-0.62		-0.005	-0.28	**
	Future	-0.003	-0.47	*	0.010	-1.56	**	-0.004	-0.41	**	-0.005	-0.35	**
H	Past	-0.007	-0.06	**	0.007	-1.36	**	0.003	-1.01	**	-0.006	-0.14	**
	Future	-0.005	-0.20	**	0.002	-0.94	**	0.003	-0.99	**	-0.003	-0.41	**
I	Past	-0.004	-0.39	**	0.011	-1.56	**	-0.002	-0.56		-0.007	-0.22	**
	Future	-0.002	-0.51		0.010	-1.49	**	-0.004	-0.38	**	-0.004	-0.38	**
J	Past	-0.008	-0.07	**	0.005	-1.15	**	0.004	-1.04	**	-0.006	-0.17	**
	Future	-0.008	-0.02	**	0.002	-0.90	*	0.005	-1.18	**	-0.003	-0.46	*
K	Past	-0.011	0.27	**	0.000	-0.65		0.008	-1.64	**	-0.002	-0.51	
	Future	-0.009	0.09	**	-0.001	-0.58		0.003	-1.11	**	0.000	-0.72	
L	Past	-0.004	-0.41	**	0.012	-1.49	**	-0.003	-0.48	*	-0.006	-0.34	**
	Future	-0.003	-0.49	*	0.010	-1.32	**	-0.006	-0.36	**	-0.002	-0.54	
M	Past	-0.005	-0.33	**	0.010	-1.47	**	0.000	-0.67		-0.007	-0.23	**
	Future	-0.006	-0.31	**	0.006	-1.15	**	0.000	-0.70		-0.004	-0.40	**
N	Past	-0.009	0.03	**	0.002	-0.88	**	0.003	-1.02	**	-0.004	-0.35	**
	Future	-0.011	0.11	**	0.001	-0.73		0.005	-1.23	**	-0.001	-0.62	
R	Past	-0.009	-0.07	**	0.004	-1.00	**	0.005	-1.11	**	-0.006	-0.23	**
	Future	-0.012	0.03	**	0.003	-0.90	*	0.007	-1.22	**	-0.004	-0.41	**
O	Past	-0.011	0.21	**	-0.002	-0.47	*	0.007	-1.57	**	0.000	-0.62	
	Future	-0.010	0.18	**	-0.002	-0.50	*	0.004	-1.20	**	0.000	-0.72	*
P	Past	-0.010	0.26	**	-0.002	-0.46	**	0.004	-1.34	**	0.000	-0.68	*
	Future	-0.011	0.26	**	-0.001	-0.50	**	0.003	-1.23	**	0.000	-0.72	
Q	Past	-0.004	-0.45	*	0.012	-1.44	**	-0.003	-0.49	*	-0.007	-0.32	**
	Future	-0.003	-0.51	*	0.011	-1.33	**	-0.007	-0.32	**	-0.002	-0.55	
R	Past	-0.009	-0.07	**	0.004	-1.00	**	0.005	-1.11	**	-0.006	-0.23	**
	Future	-0.012	0.03	**	0.003	-0.90	*	0.007	-1.22	**	-0.004	-0.41	**
S	Past	-0.009	-0.04	**	0.001	-0.77		0.007	-1.37	**	-0.003	-0.39	**
	Future	-0.012	0.10	**	0.001	-0.76		0.005	-1.18	**	-0.001	-0.61	
T	Past	-0.007	-0.33	**	0.012	-1.42	**	-0.002	-0.54		-0.005	-0.41	**
	Future	-0.005	-0.46	*	0.010	-1.26	**	-0.008	-0.29	**	0.000	-0.65	
U	Past	-0.007	-0.34	**	0.014	-1.52	**	-0.003	-0.53		-0.007	-0.30	**
	Future	-0.007	-0.35	**	0.008	-1.15	**	-0.001	-0.63		-0.003	-0.53	
V	Past	-0.012	-0.10	**	0.010	-1.28	**	-0.001	-0.63		-0.001	-0.62	*
	Future	-0.009	-0.26	**	0.007	-1.07	**	-0.004	-0.46	**	0.002	-0.81	
W	Past	-0.007	-0.37	**	0.015	-1.48	**	-0.006	-0.41	**	-0.004	-0.49	*
	Future	-0.005	-0.45	*	0.009	-1.09	**	-0.006	-0.44	**	0.001	-0.70	*
X	Past	-0.009	-0.24	**	0.009	-1.20	**	-0.003	-0.54		0.000	-0.69	
	Future	-0.006	-0.40	**	0.004	-0.89	**	-0.003	-0.54		0.003	-0.81	
Y	Past	-0.011	-0.19	**	0.009	-1.18	**	-0.004	-0.47	*	0.002	-0.79	*
	Future	-0.007	-0.37	**	0.005	-0.91	**	-0.006	-0.42	**	0.005	-0.93	**

Table 21 Probit estimates of monthly number of precipitation events (>3mm). The table reports the probit parameters β0 and β1, as well as the model significance p. ** indicates a p-value <0.01; *indicates p-value <0.05.

GRID		DJF			MAM			JJA			SON		
		β_1	β_0	p	β_1	β_0	p	β_1	β_0	p	β_1	β_0	p
A	Past	-0.086	-0.03	**	0.061	-1.22	**	0.083	-1.42	**	-0.130	0.27	**
	Future	-0.076	-0.12	**	0.075	-1.32	**	0.041	-1.01	**	-0.079	-0.10	**
B	Past	-0.087	-0.08	**	0.068	-1.24	**	0.066	-1.21	**	-0.119	0.12	**
	Future	-0.061	-0.27	**	0.081	-1.30	**	0.036	-0.94	**	-0.095	-0.07	**
C	Past	-0.115	0.20	**	0.050	-1.15	**	0.101	-1.66	**	-0.094	0.07	**
	Future	-0.109	0.15	**	0.059	-1.23	**	0.063	-1.27	**	-0.065	-0.15	**
D	Past	-0.079	-0.18	**	0.093	-1.39	**	0.049	-1.03	**	-0.131	0.09	**
	Future	-0.063	-0.29	**	0.095	-1.37	**	0.031	-0.89	*	-0.106	-0.05	**
E	Past	-0.103	0.03	**	0.070	-1.28	**	0.081	-1.36	**	-0.115	0.11	**
	Future	-0.092	-0.06	**	0.073	-1.27	**	0.058	-1.14	**	-0.093	-0.04	**
F	Past	-0.131	0.37	**	0.022	-0.90		0.112	-1.89	**	-0.051	-0.21	**
	Future	-0.133	0.33	**	0.033	-0.99	**	0.070	-1.37	**	-0.027	-0.44	*
G	Past	-0.075	-0.26	**	0.114	-1.46	**	0.024	-0.83	*	-0.122	-0.03	**
	Future	-0.046	-0.43	*	0.123	-1.44	**	-0.008	-0.63		-0.093	-0.21	**
H	Past	-0.124	0.20	**	0.050	-1.13	**	0.092	-1.53	**	-0.081	-0.07	**
	Future	-0.116	0.13	**	0.056	-1.17	**	0.076	-1.35	**	-0.076	-0.11	**
I	Past	-0.070	-0.28	**	0.111	-1.43	**	0.022	-0.81		-0.103	-0.12	**
	Future	-0.052	-0.40	**	0.137	-1.52	**	-0.023	-0.55		-0.080	-0.27	**
J	Past	-0.126	0.17	**	0.039	-1.02	**	0.104	-1.64	**	-0.086	-0.06	**
	Future	-0.132	0.19	**	0.029	-0.92	*	0.102	-1.61	**	-0.063	-0.21	**
K	Past	-0.136	0.35	**	0.001	-0.69		0.145	-2.36	**	-0.044	-0.28	**
	Future	-0.143	0.34	**	-0.004	-0.64		0.117	-1.91	**	-0.025	-0.46	*
L	Past	-0.071	-0.33	**	0.149	-1.53	**	-0.017	-0.59		-0.085	-0.27	**
	Future	-0.035	-0.52		0.166	-1.52	**	-0.092	-0.28	**	-0.049	-0.46	*
M	Past	-0.103	-0.10	**	0.088	-1.30	**	0.046	-0.98	**	-0.089	-0.17	**
	Future	-0.094	-0.18	**	0.089	-1.25	**	0.032	-0.87	*	-0.068	-0.30	**
N	Past	-0.132	0.18	**	0.013	-0.78		0.122	-1.85	**	-0.067	-0.18	**
	Future	-0.158	0.28	**	0.000	-0.67		0.128	-1.85	**	-0.040	-0.38	**
O	Past	-0.138	0.31	**	-0.013	-0.55		0.151	-2.42	**	-0.034	-0.37	**
	Future	-0.160	0.39	**	-0.020	-0.50		0.134	-2.12	**	-0.014	-0.55	
P	Past	-0.154	0.47	**	-0.006	-0.61		0.142	-2.39	**	-0.026	-0.43	*
	Future	-0.157	0.46	**	-0.022	-0.47	*	0.127	-2.13	**	-0.006	-0.61	
Q	Past	-0.066	-0.38	**	0.152	-1.50	**	-0.026	-0.55		-0.089	-0.28	**
	Future	-0.045	-0.48	*	0.143	-1.37	**	-0.073	-0.37	**	-0.039	-0.51	
R	Past	-0.136	0.09	**	0.045	-1.02	**	0.084	-1.33	**	-0.069	-0.24	**
	Future	-0.151	0.13	**	0.033	-0.91	*	0.096	-1.38	**	-0.054	-0.34	**
S	Past	-0.118	0.08	**	0.009	-0.75		0.120	-1.76	**	-0.059	-0.25	**
	Future	-0.133	0.13	**	0.003	-0.70		0.113	-1.64	**	-0.035	-0.42	**
T	Past	-0.099	-0.25	**	0.168	-1.57	**	-0.033	-0.52		-0.061	-0.40	**
	Future	-0.053	-0.46	*	0.148	-1.38	**	-0.098	-0.29	**	-0.015	-0.61	
U	Past	-0.074	-0.34	**	0.131	-1.39	**	-0.009	-0.63		-0.082	-0.31	**
	Future	-0.088	-0.32	**	0.118	-1.25	**	-0.019	-0.59		-0.036	-0.52	
V	Past	-0.102	-0.21	**	0.150	-1.50	**	-0.032	-0.52		-0.037	-0.50	
	Future	-0.081	-0.34	**	0.130	-1.30	**	-0.080	-0.34	**	0.009	-0.71	
W	Past	-0.061	-0.42	**	0.153	-1.43	**	-0.062	-0.42	**	-0.045	-0.49	*
	Future	-0.046	-0.51		0.120	-1.15	**	-0.115	-0.29	**	0.010	-0.71	
X	Past	-0.100	-0.25	**	0.132	-1.36	**	-0.045	-0.47	*	-0.008	-0.63	*
	Future	-0.052	-0.47	*	0.075	-0.99	**	-0.072	-0.40	**	0.033	-0.81	*
Y	Past	-0.038	-0.52	*	0.112	-1.24	**	-0.047	-0.46	*	0.015	-0.74	*
	Future	-0.107	-0.22	**	0.061	-0.94	**	-0.111	-0.26	**	0.063	-0.95	**

5.4. Discussion of results

The objective of study was to understand the extent of climate change patterns across a regional watershed. The descriptive analyses of precipitation characteristics were informative, as they revealed significant changes in monthly precipitation totals and numbers of events. In addition, these analyses showed an overall significant decrease of mean precipitation total during the seasonal periods of MAM and JJA. The decreases seemed to be partially compensated for by an increase in mean precipitation during SON. However, those comparative analyses were not sufficient to explain fully the changes in precipitation regimes. An examination of the kernel density estimates of the past and future precipitation gave a realistic picture of the range of changes attributable to climate change. The matching test performed between the past and future precipitation series exhibited significant dissimilarities, which confirmed results from the kernel density analysis. Comparing the precipitation time series, we observed irregular precipitation peaks particularly with the future climate scenario. However, the Mann-Kendall trend analysis did not reveal the tendency of these peaks in the time series. We applied a systematic approach based on probit analyses, which permitted to capture the changes in precipitation patterns. The signals of changes appeared heterogeneous across the precipitation ranges and within the seasons. Such observations corroborated results reported by Kalra and Ahmad (2011) who analyzed trend changes in precipitation across the Colorado River basin. Along with the seasonal trends associated with changes, we detected some spatial patterns as well. Interestingly, we were able to evaluate the

magnitudes of changes within the seasons DJF, MAM, JJA and SON; and across the entire watershed.

The probabilistic analysis of these changes suggested shifts occurring in precipitation characteristics (monthly total and number of events) within the seasons. Tebaldi et al. (2004) brought out similar changes in precipitation density function and reported high probability density regions. Likewise, our analysis indicated the presence of high density of changes in the PDFs of precipitation characteristics. In order to better explore the changes, we developed maps of plausible perturbations in future precipitation regimes. The relevance of such maps of probabilistic impacts was shown through previous studies on climate change impact in water resources (Crosbie et al., 2013; Palmer and Raisanen, 2002). From the maps, we observed that the magnitudes of the changes gradually vary from East to West at Q2 and Q3 during the seasons MAM and JJA. Analyzing historical precipitation series, Sohoulande Djebou et al. (2014) observed summer (JJA) as the wettest season in the region. Likewise, Oreskes et al. (2010) identified summer precipitation as a critical component for water supply, agricultural productivity, risk of floods and droughts, particularly in the context of changing climate. At Q3, we observed a prevailing decrease of probabilities for both precipitation total and number of events during JJA. The implication of this plausible drift of JJA precipitation total and number of events is critical, as it may disturb local ecosystems in the future. Whereas these maps of changes in probabilities may be considered as a comprehensive tool for water managers in the Texas Gulf watershed, our method in itself seems promising. Actually,

such a probabilistic way for climate change assessment seems flexible and can be replicated with any watershed.

Recently, Lespinas et al. (2014) explored the impact of climate change on future water resources and outlined substantial discrepancy within seasons. They explained the relevance of providing seasonal insights in climate change studies. For instance, the four seasons spotted in our study, exhibit various signals, which may differently affect hydrological processes at the watershed scale. The analysis shows different situations among quartiles of precipitation values. Recently, Ntegeka et al. (2014) investigated changes in future precipitation scenarios by using a quantile-based approach. Even though their method was not probabilistic, the quantile consideration was useful to explore the changes over the entire range of precipitation distribution.

The probabilistic method presented in this paper is meant for a double objective. On one hand, it enables to display the magnitude of plausible changes associated with future climate scenario. On the other hand, we are able to explore potential drifts within seasons. However, the method should not be considered as a substitute to other technics of climate impact assessment and should be used along with. The seasonal drifts are particularly displayed by Figure 36 and Figure 37. For instance, in Figure 36, grid A shows a continuous probability decrease for seasons MAM and JJA. This decreasing trend is compensated for by an increasing trend observed with the probability curves of DJF and SON. However, the tendency is more or less different for grids H, Q and X, confirming the spatial variability inferred earlier.

5.5. Conclusions

Under the spectrum of climate change, projected scenarios vary within models (Christensen and Lettenmaier, 2007). Advance in the domain resulted into agreements on the capacity of regional climate models to simulate realistic scenarios (Lespinas et al., 2014; Wehner, 2013). This consent on RCMs reliability was crucial for studies addressing the climate change impact on water resources (Butcher et al., 2014; Ntegeka et al., 2014; Graham, 2007). Particularly, Wehner (2013) documented the ability of the the NARCAAP's RCMs to better project precipitation over the contiguous United States region. For instance, our study tagets the NARCCAP's RCM3-GFDL simulations of precipitation and evaluates the ampleness of the changes likely to occure in the future. The paper examines climate change effects using different statistics. The primary results are informative as they provide mean tendency of the effects of climate change. However, limitation were noticeable. Later we describe and employ a probabibilistic and quantile based approach which reveals changes in ample detail. We find distinct seasonal patterns associated with different quantiles of precipitation values. We find substantial plausible changes across the Texas Gulf watershed. The gradient of these changes suggests a spatial weight. However, their magnitudes exhibit a seasonality pattern. Wehner (2013) described the biophysical and atmospheric features affecting seasonal precipitation in the NARCAAP's simulations. Subsequently, the seasonality signals presesented in this study, may be a feed-back of future pertubations associated to the biophysical and atmospheric features reported by Wehner (2013).

Overall, our study is a meaningful contribution that may lead to improved understanding of climate change assessments. The results may be valued beyond the simple aspect of a case study and be subsequently exploited by water manager in the Texas Gulf catchment. The opportunity to probabilistically explore changes in seasonal precipitation patterns is relevant for better insights regarding climate change impact. However, we may view the probabilistic approach as complementary method. The results from our probabilistic procedure seem particularly insightful. According to News et al. (2007) the probabilistic assessment of climate change, is more informative as it provide exhaustive detail useful for quantifying potential risk. At the scale of the Texas gulf watershed, our probabilistic impact assessment may be incorporate to risk-based decision making. However, the spatial disparity observed across the watershed needs to get particular attention. Indeed, Crosbie et al (2013) emphasized on the consistency of considering the spatial specificities in managing response to climate change. Likewise, the specificities observed within events range should be worthwhile as well. Indeed, the consequence of a minor change of probabilities are differently manageable according to the range corresponding to the event; i.e. a minor change in extreme events occurrence may turn more damageable compared to an equivalent change in middle range events. In accordance with the results discussed in this paper, we can conclude on the capacity of our method to provide an exhaustive perceptivity of plausible pertubations in precipation regimes. In sum, it is advisable to include probabilistic approach as a diagnostic tool in climate change assessment. However, besides precipitation, customary water management planning encompasses a wider range of hydrological cycle components. At that point, we

recognize the necessity to replicate the method as a comprehensive tool for diversified climate change scenarios. We also suggest further research to consider the method and explore aspects, such as changes in surface flow, base flow, temperature, land cover, etc.

CHAPTER VI

CONCLUSION AND RECOMMENDATIONS FOR FUTURE STUDIES

6.1. Conclusion

The dissertation research explored precipitation patterns in relation to vegetation dynamics. We resort to meaningful relationships between these two terrestrial components. The study region displays relevant spatial and topographic diversity which we investigated adequately in the scope of climate change impact. The regional climate is characterized by a strong seasonality. Indeed, the moisture in the southwest United States is influenced by several atmospheric forcings such as the North American Monsoon, the low jet winds, the Pacific decadal Oscillation and at certain point the El Nino Southwest Oscillation. These driving factors are consistently represented in most climate models. However, important discrepancies are often observed between climate model simulations and observations (Knight and Harrison, 2012).

Efforts aiming to improve the representation of the land atmosphere interactions are likely to result in advances for realistic simulations (Sobolowski and Pavelsky, 2012; Leung et al., 2003). We examined precipitation variability in the southwest US region using an entropy based disorder index DI, and evaluated the marginal effect of watershed topography. We found significant effects and concluded a general tendency of less disorder in complex terrain compared to plains. We quantified the effect of watershed topography on precipitation variability and came up with a magnitude of 19-27%. Specifically, we concluded the stabilizing effect of hilly relief on the JJA precipitation

characteristics. These finding are worthwhile, for the southwest U.S. region particularly, as we investigated precipitation variability and vegetation dynamics.

In fact, the southwest United States region is characterized by a westward aridity gradient which seems to drive vegetation cover. We targeted different types of vegetation cover and found that vegetation response to precipitation tends to increase with the environmental aridity. At that point, the high variability associated with aridity may result into threat for vegetation covers in the arid part of the region. However, the stabilizing effect observed for hilly regions may determine somehow the sustainability of ecosystems in the arid regions.

We employed entropy theory and examined the joint relationship between precipitation, soil moisture, temperature and NDVI. Entropy scaling showed trends toward maximum entropy and supported the goodness of coupling atmospheric variables in vegetation dynamics analysis. We retrieved algorithms to describe both marginal and interactive relationship between these atmospheric variables and vegetation growth indices. We came up with a nested statistical model for vegetation pattern estimation. In particular, the couple comprising soil moisture and temperature was able to explain up to 68% of NDVI variation. However, the marginal weight of precipitation was the most important.

We explored the projected patterns in future precipitation by using NARCCAP's RCM3-GFDL simulations. We described a probabilistic method which shows a promising capacity for depicting climate change impact within the entire precipitation range. The analysis, revealed a prominent spatial weigh (Crosbie et al; 2013), which we considered

as relevant for future water resources planning. The climate change impact on precipitation regimes, reflected well meaningful drifts within the regular seasons. At the watershed scale, the magnitude of the changes in probability varies very much and tends to be related to precipitation gradient. However, the consequence of a minor change of probabilities of event occurrence depend on the range. Therefore, it is critical to examine the changes in relation with the ranges.

In sum, the study demonstrated the capacity to comprehend precipitation variability and vegetation dynamics and consistently hypothesize on plausible impact associated with climate change. More likely, we may expect vegetation of the west and arid part of the study region more vulnerable to climate change. Knowing the relevant role of vegetation covers in hydrological processes, it is clear that an alteration in vegetation dynamics patterns may cause perturbation in hydrological processes. However, the ecosystems in the east and humid part of the Southwest U.S. may benefit a buffering effect and show less vulnerability in the future.

Through this study, we obtained realistic insights on vegetation behavior under precipitation variability and climate change by addressing each of the specific objectives stated in the chapter I. The outcomes of the study may be wisely considered in vegetation, climate and hydrological modelling. Results will be potentially useful for water resource planning and risk-based decision making. However, we recognize that potential improvements will be achieved through future research works.

6.2. Recommendations

We propose further research, and specifically, we suggest the following:

(i) Extend the study domain to a continental and global scale and use reanalysis data in order to get larger time period and finer temporal resolution. Indeed, most of our analyses were conducted with a biweekly and monthly temporal resolutions. However, the entropy scaling results show the relevance of finer time scales which tend to be more informative.

(ii) Conduct a similar study by using different remote sensing products, such as EVI and SAVI particularly in humid and arid region, respectively.

(iii) Investigate the probabilistic climate change impact by targeting diversified scenarios of climate change. Actually, one limitation of the probabilistic assessment of future climate impact is related to initial assumptions sustaining the climate scenario (News et al., 2007). For instance in our study, the probabilistic impact expounded for future precipitation patterns in the Texas Gulf watershed is conditioned by the assumption made through the SRES-A2 scenario.

(iv) Research on the adequate way to include probabilistic impact projection in hydrological models. Whereas research on probabilistic climate change impact is getting attention, the study aiming to include the results in hydrological models need to be addressed as well.

REFERENCES

Ahmad, S., Kalra, A, Stephen, H., 2010. Estimating soil moisture using remote sensing data: a machine learning approach. Advances in Water Resources 33, 1, 69-80.

Ahmed, K. F., Wang, G., Silander, J., Wilson, A. M., Allen, J. M., Horton, R., Anyah, R., 2013. Statistical downscaling and bias correction of climate model outputs for climate change impact assessment in the U.S. northeast. Global and Planetary Change 100, 0, 320-332.

Baeriswyl, P. A., Rebetez, M., 1997. Regionalization of precipitation in Switzerland by means of principal component analysis. Theoretical and Appl. Climatol. 58, 1-2, 31-41.

Bresloff, C. J., Nguyen, U., Glenn, E. P., Waugh, J., Nagler, P. L., 2013. Effects of grazing on leaf area index, fractional cover and evapotranspiration by a desert phreatophyte community at a former uranium mill site on the Colorado Plateau. Journal of Environmental Management 114, 92-104.

Brunsell, N. A., Young, C. B., 2008. Land surface response to precipitation events using MODIS and NEXRAD data. International Journal of Remote Sensing, 29, 7, 1965-1982.

Bürger, G., Schulla, J., Werner, A. T., 2011. Estimates of future flow, including extremes, of the Columbia River headwaters. Water Resources Research, 47, 10, 1-18.

Butcher, J. B., Johnson, T. E., Nover, D., Sarkar, S., 2014. Incorporating the effects of increased atmospheric CO2 in watershed model projections of climate change impacts. Journal of Hydrology, 513, 322-334.

Cai, W. J., Purich, A., Cowan, T., van Rensch, P., Weller, E., 2014. Did climate change-induced rainfall trends contribute to the Australian millennium drought? Journal of Climate, 27, 9, 3145-3168.

Carlson, T. N., Ripley, D. A., 1997.On the relation between NDVI, fractional vegetation cover, and leaf area index. Remote Sensing of Environment, 62, 3, 241-252.

Changnon Jr., S. A., Vogel, J. L., 1981. Hydroclimatological characteristics of isolated severe rainstorms. Water Resour. Res. 17, (6), 1694–1700.

Chen, T., de Jeu, R. A. M., Liu, Y. Y., van der Werf, G. R., Dolman, A. J., 2014. Using satellite based soil moisture to quantify the water driven variability in NDVI: a case study over mainland australia. Remote Sensing of Environment 140, 0: 330-38.

Chiew, F. H. S., Teng, J., Vaze, J., Post, D. A., Perraud, J. M., Kirono, D. G. C., Viney, N. R., 2009. Estimating climate change impact on runoff across southeast Australia: Method, results, and implications of the modeling method. Water Resources Research, 45, 10, 1-17.

Christensen, N. S., Lettenmaier, D. P., 2007. A multimodel ensemble approach to assessment of climate change impacts on the hydrology and water resources of the Colorado River Basin. Hydrology and Earth System Sciences, 11, 4, 1417-1434.

Clinton, N. E., Potter, C., Crabtree B., Genovese, V., Gross, P., Gong, P., 2010. Remote sensing-based time-series analysis of cheatgrass (*Bromus Tectorum* L.) Phenology. Journal of Environmental Quality 39, 3, 955-63.

Comrie, A.C., Glenn, E.C., 1998. Principal components-based regionalization of precipitation regimes across the southwest United States and northern Mexico, with an application to monsoon precipitation variability. J. Clim. Res. 10, 3, 201-215.

Crosbie, R. S., Pickett, T., Mpelasoka, F. S., Hodgson, G., Charles, S. P., Barron, O. V., 2013. An assessment of the climate change impacts on groundwater recharge at a continental scale using a probabilistic approach with an ensemble of GCMs. Climatic Change, 117, 1-2, 41-53.

Das, N. N., Entekhabi, D., Njoku, E. G., 2011. An algorithm for merging SMAP radiometer and radar data for high-resolution soil-moisture retrieval. IEEE Transactions on Geoscience and Remote Sensing 49, 5, 1504-12.

De Martonne E., 1926. Une nouvelle fonction climatologique: L'indice d'aridité. La Meteorologie, 449-458.

Deniz, A., Toros, H., Incecik, S., 2011. Spatial variations of climate indices in Turkey. International Journal of Climatology 31, 3, 394-403.

Dewar, R. C., 2010. Maximum entropy production and plant optimization theories. Philosophical Transactions of the Royal Society B-Biological Sciences 365, 1545: 1429-35.

Di Luzio, M., Johnson, G.L., Daly, C., Eischeid, J.K., Arnold, J.G., 2008. Constructing retrospective gridded daily precipitation and temperature datasets for the conterminous United States. J. Appl. Meteorol. and Climatol.. 47, 2, 475-97.

Di, L., Rundquist, D.C., Han, L., 1994. Modelling relationships between NDVI and precipitation. International J. Remote Sensing, 15, 10, 2121-2136.

Dore, M. H. I., 2005. Climate change and changes in global precipitation patterns: What do we know? Environment International, 31, 8, 1167-1181.

Duan, Q., Djidjeli, K., Price, W. G., Twizell, E. H., 1998. A rational cubic spline based on function values. Computers and Graphics 22, 4, 479-86.

Duursma, R., A., Barton, C., V., M., Lin, Y., S., Medlyn, B., E., Eamus, D., Tissue, D., T., Ellsworth D., S., McMurtrie, R., E., 2014. The peaked response of transpiration rate to vapour pressure deficit in field conditions can be explained by the temperature optimum of photosynthesis. Agricultural and Forest Meteorology 189–190, 2-10.

Easterling, D.R., Karl, T.R., Gallo, K.P., Robinson, D.A., Trenberth, K.E., Dai, A., 2000. Observed climate variability and change of relevance to the biosphere. J. Geophys. Res. Atmospheres. 105, D15, 20101-14.

Eidenshink, J. C., 2006. A 16-year time series of 1 km AVHRR satellite data of the conterminous United States and Alaska, Photogrammetric. Engineering and Remote Sensing 72, 1027-1035.

Entekhabi, D., Njoku, E. G., O'Neill, P. E., Kellogg,K. H., Crow, W. T., Edelstein, W. N., Entin, J. K., et al., 2010. The soil moisture active passive (SMAP) mission. Proceedings of the IEEE 98, 5, 704-16.

Fang, J., Piao, S., Zhou, L., He, J., Wei, F., Myneni, R. B., Tucker, C. J., Tan, K., 2005. Precipitation patterns alter growth of temperate vegetation. Geophysical research letters, 32, 21, 1-5.

Ford, T. W., Quiring, S. M., 2013. Comparison and application of multiple methods for temporal interpolation of daily soil moisture. Int. Journal of Climatology. 34, 2604-21

Frauenfeld, O. W., Davis, R. E., 2002. Midlatitude circulation patterns associated with decadal and interannual pacific ocean variability. Geophys. Res. Lett. 29, 24, 2221, 1-4.

Gao, X. J., Giorgi, F., 2008. Increased aridity in the mediterranean region under greenhouse gas forcing estimated from high resolution simulations with a regional climate model. Global and Planetary Change 62, 3-4, 195-209.

Giannini, A., Saravanan, R., Chang, P., 2003. Oceanic forcing of sahel precipitation on interannual to interdecadal time scales. Science. 302, 5647, 1027-30.

Graham, L. P., Hagemann, S., Jaun, S., Beniston, M., 2007. On interpreting hydrological change from regional climate models. Climatic Change, 81, 97-122.

Groisman P. Y., Knight, R.W., Karl, T.R., Easterling, D.R., Sun, B.M., Lawrimore, J.H., 2004. Contemporary changes of the hydrological cycle over the contiguous united states: trends derived from in situ observations. J. Hydrometeorol. 5, 1, 64-85.

Groves, D. G., Yates, D., Tebaldi, C., 2008. Developing and applying uncertain global climate change projections for regional water management planning. Water Resources Research, 44, 12, 1-16.

Guilford, J. P., 1941. The phi coefficient and chi square as indices of item validity. Psychometrika, 6, 1, 11-19.

Gutzler, D.S., 2000. Covariability of spring snowpack and summer precipitation across the southwest United States. J. Clim. 13, 22, 4018-27.

Hamed, K. H., 2008. Trend detection in hydrologic data: The Mann-Kendall trend test under the scaling hypothesis. Journal of Hydrology, 349, 3-4, 350-363.

Hand, L.M., Shepherd, J.M., 2009. An investigation of warm-season spatial precipitation variability in Oklahoma City: possible linkages to urbanization and prevailing wind. J. Appl. Meteorol. Climatol. 48, 2, 251-69.

Hartigan, J.A., Wong, M.A., 1979. A K-means clustering algorithm. Applied Statistics, 28, 100-108.

Haylock, M. R., et al., 2006: Trends in total and extreme south american rainfall in 1960–2000 and links with sea surface temperature. J. Climate, 19, 1490–1512.

Hermance, J. F., Jacob, R. W., Bradley, B. A., Mustard, J. F., 2007. Extracting phenological signals from multiyear AVHRR NDVI time series: framework for applying high-order annual splines with roughness damping. IEEE Transactions on Geoscience and Remote Sensing 45, 10, 3264-76.

Higgins, R.W., Shi, W., 2001. Intercomparison of the principal modes of interannual and intraseasonal variability of the North American Monsoon system. J. Clim. 14, 3, 403-17.

Higgins, R.W., Yao, Y., Wang, X.L., 1997. Influence of the North American Monsoon system on the US summer precipitation regime. J. Clim. 10, 10, 2600-22.

Hirsch, R. M., Slack, J. R., Smith, R. A., 1982. Techniques of trend analysis for monthly water-quality data. Water Resources Research 18, 1, 107-21.

Homer, C., Dewitz, J., Fry, J., Coan, M., Hossain, N., Larson, C., Herold, N., McKerrow, A., VanDriel, J.N., Wickham, J., 2007. Completion of the 2001 national land cover database for the conterminous United States. Photogrammetric Engineering and Remote Sensing, 73, 4, 337-341.

Homer, C., Huang, C., Yang, L., Wylie, B., Coan, M., 2004. Development of a 2001 national landcover database for the United States. Photogrammetric Engineering and Remote Sensing 70, 7, 829-840.

Huete, A. R., 1988. A soil-adjusted vegetation index (SAVI). Remote sensing of environment, 25, 3, 295-309.

Huete, A., Didan K., Miura T., Rodriguez E. P., Gao X. and L. G. Ferreira, 2002. Overview of the radiometric and biophysical performance of the MODIS vegetation indices. Remote Sensing of Environment 83, 1-2, 195-213.

Huntington, T. G., 2006. Evidence for intensification of the global water cycle: review and synthesis. Journal of Hydrology 319, 1–4, 83-95.

Ichii, K., Kawabata, A., Yamaguchi, Y., 2002. Global correlation analysis for NDVI and climatic variables and NDVI trends: 1982-1990. International Journal of Remote Sensing 23, 18, 3873-78.

IPCC, 2012. Managing the risks of extreme events and disasters to advance climate change adaptation. a special report of working groups i and ii of the intergovernmental panel on climate change [Field, C.B., V. Barros, T.F. Stocker, D. Qin, D.J. Dokken, K.L. Ebi,

M.D. Mastrandrea, K.J. Mach, G.-K. Plattner, S.K. Allen, M. Tignor, and P.M. Midgley (eds.)]. Cambridge University Press, Cambridge, UK, and New York, NY, USA, 582.

Jann, B., 2007. Univariate kernel density estimation. Statistical Software Component, S456410. http://fmwww.bc.edu/RePEc/bocode/k/kdens.pdf.

Jayakrishnan, R., Srinivasan, R., Arnold J. G., 2004. Comparison of raingage and wsr-88d stage III precipitation data over the Texas-Gulf basin. J. Hydrol. 292, 1-4, 135-52.

Joseph, T., Whitehead, D., Turnbull, M., H., 2014. Soil water availability influences the temperature response of photosynthesis and respiration in a grass and a woody shrub. Functional Plant Biology, http://dx.doi.org/10.1071/FP13237.

Junk, W. J., S. Q. An, C. M. Finlayson, B. Gopal, J. Kvet, S. A. Mitchell, W. J. Mitsch, and R. D. Robarts 2013. Current state of knowledge regarding the world's wetlands and their future under global climate change: a synthesis. Aquatic Sciences 75, 1, 151-67.

Kaiser, H. F. 1958. The varimax criterion for analytic rotation in factor-analysis. Psychometrika 23, 3, 187-200.

Kalra, A., Ahmad, S., 2011. Evaluating changes and estimating seasonal precipitation for the Colorado River Basin using a stochastic nonparametric disaggregation technique. Water Resources Research, 47, 5, 1-26.

Kawabata, A., Ichii, K., Yamaguchi, Y., 2001. Global monitoring of interannual changes in vegetation activities using NDVI and its relationships to temperature and precipitation. Int. Journal of Remote Sensing 22, 7: 1377-82.

Kawachi, T., Maruyama, T., Singh V.P., 2001. Precipitation entropy for delineation of water resources zones in Japan. J. Hydrol. 246, 36-44.

Knapp, A. K., Smith, M. D., 2001. Variation among biomes in temporal dynamics of above ground primary production. Science 291, 5503: 481-84.

Knight, J., Harrison, S., 2012. The impacts of climate change on terrestrial earth surface systems. Nature Clim. Change. 3, 1, 24-29.

Krasovskaia, I., 1997. Entropy-based grouping of river flow regimes. J. Hydrology, 202, 1-4, 173-91.

Krishnamurthy, V., Shukla, J., 2000. Intraseasonal and interannual variability of precipitation over India. J. Clim. 13, 24, 4366-77.

Legates, D. R., Mahmood, R., Levia, D. F., DeLiberty, T. L., Quiring, S. M., Houser, C., Nelson, F. E., 2011. Soil moisture: a central and unifying theme in physical geography. Progress in Physical Geography 35, 1: 65-86.

Lespinas, F., Ludwig, W., Heussner, S., 2014. Hydrological and climatic uncertainties associated with modeling the impact of climate change on water resources of small Mediterranean coastal rivers. Journal of Hydrology, 511, 403-422.

Leung, L.R., Yun Q., Bian, X., 2003. Hydroclimate of the western United States based on observations and regional climate simulation of 1981–2000. Part I: Seasonal Statistics. J. Clim. 16, 12, 1892-911.

Liu, H., Huete, A., 1995. A feedback based modification of the NDVI to minimize canopy background and atmospheric noise. Geoscience and Remote Sensing, IEEE, 33, 2, 457-465.

Liu, J. H., Wu, J. J., Wu, Z. T., Liu, M., 2013. Response of NDVI dynamics to precipitation in the Beijing-Tianjin sandstorm source region. International Journal of Remote Sensing 34, 15, 5331-50.

Lobell, D. B., Lesch, S. M., Corwin D. L., Ulmer M. G., Anderson K. A., Potts D. J., Doolittle J. A., Matos, M. R., Baltes, M. J., 2010. Regional-scale assessment of soil salinity in the Red River Valley using multi-year MODIS EVI and NDVI. J. Env. Quality 39, 1: 35-41.

Los, S. O., 2013. Analysis of trends in fused AVHRR and MODIS NDVI data for 1982–2006: Indication for a CO2 fertilization effect in global vegetation, Global Biogeochemical Cycles, 27, 318-330.

Lotsch, A., Friedl, M. A., Anderson, B. T., Tucker, C. J., 2003. Coupled vegetation-precipitation variability observed from satellite and climate records. Geophysical Research Letters 30, 14.

Lowry, J., Ramsey, R.D., Thomas, K., Shrupp, D., Sajwaj, T., Kirby, J., et al. 2007. Mapping moderate-scale land-cover over very large geographic areas within a collaborative framework: A case study of the Southwest Regional Gap Analysis Project (SWReGAP). Remote Sensing of Environment, 108: 59–73.

Maestre, F. T., Salguero-Gomez, R., Quero, J. L., 2012. It is getting hotter in here: determining and projecting the impacts of global environmental change on drylands introduction. Philosophical Transactions of the Royal Society B-Biological Sciences 367, 1606, 3062-75.

Masek, J.G., Vermote, E.F., Saleous, N.E., Wolfe, R., Hall, F.G., Huemmrich, K.F., Feng Gao, Kutler, J., Teng-Kui Lim, 2006. A Landsat surface reflectance dataset for North America, 1990-2000. Geoscience and Remote Sensing Letters, IEEE , 3,1, 68-72.

McLaughlin, S. P., 1995. An overview of the flora of the sky islands, southeastern Arizona: diversity, affinities, and insularity. biodiversity and management of the madrean archipelago: the sky islands of southwestern United States and northwestern Mexico 264, 60-70.

McRoberts, D.B., Nielsen-Gammon, J.W., 2011. A new homogenized climate division precipitation dataset for analysis of climate variability and climate change. J. Appl. Meteorol. and Climatol. 50, 6, 1187-99.

Mearns, L. O., Arritt, R., Biner, S., Bukovsky, M. S., McGinnis, S., Sain, S., . . . Snyder, M., 2012. The north american regional climate change assessment program overview of phase I results. Bulletin of the American Meteorological Society, 93, 9, 1337-1362.

Mishra, A.K., Ozger, M., Singh, V.P., 2009. An entropy-based investigation into the variability of precipitation. J. Hydrology. 370, 1-4, 139-54.

Mohino, E., Rodriguez-Fonseca, B., Losada, T., Gervois, S., Janicot, S., Bader, J., Ruti, P., Chauvin, F., 2011. Changes in the interannual SST-forced signals on West African precipitation. AGCM intercomparison. Climate Dynamics. 37, 9-10, 1707-25.

Mojena, R., 1977. Hierarchical grouping methods and stopping rules. Evaluation. Computer Journal 20, 359-63.

Nakicenovic, N., Alcamo, J., Davis, G., De Vries, B., Fenhann, J., Gaffin, S., Gregory, K., A. Grübler, Jung, T. Y., Kram, T., 2000. Special report on emissions scenarios. a

special report of working group III of the intergovernmental panel on climate change. Cambridge University Press: Cambridge, 599.

New, M., Lopez, A., Dessai, S., Wilby, R., 2007. Challenges in using probabilistic climate change information for impact assessments: an example from the water sector. Philosophical Transactions of the Royal Society a-Mathematical Physical and Engineering Sciences, 365, 1857, 2117-2131.

Nicholson, S. E., Davenport, M. L., Malo, A. R., 1990. A Comparison of the vegetation response to rainfall in the Sahel and East-Africa, Using Normalized Difference Vegetation Index from NOAA AVHRR. Climatic Change 17, 2-3: 209-41.

Njoku, E. G., Jackson, T. J., Lakshmi, V., Chan, T. K., Nghiem, S. V., 2003. Soil moisture retrieval from AMSR-E. IEEE Transactions on Geoscience and Remote Sensing 41, 2: 215-29.

Ntegeka, V., Baguis, P., Roulin, E., Willems, P., 2014. Developing tailored climate change scenarios for hydrological impact assessments. Journal of Hydrology, 508, 307-321.

O'Gorman, P.A., 2012. Sensitivity of tropical precipitation extremes to climate change. Nature Geoscience, 5, 697-700.

Ohmart, R.D., Anderson B.W., 1982. North American desert riparian ecosystems. G.L. Bender (Ed.), Reference Handbook on the Deserts of North America, Greenwood Press, Westport, CT, 433–466.

Oreskes N, Stainforth D.A., and L. A. Smith, 2010. Adaptation to global warming: do climate models tell us what we need to know?. Philosophy Sc. 77, 5, 1012-1028.

Overpeck, J.T., Meehl, G.A., Bony, S., Easterling, D.R, 2011. Climate data challenges in the 21st century. Science. 331, 6018, 700-02.

Palmer, T. N., & Ralsanen, J., 2002. Quantifying the risk of extreme seasonal precipitation events in a changing climate. Nature, 415, 6871, 512-514.

Pecher, C., Tasser, E., Walde, J., Tappeiner, U. 2013. Typology of alpine region using spatial-pattern indicators. Ecological Indicators 24, 37-47.

Peixoto, J. P., Oort, A. H., De Almeida, M., Tomé, A., 1991. Entropy budget of the atmosphere, J. Geophys. Res., 96, D6, 10981–10988.

Pellant, M., Abbey, B., Karl, S., 2004. Restoring the Great Basin desert, U.S.A.: integrating science, management and people. Environmental Monitoring and Assessment, 99, 169–179

Pellarin, T., Tran, T., Cohard, J. M., Galle, S., Laurent, J. P., de Rosnay, P., Vischel, T., 2009. Soil moisture mapping over West Africa with a 30-min temporal resolution using amsr-e observations and a satellite-based rainfall product. Hydrology and Earth System Sciences 13, 10, 1887-96.

Pettorelli, N., Pelletier, F., von Hardenberg, A., Festa-Bianchet, M., Cote, S. D., 2007. Early onset of vegetation growth vs. rapid green-up: impacts on Juvenile Mountain ungulates. Ecology 88, 2, 381-90.

Pierce, D. W., Das, T., Cayan, D. R., Maurer, E. P., Miller, N. L., Bao, Y., . . . Tyree, M., 2013. Probabilistic estimates of future changes in California temperature and precipitation using statistical and dynamical downscaling. Climate Dynamics, 40, 3-4, 839-856.

Ratkowsky, D. A., 1984. A stopping rule and clustering method of wide applicability. Botanical Gazette 145, 4: 518-23.

Reed, B.C., 2006. Trend analysis of time-series phenology of North America derived from satellite data, GIScience and Remote Sensing, 43, 1, 24-38.

Regonda, S. K., Rajagopalan, B., Clark, M., Pitlick, J., 2005. Seasonal cycle shifts in hydroclimatology over the Western United States. Journal of Climate 18, 2, 372-384.

Reich, P. B., Wright, I. J., Lusk, C. H., 2007. Predicting leaf physiology from simple plant and climate attributes: a global glopnet analysis. Ecological Applications 17, 7, 1982-88.

Richards, L. A., Weaver, L. R., 1943. Fifteen-atmosphere percentage as related to the permanent wilting percentage. Soil Science 56, 5, 331-40.

Rigge, M., Wylie, B., Gu, Y. X., Belnap J., Phuyal , K., Tieszen, L., 2013. Monitoring the status of forests and rangelands in the western United States using ecosystem performance anomalies. International Journal of Remote Sensing 34, 11, 4049-68.

Ritchie, J.T., 1981. Soil water availability. Plant Soil, 58, 327–338.

Roe, G. H., 2005. Orographic precipitation. Annual Review of Earth and Planetary Sciences, 33, 645-71.

Rozhenko, A. I., 2010. A new method for finding the optimal smoothing parameter for the abstract smoothing spline. Journal of Approximation Theory 162, 6, 1117-27.

Sahin, S., 2012. An aridity index defined by precipitation and specific humidity. Journal of Hydrology 444, 199-208.

Salguero-Gomez, R., Siewert, W., Casper, B. B., Tielborger, K., 2012. A demographic approach to study effects of climate change in desert plants. Philosophical Transactions of the Royal Society B-Biological Sciences 367, 1606, 3100-14.

Salve, R., Sudderth, E.A., St Clair, S.B., Torn, M.S., 2011. Effect of grassland vegetation type on the responses of hydrological processes to seasonal precipitation patterns. J. Hydrol. 410, 1-2, 51-61.

Seager, R., Ting, M., Held, I., Kushnir, Y., Lu, J., Vecchi, G., Huang, H.P., Harnik, N., Leetmaa, A., Lau, N. C., Li, C., Velez, J., Naik, N., 2007. Model projections of an imminent transition to a more arid climate in Southwestern North America. Science 316, 1181–1184.

Seaman, D. E., Powell, R. A., 1996. An evaluation of the accuracy of kernel density estimators for home range analysis. Ecology, 77, 7, 2075-2085.

Seneviratne, S. I., Koster, R. D., Guo,Z. C., Dirmeyer, P. A., Kowalczyk, E., Lawrence, D., Liu, P., et al., 2006. Soil moisture memory in AGCM simulations: analysis of global land-atmosphere coupling experiment (GLACE) data. Journal of Hydrometeorology 7, 5, 1090-112.

Shannon, C.E., 1948. A mathematical theory of communication, The Bell Sys. Tech. J., 27, 379-423, 623-656.

Shepherd, J.M., Pierce, H., Negri, A.J., 2002. Rainfall modification by major urban areas: observations from spaceborne rain radar on the TRMM satellite. J. Appl. Meteor., 41, 689-701.

Sheppard, P.R., Comrie, A.C., Packin, G.D., Angersbach, K., Hughes, M.K., 2002. The climate of the U.S. Southwest. Clim. Res. 21, 3, 219-38.

Sillett, T. S., Holmes, R. T., Sherry, T. W., 2000. Impacts of a global climate cycle on population dynamics of a migratory songbird. Science 288, 5473, 2040-2042.

Silverman, B. W., 1986. Density estimation for statistics and data analysis, 26, CRC press.

Singh, V. P., 1997. The use of entropy in hydrology and water resources. Hydrological Processes 11, 6, 587-626.

Singh, V. P., 2013. Entropy theory and its application in environmental and water engineering. Publisher, Wiley. 666.

Singh, V.P., 2011. Hydrologic synthesis using entropy theory: A review. Journal of Hydrologic Engineering, ASCE, 16, 5, 421-433.

Sitch, S., Smith, B., Prentice, I. C., Arneth, A., Bondeau, A., Cramer, W., Kaplan, J. O., et al., 2003. Evaluation of ecosystem dynamics, plant geography and terrestrial carbon cycling in the LPJ dynamic global vegetation model. Global Change Biology 9, 2, 161-85.

Slatyer, R. O., 1957. The significance of the permanent wilting percentage in studies of plant and soil water relations. The Botanical Review 15, 10, 585-636.

Slayback, D. A., Pinzon, J. E., Los, S. O., Tucker, C. J., 2003. Northern hemisphere photosynthetic trends 1982-99. Global Change Biology 9, 1, 1-15.

Sobolowski, S., Pavelsky, T., 2012. Evaluation of present and future North American Regional Climate Change Assessment Program (NARCCAP) regional climate simulations over the Southeast United States. J. Geophys. Res. 117 : D01101.

Sohoulande Djebou, D.C., Singh, V.P., Frauenfeld, O.W., 2014. Analysis of watershed topography effects on summer precipitation variability in the Southwestern United States. J.hydrol. 511C, 838-849

Swenson, R., 1989. Emergent attractors and the law of maximum-entropy production - foundations to a theory of general evolution. Systems Research 6, 3, 187-97.

Szeicz, G., 1974. Solar radiation for plant growth. Journal of Applied Ecology 11, 2: 617-36.

Tebaldi, C., Mearns, L. O., Nychka, D., Smith, R. L., 2004. Regional probabilities of precipitation change: A Bayesian analysis of multimodel simulations. Geophysical Research Letters, 31, 24.

Thomas, C. D., A. Cameron, R. E. Green, M. Bakkenes, L. J. Beaumont, Y. C. Collingham, B. F. N. Erasmus, et al. 2004. Extinction risk from climate change. Nature 427, 6970, 145-48.

Tohver, I. M., Hamlet, A. F., Lee, S.-Y., 2014. Impacts of 21st-century climate change on hydrologic extreme in the Pacific Northwest Region of North America. J. American Water Resources Association. 50, 6, 1461-76.

Vicente-Serrano, S. M., Cuadrat-Prats, J. M., Romo, A., 2006. Aridity influence on vegetation patterns in the middle ebro valley (Spain): evaluation by means of AVHRR images and climate interpolation techniques. Journal of Arid Environments 66, 2, 353-75.

Vogelmann, J.E., Howard, S.M., Yang, L., Larson, C. R., Wylie, B. K., Van Driel, J. N., 2001. Completion of the 1990's national land cover data set for the conterminous united states, photogrammetric. Engineering and Remote Sensing, 67, 650-662.

Vorosmarty, C. J., Federer, C. A., Schloss, A. L., 1998. Evaporation functions compared on us watersheds: possible implications for global-scale water balance and terrestrial ecosystem modeling. Journal of Hydrology 207, 3-4, 147-69.

Wagner, W., Scipal, K., Pathe, C., Gerten, D., Lucht, W., Rudolf, B., 2003. Evaluation of the agreement between the first global remotely sensed soil moisture data with model and precipitation data. Journal of Geophysical Research-Atmospheres 108, D19, 4611, 1-17.

Wang, J., Rich, P. M., Price, K. P., 2003. Temporal responses of NDVI to precipitation and temperature in the central Great Plains, USA. International Journal of Remote Sensing 24, 11, 2345-64.

Wang, S., Fu, B. J., Gao, G. Y., Liu, Y., Zhou, J., 2013. Responses of soil moisture in different land cover types to rainfall events in a re-vegetation catchment area of the Loess Plateau, China. Catena 101, 122-28.

Wang, S.Y., Gillies, R.R., Takle, E.S., Gutowski, W.J., 2009. Evaluation of precipitation in the intermountain region as simulated by the NARCCAP regional climate models. Geophys. Res. Lett. 36, 11. L11704, 1-6.

Webb, R. H., Leake, S. A., 2006. Ground-water surface-water interactions and long-term change in riverine riparian vegetation in the southwestern United States. J. Hydrol. , 320, 3-4, 302–323.

Wehner, M. F., 2013. Very extreme seasonal precipitation in the NARCCAP ensemble: model performance and projections. Climate Dynamics, 40, 1-2, 59-80.

Wehner, M., Easterling, D.R., Lawrimore, J.H., Heim, R.R., Vose, R.S., Santer, B.D., 2011. Projections of future drought in the continental United States and Mexico. J. Hydrometeorol. 12, 6, 1359-77.

Weichert, A., Bürger, G., 1998. Linear versus nonlinear techniques in downscaling. Climate Research 10, 2, 83-93.

White, D., Richman, M., Yarnal, B., 1991. Climate regionalization and rotation of principal components. Int. J. Climatol. 11, 1, 1-25.

White, M. A., Thornton, P. E., Running, S. W., 1997. A continental phenology model for monitoring vegetation responses to interannual climatic variability. Global Biogeochemical Cycles 11, 2, 217-34.

Wood, A.W., Maurer, E.P., Kumar, A., Lettenmaier, D.P., 2002. Long range experimental hydrologic forecasting for the eastern US. Journal of Geophysical Research 107, D20, 4429.

Yue, S., Pilon, P., & Cavadias, G., 2002. Power of the Mann-Kendall and Spearman's rho tests for detecting monotonic trends in hydrological series. Journal of Hydrology, 264, 1-4, 262-263.